ANL-7105

Argonne National Laboratory

REACTOR DEVELOPMENT PROGRAM

PROGRESS REPORT

September 1965

Oct. to Gene Korn

Printed in USA. Price $3.00. Available from the Clearinghouse for Federal Scientific and Technical Information, National Bureau of Standards, U. S. Department of Commerce, Springfield, Virginia

ANL-7105
Reactor Technology
(TID-4500, 45th Ed.)
AEC Research and
Development Report

ARGONNE NATIONAL LABORATORY
9700 South Cass Avenue
Argonne, Illinois 60440

0560

REACTOR DEVELOPMENT PROGRAM PROGRESS REPORT

September 1965

Albert V. Crewe, Laboratory Director
Stephen Lawroski, Associate Laboratory Director

Division	Director
Chemical Engineering	R. C. Vogel
Idaho	M. Novick
Metallurgy	F. G. Foote
Reactor Engineering	L. J. Koch
Reactor Physics	R. Avery
Remote Control	R. C. Goertz

Report coordinated by
R. M. Adams and A. Glassner

Issued October 20, 1965

Operated by The University of Chicago
under
Contract W-31-109-eng-38
with the
U. S. Atomic Energy Commission

FOREWORD

The Reactor Development Program Progress Report, issued monthly, is intended to be a means of reporting those items of significant technical progress which have occurred in both the specific reactor projects and the general engineering research and development programs. The report is organized in a way which, it is hoped, gives the clearest, most logical overall view of progress. The budget classification is followed only in broad outline, and no attempt is made to report separately on each sub-activity number. Further, since the intent is to report only items of significant progress, not all activities are reported each month. In order to issue this report as soon as possible after the end of the month editorial work must necessarily be limited. Also, since this is an informal progress report, the results and data presented should be understood to be preliminary and subject to change unless otherwise stated.

The issuance of these reports is not intended to constitute publication in any sense of the word. Final results either will be submitted for publication in regular professional journals or will be published in the form of ANL topical reports.

The last six reports issued in this series are:

March 1965	ANL-7028
April 1965	ANL-7045
May 1965	ANL-7046
June 1965	ANL-7071
July 1965	ANL-7082
August 1965	ANL-7090

REACTOR DEVELOPMENT PROGRAM

Highlights of Project Activities for September 1965

EBR-II

Formal dedication cermonies were held at EBR-II on September 13.

Burnup to the extent of 1.21 a/o was achieved as of September 20.

FARET

All design packages, except V and IX, which have been ready since early June, have been signed and issued. Authorization for Title III work has not yet been issued, which is producing problems with regard to scheduling of construction and estimation of costs.

A FARET Core I report was prepared and submitted to the AEC early in September. This report delineates the design of Core I and the R and D program necessary for its fabrication.

ZPPR

The coring of the Gravel Gertie structure was completed. Preliminary results show that there was uranium present during the test and that there is a uranium gradient in the gravel. No uranium above background levels can be detected in the top 5 ft of gravel.

Preliminary tests of the high velocity filtration characteristics of the sand portion of the ZPPR gravel-sand roof have been started.

AARR

The architect-engineer for the AARR project, Burns and Roe, Inc., has completed the initial planning phase of the Title I effort, and has been authorized to proceed with the principal design phase.

Experiments have been performed in the Criticality Facility to supply information needed in selecting the optimum arrangement of nuclear instrumentation for the AARR core. Additional reactivity calculations were carried out to determine the effect of voids in the core and internal thermal column, with boron added to the core as burnable poison. An initial set of three approximately full-size europia-stainless steel control blades has been received for worth measurements in the Criticality Facility, and for hydraulic and corrosion testing.

A prototype aluminum core support grid has been machined from 6-in. thick plate, and is being set up for an experimental stress study.

Materials compatibility tests are being conducted at Oak Ridge National Laboratory on samples of beryllium, aluminum and stainless steel in various ratios of exposed surface area. Initial tests with beryllium indicate somewhat lower corrosion rates as the exposed surface area is increased.

REACTOR DEVELOPMENT PROGRAM

Highlights of Project Activities for September 1965

EBR-II

Formal dedication ceremonies were held at EBR-II on September 13.

Surging to the extent of 1.21 MW was achieved as of September 20.

EARET

All design packages, except V and IX, which have been ready since early June, have been signed and released. Authorization for Title III work has not yet been issued, which is producing problems with regard to scheduling of construction and estimation of costs.

A EARET Core I report was prepared and submitted to the AEC early in September. This report delineates the design of Core I and the R and D program necessary for its fabrication.

ZPPR

The coring of the Gravel Gertie structure was completed. Preliminary results show that there was uranium present during the test and that there is uranium present in the gravel to uranium above background levels can be detected up to 5 ft or gravel.

Preliminary tests of the high velocity flow characteristics of the sand portion of the ZPPR gravel-sand roof have been started.

AARR

The architect-engineer for the AARR project, Burns and Roe, Inc., has completed the initial planning phase of the Title I effort, and has been authorized to proceed with the principal design phase.

Experiments have been performed inside Criticality Facility to supply information needed in selecting the optimum arrangement of nuclear instrumentation for the AARR core. Additional reactivity calculations were carried out to determine the effect of voids in the core and internal thermal column, with boron added to the core as a removable poison. An initial set of three approximately full-size europia-stainless steel control blades has been received for worth measurements in the Criticality Facility and for hydraulic and corrosion testing.

A prototype aluminum core support grid has been machined from 6-in. thick plate, and is being set up for an experimental stress study.

Materials compatibility tests are being conducted at Oak Ridge National Laboratory on samples of beryllium, aluminum and stainless steel in various ratios of exposed surface area. Initial tests with beryllium indicate somewhat lower corrosion rates as the exposed surface area is increased.

TABLE OF CONTENTS

		Page
I.	LIQUID-METAL-COOLED REACTORS	1
A.	EBR-II	1
1.	Operations	1
2.	Systems and Components	1
3.	Reactor Physics	3
4.	Surveillance of Mark-I Fuel	3
5.	Fuel Cycle Facility	8
B.	FARET	9
1.	General	9
2.	Mock-up for FARET Cell Handling Operations	10
3.	Shielding Windows	11
4.	Penetration of Tank Cover for Cable Take-up and Cable Support	11
5.	Modeling Studies	14
6.	In-core Instrumentation	15
7.	Fuel Assembly Sodium Flow Test Loop	18
8.	FARET Criticals (ZPR-3)	18
C.	General Fast Reactor Physics	21
1.	ZPR-6	21
2.	ZPPR	21
D.	General Fast Reactor Fuel Development	22
1.	Metallic Fuels	22
2.	Jacket Materials	26
3.	Carbide Fuel Elements	27
4.	Corrosion	28
5.	Irradiation Testing	29
6.	Zero-power Reactors	31
E.	General Fast Reactor Fuel Reprocessing Development	32
1.	Skull Reclamation Process	32
2.	Pyrochemical Processes	34

TABLE OF CONTENTS

		Page
II.	GENERAL REACTOR TECHNOLOGY	36
A.	Experimental Reactor and Nuclear Physics	36
1.	Electron Excitation of ZnS(Ag)	36
2.	On-line Computer Application	37
3.	Nuclear Constants	38
B.	Theoretical Reactor Physics	40
1.	Effects of Randomness on Group Cross Sections	40
C.	High-temperature Materials	41
1.	Ceramic Fuel Materials	41
2.	Liquid-metal Corrosion	44
3.	Irradiation Testing	44
D.	Other Reactor Fuels and Materials Development	47
1.	Nondestructive Testing	47
E.	Engineering Development	49
1.	Two-phase Flow	49
2.	Boiling Liquid-metal Technology	49
3.	General Heat Transfer	50
4.	Manipulators for Handling Radioactive Materials	50
F.	Chemical Separations	51
1.	Fluorination and Volatility Separations Processes	51
G.	Sodium Coolant Chemistry	56
1.	Chemistry of Carbon in Liquid Sodium	56
2.	Control of Sodium Oxide Impurity	58
H.	Plutonium Recycle Reactors	58
1.	EBWR Plutonium Recycle	58

TABLE OF CONTENTS

	Page
III. ADVANCED SYSTEMS RESEARCH AND DEVELOPMENT	59
A. Argonne Advanced Research Reactor (AARR)	59
1. General	59
2. Critical Experiments	59
3. Theoretical Analyses of the Critical-facility Reactors	60
4. Heat Transfer	62
5. Fuel and Materials Development	66
6. Development of Reactor Components	66
7. Primary System and Components	67
B. Magnetohydrodynamics	67
1. Liquid-metal Generator Studies	67
2. MHD Condensing Injector	68
C. Energy-conversion Systems	68
1. Regenerative EMF Cells	68
2. Bimetallic Cells	70
IV. NUCLEAR SAFETY	72
A. Reactor Kinetics	72
1. Equation of State for Fast Reactor Accidents	72
2. Transients with Thorium-Uranium Fuel	73
3. Remotely Controlled Camera Stage for Hot Cell Examinations	75
4. Fast Neutron Hodoscope	76
5. Fast Reactor Safety	76
6. Fast Reactor Control	77
B. TREAT	80
1. Operations	80
2. Large TREAT Loop	80
C. Chemical and Associated Energy-transfer Problems in Reactor Safety	81
1. Metal-Water Reactions	81
V. PUBLICATIONS	85

I. LIQUID-METAL-COOLED REACTORS

A. EBR-II

1. Operations

The reactor was made critical on September 3 to initiate a power run for the next incremental burnup in the row 3 subassemblies. Two experimental subassemblies, XGO5 and XGO6, had been installed in row 4. One-day operation at a maximum power of 50 kW showed that no further loading changes were necessary to reach the goal of 1.21 a/o maximum burnup.

By intermittent operation at or below 500 kW, control rods No. 3 and 10 were calibrated by the period technique and other control rods were calibrated against these two. Reactor power was raised incrementally to 45 MW while taking measurements for determination of power coefficients.

Operation continued until September 20 to achieve the desired burnup and the reactor was then shut down while power coefficient measurements were repeated.

The delayed-neutron monitor (Fuel Element Rupture Detector) exhibited some degree of instability, apparently due to noise.

Fission product gases reached equilibrium in the primary argon gas at levels previously encountered as follows: Xe^{133}, 4×10^{-3} μCi/ml; Xe^{135}, 1×10^{-3} μCi/ml.

On September 13, EBR-II dedication ceremonies were held. AEC Commissioner Gerald Tape attended, as well as other government, The University of Chicago, Argonne, and community officials.

A total of 79,734 MWdt has been accumulated in reactor operation to date; 391 MWdt of operation were accumulated in the last power run described above.

2. Systems and Components

a. Control Rod Drives. The gripper jaw mechanism of control rod drive No. 9, which was removed from the primary tank last month (see Progress Report for August 1965, ANL-7090, p. 1), could not be examined closely because of its radioactivity (approximately 50 R/hr at 6 in.). The sensing rod of this drive was stuck in the "UP" position. Cleaning of the drive has been started.

Control rod drive No. 11 was installed earlier in the No. 9 position, but would not latch readily on the control subassembly. To

determine whether the subassembly might be at fault, it was replaced by a new one. The same problem occurred.

For current operation, control rod drive No. 11 (position 9) was manually latched to the new control subassembly. After the power run, the control rod was manually unlatched.

During subsequent testing to investigate this problem, the control drive was latched to the subassembly with the reactor cover up. The same problem was encountered.

A dummy control subassembly with a top adapter "mushroom" of 0.955-in. OD (0.020 in. less than standard) was placed in position No. 9. Also, a second modification of this dummy subassembly was made by machining 0.020 in. off the underside of the "mushroom." Neither expedient improved the latching of the gripper.

b. Rotating Shield Plug-seal Troughs. By a vacuum cleaning technique approximately $21\frac{1}{2}$ lb of black powdery oxide, modules, and metal were removed from the large plug (a total to date of $23\frac{1}{2}$ lb). Small-plug cleaning, begun this month, yielded approximately $2\frac{1}{2}$ lb of the same type of material. No attempt has been made to separate the recovered oxide from the metal.

The oxide removal seems to allow the large shield plug to rotate with somewhat less heating; the last melting time (to obtain plug rotation) was approximately 40 hr versus the 56 hr required before the cleaning operation. The small plug does not seem to present as great a problem and appears to have less black powder on the surface.

An attempt was made to clean the upper-level thermocouple wells with a wire brush to determine the effect upon indicated temperatures. However, below the surface of the molten alloy, deposits apparently hindered brushing action. Vertical temperature profiles at several large plug locations have been taken. The minimum temperature at the surface of the alloy was 355°F; the maximum temperature was 528°F near the bottom of the trough.

Two samples of "nodular" oxides from the large plug seal trough were chemically analyzed and found to contain 6 w/o and 13 w/o sodium (expressed as sodium oxide), respectively. These results are in agreement with previous analyses (see Progress Report for July 1965, ANL-7082, p. 2).

c. Improved Pump for Secondary System. In April 1964, prior to start of the Approach to Power, a leak developed in the secondary-system pump due to cracks (fatigue failures) in the pump duct wall caused by duct vibration. The vibration resulted from deficiencies in the pump design which produced deleterious differential pressure conditions across the wall at high flow rates.

After repair and reinstallation of the pump, flow has been limited to 5500 gpm as a result of downrating of the pump by the manufacturer (from the original 6500-gpm capacity). This is adequate for reactor operation at 45-50 MW. However, use of the very high flow rates required for full reactor power (62.5 MW) presumably would unduly increase the probability of failure.

To enable future full power operation with minimal risk of extended plant shutdown due to a secondary-pump failure, a linear induction pump of 6500-gpm capacity at 53 psi head is being procured. Design improvements are expected to include a redesigned inlet transition member, to reduce pressure drop, and elimination of internal spacer supports in the duct. Delivery time is estimated by the successful bidder at 10 months.

3. Reactor Physics

Power coefficients were taken during the startup and shutdown of the reactor during the September 9-20 run. The shape of the power coefficient curve was qualitatively the same as previously; the overall magnitude of the power coefficient was 73 and 77 Ih, respectively. The total reactivity lost during the 391 MWd run was 60 Ih.

Data from the drops of the stainless steel control rod taken during the previous run (starting at 2400 MWd and ending at 2920 MWd indicated no changes in the prompt power coefficient.

4. Surveillance of Mark I Fuel

A surveillance program to determine the condition of the EBR-II Mark I fuel is being conducted at both the Idaho and Illinois sites. Measurements at Idaho include sodium-level and bond condition, internal gas pressure, and diameter checks of the jacketed fuel by "go, no-go" gaging. Examinations at Illinois presently include dimensional and density measurements of both jacketed and stripped fuel, metallographic inspection, and furnace heating tests. Burst tests on the fuel jackets are scheduled to begin shortly at Illinois.

The primary objective of the surveillance program is to enable EBR-II to achieve the maximum burnup in the fuel short of excessive fission product release into the primary coolant. Frequent inspection of the fuel as reactor operation proceeds is relied upon to furnish the information necessary to determine the ability of the fuel to accumulate additional burnup.

The reactor was permitted to continue to approximately 0.8 a/o burnup (maximum) while fuel was being examined from lower burnup levels. It appeared that from then on it would be more prudent not to start up the

reactor until results from the last fuel examination were available. Although this type of operation results in a low plant factor, it was considered more desirable than to increase seriously the risk of numerous unanticipated fuel-jacket failures.

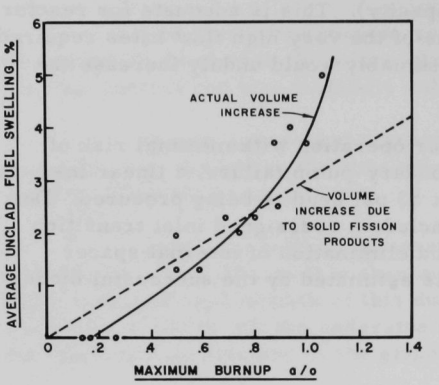

Fig. 1. Average Swelling in EBR-II Mark-I Bare Fuel (Based on Changes in Sodium Level).

Fuel has now been removed from the reactor for examination after 1.21 a/o burnup (maximum). The data available from previous examinations indicate that the unclad fuel is increasing in volume at an accelerating rate, as is shown in Fig. 1. Since the pressure-volume relationship in the jacketed fuel rod is now such that a small increase in fuel volume causes a large increase in internal pressure, it is evident that two strongly reinforcing functions are acting. In other words, small increments of burnup now result in large increments in jacket stress, assuming that the jacket does not show plastic deformation.

Increases of fuel volume over ~8% can be accommodated without jacket failure only if the jacket develops plastic strain. Whether or not plastic strain can be counted upon in the reactor to relieve high jacket stresses before rupture is as yet unanswered. The burst tests are intended to provide information on the available ductility in the irradiated jackets at reactor operating temperatures.

In addition, the furnace heating tests now in progress supply helpful information on available ductility in jackets. Their primary purpose, however, is to provide an indication of the capability of the jacketed fuel to resist dimensional changes or of the jacket to resist rupture because of temperature rises that could conceivably occur in the reactor core because of slower coolant flow.

In the furnace heating experiments, the jacketed fuel rods are heated to progressively higher temperatures of 550, 600, 650, 700, and 750°C. After being held for 5 min at each temperature, the rods are cooled to room temperature, leak-tested, and measured for dimensional and density changes. After the final heating to 750°C, the jackets are removed and the bare fuel pins similarly measured for dimensional and density changes.

The results with 5 rods thus far tested are summarized in Table I. Since the original diameter of the jacketed fuel was 4.42 mm and of the bare fuel pin 3.66 mm, it can be seen that significant dimensional changes

do not occur below 750°C. Furthermore, fuel volume increases of over 11% can occur without increasing the volume of the jacketed rod more than 0.5%. No leaks were observed to have developed in any of the jacketed rods as a result of the heating tests, with the possible exception of Rod No. E-37. A questionable leak indication on the first leak test after the 750°C anneal could not be reproduced.

TABLE I. Results from Furnace Heating Tests of EBR-II Mark-I Jacketed Fuel Rods

Rod No.	Maximum Burnup, a/o	Temp, °C	Avg Diameter, in.	Volume Change, %
A-7	1.0	Start	0.174	-
		570	-	-0.01
		600	0.176	+0.34
		650	0.175	-0.10
		700	0.174	-0.03
		750	0.174	+0.42
(Unclad Fuel)		750	0.151	+0.58
E-48	1.0	Start	0.174	-
		570	-	+0.77
		600	0.174	+0.32
		650	0.174	-0.03
		700	0.174	-0.05
		750	0.174	+0.30
(Unclad Fuel)		750	0.149	+11.17
E-74	1.0	Start	0.175	-
		555	-	+0.04
		600	-	+0.03
		645	-	+0.03
		700	-	-0.06
		750	-	-0.02
		775	0.177	+0.36
(Unclad Fuel)		775	0.150	+10.38
E-37	1.1	Start	0.173	-
		560	0.173	+0.01
		600	0.174	-0.01
		650	0.175	-0.01
		700	0.174	-0.03
		750	0.175	+0.45
(Unclad Fuel)		750	0.150	+10.89
E-38	1.1	Start	0.175	-
		560	0.174	+0.02
		600	0.174	0
		650	0.175	+0.01
		700	0.175	-0.01
		750	0.175	+0.45
(Unclad Fuel)		750	0.151	+11.11

The heating tests to date provide considerable encouragement that the EBR-II Mark-I fuel with as much as 1.1 a/o burnup is capable of withstanding, without jacket rupture, jacket temperature excursions of at least 200°C above normal operating conditions.

Fuel elements from subassemblies S-602 and C-136, representing maximum burnup levels of 1.01 and 1.06 a/o, have been examined. The data from these units have been combined with those obtained previously, and are presented graphically in Figs. 2 and 3, which show the sodium levels and void volumes as functions of maximum fuel burnup in the assembly.

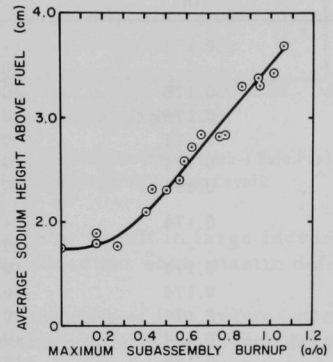

Fig. 2. Variation of Sodium Level with Burnup

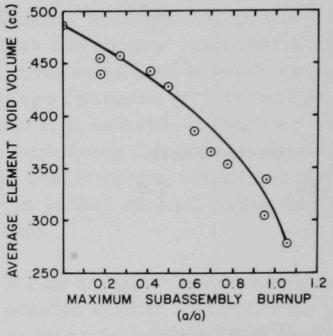

Fig. 3. Variation of Void Volume with Burnup

In Fig. 4, the sodium-level and void-volume data have been combined to show the fuel swelling as burnup progresses. This curve is based on the assumptions that changes of fuel volume are manifest as linear changes in sodium level and that the decrease in void volume is caused by an equal change in fuel volume. The slope of this curve is only slightly greater than could be attributed to accumulation of solid fission products. Perhaps more significant is the fact that no gross swelling has been observed during 45-MW operation.

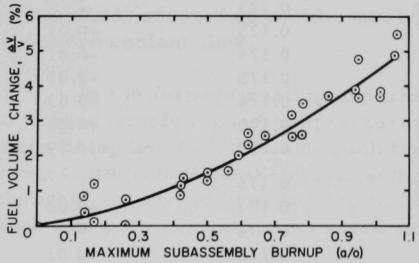

Fig. 4. Fuel Volume Change with Burnup

Measurement and visual inspection of individual rods (10 each) from subassemblies L-410, B-314,

C-131, S-601, and C-145 have also been completed. The ranges observed in increases in diameter are summarized in Table II. This information is of value in correlating the data obtained on volume increase as indicated by sodium level and void volume measurements. Measurements before and after irradiation indicate a minimum diameter change based on the assumption that the maximum values occur at the same rod position. A maximum possible diameter change can be ascertained by comparing the minimum preirradiation diameter with measurement of the maximum postirradiation diameter.

TABLE II. Summary of Diameter Increases Observed

Subassembly	Calculated Maximum Burnup, a/o	(10 rods from each subassembly) Increase in Maximum Diameter (post-pre), in.
B-314	0.59	0.000-0.001
L-410	0.67	0.001-0.006
C-141	0.78	0.000-0.002
S-601	0.86	0.003-0.006
C-145	0.94	0.002-0.006

Table III presents a comparison of the indicated volume change of the fuel as derived from the independent measurements of sodium level and void volume.

TABLE III. Comparison of Fuel Volume Change as Indicated by Measurements of Sodium Level and Void Volume

	Calculated Burnup		Volume Increase (%)	
Subassembly	Maximum a/o	Average a/o	Sodium Level*	Void Volume**
C-140	0.26	0.22	0.07	0.79
C-112	0.42	0.38	0.89	1.18
C-143	0.50	0.43	1.34	1.55
C-122	0.63	0.53	2.32	2.69
C-103	0.75	0.63	2.57	3.19
C-141	0.79	0.62	2.62	3.51
C-145	0.94	0.79	3.90	No valid data
C-138	0.95	0.81	3.73	3.90
C-136	1.06	0.87	4.93	5.51

*Based on an initial sodium level of 0.688 in. above the fuel.
**Based on an initial void volume of 0.487 cc.

Subassemblies C-104 and C-142, which represent maximum burnup levels of 1.21 a/o, are presently being examined.

5. Fuel Cycle Facility

a. Fuel Handling. Forty-one subassembly transfers involving both the reactor grid and the storage basket were performed during the month.

b. Fuel Processing and Fabrication. An irradiated control rod subassembly (S-601, of 1.0 max a/o burnup) was received from the reactor, dismantled, examined, and processed. Six refabricated subassemblies were transferred to the reactor.

About 300 elements were decanned during the period. A graphite bearing on the upper drive shaft of the decanner seized, and the unit was replaced with a spare while the malfunctioning decanner is being decontaminated and repaired.

Nine melt-refining runs and corresponding skull-oxidation runs were completed. Ingot yields ranged from 90.8 to 96.2%, with one exception in which some oxidized charge material was used and the yield was 87%. The ingots produced provided part of the material for 10 injection-casting runs in which the average yield of metal cast was 70.5%.

In the processing of 1120 pregnant molds from 11 injection-casting runs, the yield of acceptable rods was 64%. Principal causes for rejection were castings too short to shear, castings short after shearing, diameter defects, and porosity. Assembly, welding, leak testing, bonding, and bond testing operations were carried out, and 364 acceptable elements were transferred for use in subassembly manufacture (additional acceptable elements are in process). Five core-type assemblies were fabricated. Poor welds noted on one assembly suggested removal of the welding guns for examination. The electrodes were found to be worn and were replaced.

c. Blanket Decanner. Preoperational tests of a decanning machine for the EBR-II blanket elements have been completed and the machine is being shipped to Idaho for installation in the Argon Cell of the Fuel Cycle Facility.

The decanner will accommodate either the short blanket elements from the core and blanket subassemblies or the long elements from the blanket subassemblies. The short elements contain two, 0.316 in. dia x 9 in. long, uranium rods; the long elements contain five, 0.433 in. dia x 11 in. long, uranium rods. The elements are loaded into a suitable length-transfer magazine in the Air Cell, transferred to the Argon Cell, and the transfer magazine is then placed in position on the decanner. The elements are individually placed into the decanner with a master-slave manipulator. Each element is then lowered by the feed mechanism against the stop plate to gauge the location of the cut. The cladding is cut near the ends of the uranium rods contained in the element by rotating the element as it is forced against a rolling cutter.

The short lengths of elements are placed in the heated magazine with the master-slave manipulator. The heated magazine is maintained at 600°F; about 2 min are required to melt the sodium bonding between the uranium rod and the cladding. A stepped hole just below the heated magazine retains the cladding while the rod is pushed out by a pneumatically powered ram. The stepped hole is then opened and the cladding is allowed to fall into a scrap container.

The entire machine is designed for moderate ease of remote repair of its subassemblies. Locating pins, guide surfaces, lifting handles and captive screws were used throughout to facilitate this.

Utilization of a master-slave manipulator for most of the handling, indexing, and positioning operations has allowed this machine to be much simpler than if switch-controlled manipulators were used or if the machine were built to incorporate all of these functions.

B. FARET

1. General

There has been no change in the status of the Architect-Engineer's portion of the Title II design during the month. The design is essentially complete and all design packages have been signed and issued, except Packages V and IX. The latter package drawings and specifications have been ready for signature since early June. Approval is being withheld until firm guidance has been received from the Commission relative to the start of construction.

Pending authorization to proceed with Title III, work at the Architect-Engineer offices is at a very low level, requiring approximately 3 or 4 men full time. The efforts of these people have been directed toward the following:

a. Minor revisions of design Packages III, Liquid Metal Heat Exchangers, and IV, Liquid Metal Pumps. A formal revision of these design packages is not planned until authorization to proceed with procurement has been received from the Commission.

b. Bechtel is also currently working on minor revisions of a number of other specifications, including those for liquid metal valves, piping, and general cleaning procedures.

A group at Bechtel is also reviewing the general project design quality of Title II. The specific objectives in this effort include the following:

(a) To identify errors, omissions or oversights which could result in fabrication-quality problems caused by furnished equipment or facility construction;

(b) To identify additional requirements which could be imposed to increase confidence in obtaining presently specified equipment and facility quality;

(c) To identify additional requirements where such upgrading may be advisable;

(d) To examine agreed-upon, selected, current design criteria which, if modified, will result in a design with a higher confidence level.

The review of the project design is being concentrated primarily on the more critical regions, such as those in the reactor vessel cavity; system components, such as liquid metal pumps, heat exchangers, instrumentation, and the containment liner.

The Laboratory is continuing to review various FARET equipment drafts for bid invitations submitted by UE & C. To date, these reviews are essentially complete and are coordinated with UE & C for the liquid metal pumps, heat exchangers, and instrumentation. Other bid packages for which UE & C has submitted material to the Laboratory for review include cleaning procedures; boilers; stainless steel tanks; cell, vault and cavity liners; and the personnel air locks.

The current delay in authorizing the initiation of Title III continues to multiply schedule and cost-estimating problems. The liquid metal heat exchanger procurement, Package III, and the liquid metal pumps procurement, Package IV, are now dominating factors in establishing the construction schedule. In addition, costs continue to increase as a consequence of changing market conditions. Because of continued uncertainties in the current project planning, the Laboratory is reviewing the extent of the work at Bechtel necessary to cope with the discontinuity in engineering activities.

2. Mock-up for FARET Cell Handling Operations

The remote operating functions of the reactor cell equipment require prior evaluation of the in-cell handling operations, which include the effects of variations in operator position, window and lighting arrangements, considerations of crane and manipulator mounting locations, and cell area to be reached. This evaluation will be studied by means of a mock-up of reactor vessel top section, a viewing window, manipulator, special purpose crane, lights, mirrors, closed circuit TV, fuel cut-off machine cable feed troughs, pneumatic and electrical connectors, floor storage pits, scrap disposal equipment, and others as desired.

3. Shielding Windows

The specifications for shielding windows are being redrafted to modify the performance specification. The new specifications are in two parts, the first set specifying the requirements for the glass slabs and the second set for the fabrication and assembly according to ANL-furnished drawings. The glass slabs would be made by competent glass manufacturers and delivered to the window-frame manufacturer for final assembly. This procedure should enable a number of fabricating shops to enter into the bidding without having to assume responsibility for meeting the glass requirements. The separate glass procurement can be followed more competently by ANL personnel intimately familiar with the complex shielding and viewing requirements.

The new design (see Fig. 5) calls for shielding equivalent to a 5-ft-thick wall of ordinary concrete whereas the first specifications called for heavy concrete equivalent. The tank unit has been laid out so that in its interior can be used either two 4-in.-thick slabs of 6.2 (T_2 and T_3) density glass or two 8-in.-thick slabs of 3.3 density glass with virtually no change in the viewing angles of the window or in the shielding capability.

Depending on what optional glass combination listed in the glass specifications is most economically available, the expected light transmittance could vary from 14.5% as a minimum to about 22.5% as a maximum. Although high light transmittance is desirable, even the low value of light transmittance is comparable to window transmittance at the Fuel Cycle Facility of EBR-II and is acceptable.

4. Penetration of Tank Cover for Cable Take-up and Cable Support

A mock-up of the penetration of the tank cover for take up of the electrical cable of the control rod drive (see Fig. 6) has been designated and fabricated.

These penetrations are planned to bring the cable leads of the control rod drives from the cell to the outside. Since the drives are attached to the head and move up and down with the head for refuelling, free movement of the cables is necessary. Cable take-up reels are used to maintain cable tension during movement of the reactor vessel cover. This mechanism is contained within a vertical steel tank located at the north end of the cell. Some eighty electrical cables enter the steel tank at the top flange through leak- and pressure-resistant penetrations. The cables are supported by an intermediate support plate installed below the tank cover.

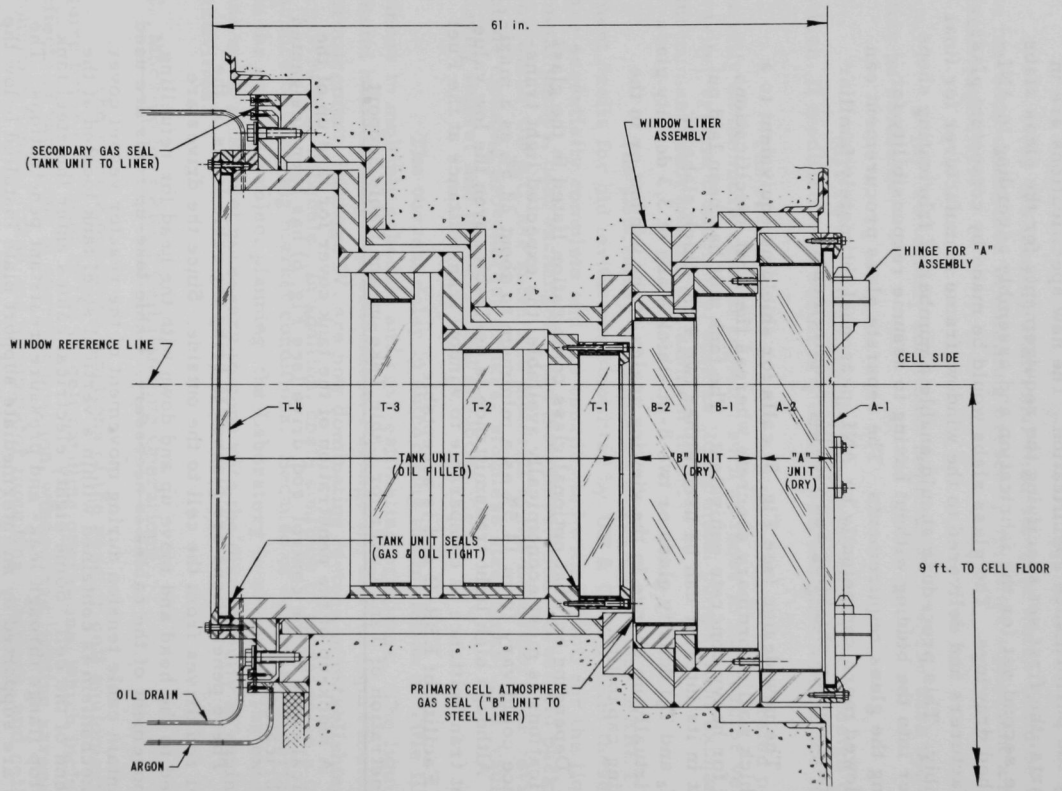

Fig. 5. Vertical Section through FARET Cell Shielding Window

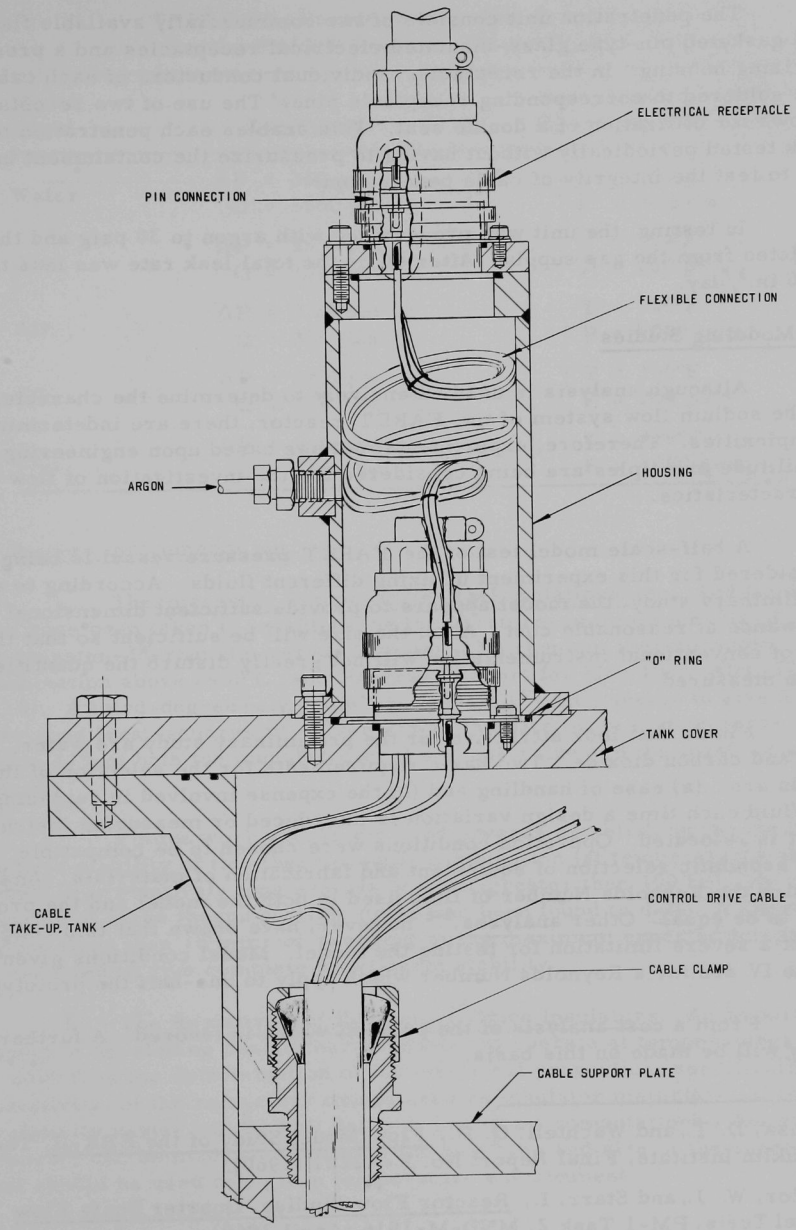

Fig. 6. Penetration of Tank Cover for Cable Take-up

The penetration unit consists of two commercially available flanged and gasketed pin-type glass-insulated electrical receptacles and a pressurizing housing. In the receptacles, individual conductors of each cable are soldered to corresponding receptacle pins. The use of two receptacles allows for utilization of a double seal. This enables each penetration to be leak tested periodically without having to pressurize the containment building to test the integrity of cable penetration.

In testing, the unit was pressurized with argon to 30 psig and then isolated from the gas supply. After 40 hr the total leak rate was less than 0.06 $in.^3$/day.

5. Modeling Studies

Although analysis is used extensively to determine the characteristics of the sodium flow system of the FARET reactor, there are indeterminable complexities. Therefore, experimental studies based upon engineering similitude principles are being considered for the investigation of flow characteristics.

A half-scale model test of the FARET pressure vessel is being considered for this experiment utilizing different fluids. According to a preliminary study, the model appears to provide sufficient dimensional allowance at reasonable cost. Also, the size will be sufficient so that the use of conventional instrumentation will not greatly disturb the quantities to be measured.

Fluids that look attractive for the preliminary study are water, air, and carbon dioxide. Two basic requirements for the selection of the fluids are: (a) ease of handling and (b) the expense involved in replacing the fluid each time a design variation is introduced or measuring instrument is relocated. Operation conditions were chosen to be compatible with economic selection of equipment and fabrication of materials. Analyses require the Reynolds Number of fluid used in both the model and the prototype to be equal. Other analyses,[1,2] however, have shown that this condition is not a severe limitation for testing the model. Model conditions given in Table IV are for a Reynolds Number which apply to one-half the prototype.

From a cost analysis of the project, water is favored. A further study will be made on this basis.

---

[1]Rymsa, D. T., and Wachtell, G. P., Flow Model Study of the EBR-II, The Franklin Institute, Final Report No. F-A2201 (1960).

[2]Taylor, W. J., and Starr, I., Reactor Flow Studies, Quarter Scale Flow Model Tests, PM-1 Task 2, MND-M-1916 (April 1960).

TABLE IV. Expected Operating Condition for the FARET Pressure Vessel Model

Model Fluid	Model Conditions	Approximate System Operating Conditions
Water	ΔP = 244 psi Q = 2850 gpm	T = 160°F P = 50 psia
Air	ΔP = 36.5 psi Q = 1580 cfm	T = 100°F P = 200 psia
Air	ΔP = 7.28 psi Q = 316 cfm	T = 100°F P = 1000 psia
CO_2	ΔP = 18.4 psi Q = 922 cfm	T = 100°F P = 200 psia
CO_2	ΔP = 6.46 psi Q = 656 cfm	T = 100°F P = 1000 psia

6. In-core Instrumentation

a. Thermocouple Temperature-EMF Relationships. Additional data have been taken to establish the temperature-emf relationship of the tungsten-3% rhenium versus tungsten-25% rhenium thermocouple combination above 2400°C (see Progress Report for May 1965, ANL-7046, p. 10). A third-degree polynomial ($A_0 + A_1t + A_2t^2 + A_3t^3$) seems to give a very good least-squares fit. Over 97% of the data taken to date agree to within ±1% of both the manufacturers' average value and the least-square values.

Future work will be directed towards establishing the thermoelectric stability of this thermocouple combination (at temperatures above 2400°C) for relatively long periods of time (greater than 100 hr). No indication of large thermoelectric drifts has been found to date. A short period (less than 15 min) of preaging at the maximum expected temperature is required to give complete short-term stability.

b. The Resistivity of Refractory Oxide Insulators. An important aspect of developing usable thermocouples to operate at temperatures up to 2800°C is the determination of the electrical properties, specifically the resistivity, of the refractory oxides used as insulator materials. If these resistivity values can be well defined, important computations ("hot zone errors") can be made to determine the best type and size of thermocouple that should be used in a given temperature environment.

Thoria appears to be the only refractory oxide suitable for use as electrical insulation in sheath-type thermocouple assemblies at temperatures above 2300°C. The reasons are:

(i) It has a high melting point (~3300°C).

(ii) It is reported to be completely compatible with refractory metals such as tantalum, tungsten, rhenium, molybdenum, and alloys of these elements which are used both as sheath and wire elements.

(iii) It has a low electrical resistivity at temperatures above 2300°C.

The resistivity of typical refractory oxide insulator beads used in thermocouples is being determined. Both the so-called "crushable" and "vitrified" types of insulators are used. Differences exist in the resistivity values of these two types, principally because of different contact area between the wires and insulation. The "crushable" type of insulation produces the greatest ratio of wire-to-insulation contact area and will probably produce the lowest resistivity. The "vitrified" type of insulator is slip fit over the wires and will produce point or line contacts of higher resistivity.

Alumina was selected as a reference material. Measurements are to be made according to ASTM Standard Methods of Test for Electrical Resistance of Insulating Materials, ASTM Designation: D257-61. The volume resistivity is calculated from

$$\rho_v = \frac{2\pi L R_v}{\ell n (D_2/D_1)} \text{ ohm-cm},$$

where L is the length of the specimen in cm, R_v is the measured volume resistance in ohms, D_2 is the largest specimen diameter, and D_1 is the smallest specimen diameter. This equation is a variation from that recommended by the ASTM, but is believed to give a more accurate result.

TABLE V. Resistivity of Alumina at Various Temperatures

Temperature, °C	Resistivity, ohm-cm	
	Average from Literature	Measured for Vitrified Alumina
800	1×10^8	2×10^7
1000	1×10^6	3×10^6
1200	7×10^4	5.5×10^5
1400	1.5×10^4	1×10^5
1600	3×10^3	2×10^4
1800	5×10^2	3×10^3
1900	2.5×10^2	1×10^3

In Table V are listed the preliminary volume resistivities of a "vitrified" alumina insulator at various temperatures. Also listed are average values obtained from the literature. The measured values are generally higher than the literature values.

At the completion of the above test, the alumina

insulator bead had shrunk about 3%, which throws some doubt on the measured resistivity values. Since the beads used had been sintered at 1650°C, further sintering at higher temperatures (~1950°C) occurred.

A white alumina bead was fired for 3 hr at 1950°C in helium. Upon removal, the bead had shrunk about 10% and had turned a dull black color suggesting a stoichiometric change. The resistivity of the alumina at room temperature had decreased to one-fourth its initial value. Preliminary tests indicate that firing in an air environment returns the bead to its original color and resistivity. The stoichiometric change will be checked by spectrographic analysis.

To determine whether thoria exhibits a similar behavior, a white sample bead was fired for 30 min at 2400°C in helium. The bead turned silver gray. After an additional 30 min at 2600°C, the bead turned darker and total shrinkage was 5%. Further firing will be made at 2800°C in helium and an oxygen-rich environment.

The fact that a stoichiometric change may take place in an inert gas environment explains the low resistivity values sometimes reported in the literature. Proper sintering of the beads may solve this problem and consequently improve the thermocouple performance.

c. Fuel-irradiation Experiments. Thermocouple data from the Plutonium Fuel Irradiation Experiment (see Progress Report for June 1965, ANL-7071, p. 9) have been analyzed. The capsule used had a centerline fuel thermocouple made of W-3% Re/W-25% Re wires insulated by thoria inside the fuel region and alumina outside the fuel region. The sheath was 0.062-in.-OD tantalum. The thermocouple was exposed to a calculated fast integrated neutron flux of ~2.6 x 10^{19} nvt during the 720-hr test. Approximately 20 thermal cycles occurred during this time.

This information concludes the reporting on the Fuel Irradiation Experiments.

d. Thermocouple In-pile Tests. The data obtained from a different thermocouple capsule, which may contain up to three thermocouples (see Monthly Progress Report for June 1965, ANL-7071, p. 9), have been analyzed. The W-3% Re/W-25% Re thermocouple that was used to indicate the central fuel temperature operated continuously throughout the 2-hr in-pile test to determine if the capsule design would permit a center fuel temperature of approximately 2400°C in the CP-5 reactor at maximum power. The UO_2 fuel in the capsule was spaced away from the cladding by means of tantalum rods placed so as to achieve a temperature of about 2300°C in an argon atmosphere at the maximum reactor power of 4.5 MW. Figure 7 shows the time-temperature history of the capsule. At point "A," as the reactor was being taken to 3 MW, the high-temperature scram circuit shut down the reactor when the fuel temperature reached 1950°C, a limit set for

the previous slip-fit heat-transfer experiments. After readjustment of the high-temperature scram circuit to trip at 2360°C, the reactor was restarted, and 69 min later was operating at a steady power of 4.2 MW. The indicated fuel temperature was 2180°C, very close to the design value. The fuel temperature remained practically steady for 30 min. It then increased rather abruptly to about 2300°C and finally increased suddenly to 2360°C at point "B." This shut down the reactor. The capsule was subsequently removed from the reactor.

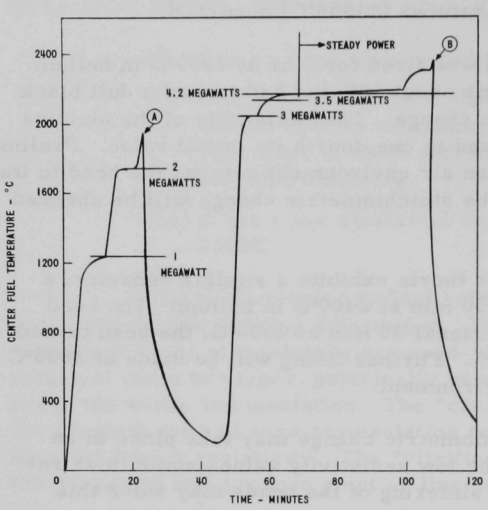

Fig. 7. Time-temperature History for Capsule HT-1

The cause of the sudden increase in temperature has not been explained. The capsule did, however, accomplish its purpose of showing that temperatures up to ~2300°C can, in fact, be achieved in the CP-5 reactor with the present capsule design.

7. Fuel Assembly Sodium Flow Test Loop

The 800-gpm sodium pump has successfully passed the manufacturer's performance test; apparently the pump will deliver a head slightly greater than the specified 320 ft of sodium. All critical parts have been inspected at the vendor's plant, and the pump has been fully accepted. The interim pump now installed in the loop will be removed and the 800-gpm pump mounting installed. Removal of the interim pump has started.

The "Conax" connector and elbow assembly for the pressure vessel had been delayed for lack of a suitable 4-in. 90°, S.R. elbow. Such an elbow was finally located and shipped to the manufacturer. The unit is now scheduled to be completed at the end of this month. The installation of this item will be done concurrently with the installation of the new pump and upon completion of the pressure vessel internals.

8. FARET Criticals (ZPR-3)

Assembly 46 was modified to produce a uniform central zone of high enrichment, called 46G, by changing the central oxide zone of 46F (see Progress Report for July 1965, ANL-7082, p.14) to a carbide zone. Since the next outer zone of 46F already was composed of this carbide composition, the result was a unified central carbide zone, approximately 10 in. in diameter and 20 in. in length.

Each drawer in the central zone contains $1\frac{1}{2}$ columns of 93% enriched uranium, $1\frac{1}{2}$ columns of plutonium, and 1 column of 31% enriched uranium. An interface view of Assembly 46G is shown in Fig. 8.

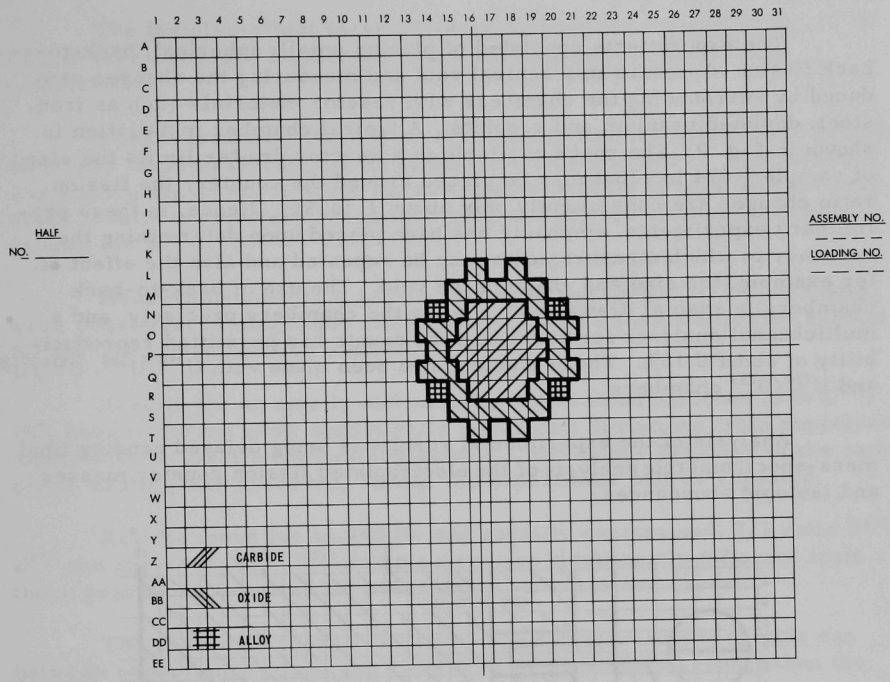

Fig. 8. Face View, Assembly 46G

Compositions of the core zones are given in Table VI. As in Assembly 46F, the uranium in the carbide zone has an average enrichment

TABLE VI. Core Zone Compositions for ZPR-3 Assembly 46G

	Composition, 10^{22} atoms/cc				Composition, 10^{22} atoms/cc		
Material	Oxide	Carbide	Alloy	Material	Oxide	Carbide	Alloy
Pu^{239} + 241	0.107	0.156	0.263	O	0.866	-	-
Pu^{240} + 242	0.005	0.008	0.013	C	0.502	1.111	-
U^{235}	0.224	0.410	0.112	Fe	1.099	1.057	1.141
U^{238}	0.459	0.472	0.848	Cr	0.295	0.284	0.307
U^{234} + 236	0.003	0.005	0.002	Ni	0.145	0.140	0.144
Na	0.843	0.843	0.843	Zr	-	-	0.317

Reflector composition: 0.211 g/cc Na, 6.38 g/cc stainless steel, 0.305 g/cc Al.

of 45% and that in the oxide zone, 33%. The higher enrichment of the carbide zone gives high threshold fission rates and is well suited for the investigation of the effects of small alterations in the environment upon threshold fission ratios.

The experiments consisted of placing small, spherical, back-to-back fission chambers in a central void and measuring the changes produced by surrounding the chambers with reactor materials such as iron, steel, depleted uranium and graphite. A typical chamber installation is shown in Fig. 9. The space available in a reactor drawer limits the size of sample (~1/4 in.) that may be placed around the counter; the fission ratio changes are consequently only about 1 to 5%. Hence, in these preliminary experiments, emphasis has been placed upon determining the accuracy to which measurements may be repeated and also the effect of, for example, the size and shape of the void. The use of back-to-back chambers, a special drawer which holds the chambers precisely, and a multichannel analyzer for recording the counts has permitted reproducibility of about 0.15%. These studies have been made with U^{238}/U^{235}, U^{236}/U^{235} and U^{234}/U^{235} chambers.

Analysis of the experimental results is being delayed pending final mass-spectrometric analysis of the electroplated fission counter masses and isotopic abundances.

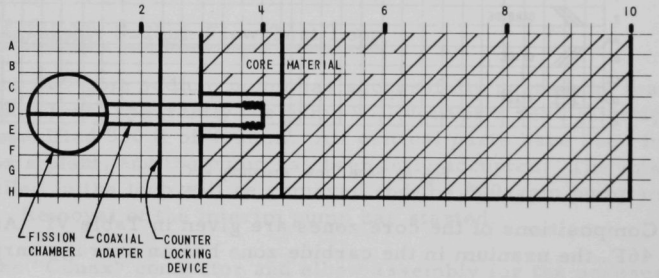

Fig. 9. Top View of Typical Chamber Installation for ZPR-3 Assembly 46G (Drawer 1-P-17)

C. General Fast Reactor Physics

1. ZPR-6

The Doppler-effect measurements planned for Assembly No. 4Z of ZPR-6 (see Progress Report for May 1965, ANL-7046, p. 14) were completed.

A measurement with a 1-in.-dia, axially constrained natural UO_2 element was made to investigate an apparent anomaly at 400°K. The anomaly was apparently an error since the new measurements agreed with the previous results everywhere but at that point and showed consistent results around 400°K.

Measurements with a 1/2-in.-dia enriched (97% U^{235}) UO_2 element were consistent in magnitude and sign with the previously reported results for the 1-in. enriched UO_2 sample.

Results for an axially and radially constrained enriched (97% U^{235}) UO_2 sample did not show statistically significant deviations from measurements with an axially constrained sample. Anomalous behavior of the sample on heating was observed, so that the experiment will be repeated.

Results found for an axially and radially constrained, 7/1 ratio U^{238}/U^{235} and enriched (97% U^{235}) sample were not significantly different from those previously reported for other axially constrained cases.

The reactivity change measured on heating an empty sample can between room temperature and 1100°K was only slightly greater than the statistical precision and is thus considered negligible.

2. ZPPR

Analysis of the containment structure of ZPPR is continuing.

The coring of the Gravel Gertie structure was completed during August. Preliminary scanning of the gravel was obtained by driving a 2-in.-dia pipe down through the gravel and by gamma scanning each hole for thorium-234, the natural daughter of the alpha decay of U^{238}. (Depleted uranium was used as the tracer in the Gravel Gertie tests.) Seven holes were logged, and analyses of these scans indicated that the casing should be located approximately 7 ft off center in a south-southeast direction (155° off north).

Samples from selected levels of gravel were analyzed chemically. The preliminary results showed uranium present during the test and a uranium gradient in the gravel. No uranium above background levels was

found on the gravel until a depth of approximately 5 ft is reached. The maximum concentration of uranium occurs approximately 10 ft down in the gravel.

Preliminary tests of the high-velocity filtration characteristics of the sand portion of the ZPPR gravel-sand roof have been started. The sand used in these tests is that which is called for in the Title II specifications and is available at the normal NRTS supply area.

The following is a status report on reactor components:

a. Reactor Bed and Tables. The vendor, Giddings & Lewis Machine Co., has received the comments on the preliminary drawing of the assembly and is incorporating these comments into the design. The electrical drawings are being prepared for review. The details of the hot rail system are also being prepared for review.

b. Matrix Drawers. All perforation dies were completed and tried out. The forming dies were completed but have not been tried out with perforated stainless steel blanks. The sizing die (for weld test and length sizing) was completed. The hole pattern was checked by ANL and comments were sent back to the vendor.

c. Matrix Tubes. The four pilot tubes were fabricated. One was shipped to ANL-Idaho and three to ANL-Illinois. These are now being inspected by ANL for specifications. All dies and jigs were completed. The test and inspection jigs are being designed.

d. Fuel-rod Drives. All castings have been bronze finished. The springs have been received. The job is approximately 25% complete.

e. Poison Rod Drives and Reactor Knees. The bid packages have been reviewed.

D. General Fast Reactor Fuel Development

1. Metallic Fuels

a. Thorium-Uranium-Plutonium Alloys. As part of our interest in Th-U-Pu alloys as potential fast reactor fuels, we are investigating pertinent features of the equilibrium phase diagram. The question of the stability range of the thorium-beta phase still needs to be answered. A high-temperature X-ray-diffraction Debye-Scherrer camera was built and calibrated with platinum. Temperatures up to 900°C were reached and excellent diffraction patterns were obtained. The room-temperature data are in agreement with the best measurements published by the National Bureau of Standards.

At 800°C a Th-2 w/o U-40 w/o Pu alloy gave diffraction patterns of α-Th, ThO_2, and PuO_2, with no indication of the bcc β-Th phase. Because of the almost complete overlap between the ThO_2 pattern and bcc β-Th pattern, the statement is based on absence of the (321) bcc line, a negative proof that may not be entirely satisfactory. The lattice parameter of the thorium phase was 5.0431 ± 0.0005 Å. By comparison the lattice parameter of pure thorium was 4.9972 ± 0.0005 Å at 800°C.

The excellent compatibility results that have been obtained with stainless steel by adding zirconium to U-Pu alloys suggested a similar approach for the Th-U-Pu alloys. The following series of Th-U-Pu alloys was tested against Type 304 stainless steel:

	Composition			
Alloy	a/o Th	a/o U	a/o Pu	a/o Zr
I	61	20	10	9
II	71	10	10	9
III	50	20	10	20
IV	60	10	10	20

After one week at a temperature of 750°C considerable interpenetration occurred both into the fuel and the cladding. It was concluded that zirconium additions to these thorium alloys do not improve their compatibility with stainless steel. However, the ternary thorium-uranium-plutonium alloys are compatible with V-20 w/o Ti alloy.

b. Improved U-Pu-based Metal Fuels. Phase relationships, compatibility with potential cladding materials, and pertinent properties of the very promising high-melting U-Pu-Zr and U-Pu-Ti alloys (see Progress Report for May 1965, ANL-7046, pp. 19-24) are being investigated.

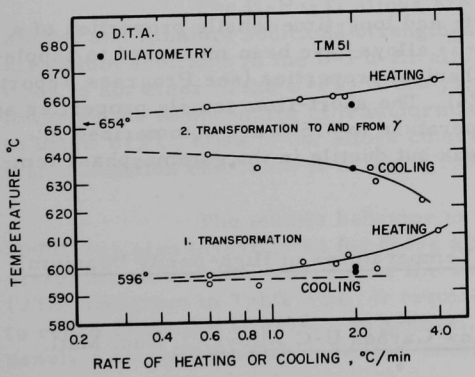

Fig. 10. Solid-state Transformations in U-15 w/o Pu-10 w/o Zr (U-12.9 a/o Pu-22.5 a/o Zr) as a Function of Heating and Cooling Rates

(i) Phase Relationships. An alloy consisting nominally of U-15 w/o Pu-10 w/o Zr, equivalent to U-12.9 a/o Pu-22.5 a/o Zr, was investigated by differential thermal analysis (DTA). Various rates of heating and cooling were employed. The results are shown in Fig. 10. The solid-state transformation data agree with those previously obtained by dilatometry at a rate of 2°C/min. Hysteresis occurred in both transformations

on heating, but only in the second transformation on cooling. The hysteresis increased with the rate of heating and cooling, as might be expected. Extrapolation to equilibrium temperatures was possible, and the observed phenomena follow the general pattern observed with high-purity uranium[3] and uranium-carbon alloys.[4] An attempt to determine the solidus temperature of the U-Pu-Zr alloy gave a value higher than 1120°C, the maximum temperature presently attainable in our DTA apparatus.

(ii) Compatibility. Further studies have been made of the phase relations in the U-Zr-Fe system to assist our understanding of the factors that relate to the good compatibility up to 800°C of U-Pu-Zr alloys with Type 304 stainless steel (see Progress Report for July 1965, ANL-7082, pp. 20-1). At 800°C ternary alloys containing up to 30 w/o Fe and from 10 to 15 w/o Zr are composed of the following phases: a solid solution of gamma uranium containing zirconium and possibly a small amount of iron; a solid solution of U_6Fe containing zirconium; and a solid solution of UFe_2 containing zirconium. The gamma and U_6Fe solid solutions are in thermodynamic equilibrium in alloys containing up to approximately 4 w/o Fe; the U_6Fe and UFe_2 solid solutions are in equilibrium in alloys containing between 15 and 30 w/o Fe. The compositional range of the ternary solid solutions based on U_6Fe has not as yet been determined.

These findings suggest that the previously observed good compatibility of U-Zr and U-Pu-Zr alloys with iron and Type 304 stainless steel may be related in part to an enhancement of the thermodynamic stability of the U_6Fe, UFe_2, and gamma-uranium phases upon the addition of zirconium. Another possible contributing factor, suggested by some findings of Clark and Rhines[5] for Al-Mg-Zr alloys, is that the diffusion composition path in the previously studied couples tends, as a whole, to bend away from the fastest diffusing component or components, which in our case is iron.

(iii) Properties. Short- and long-time tensile properties of a series of cast U-Pu-Zr and U-Pu-Ti alloys have been measured to supplement the previously reported mechanical properties (see Progress Report for May 1965, ANL-7046, pp. 19-24). The short-time tensile properties as a function of composition and temperature to 675°C are summarized in Table VII. The alloys are very weak but ductile in the gamma-phase temperature region.

---

[3]Blumenthal, B., Transformation Temperatures of High-purity Uranium, J. Nuc. Matl. 2(1), 23-30 (1960).

[4]Blumenthal, B., Constitution of Low Carbon U-C Alloys, J. Nuc. Matl. 2(3), 197-208 (1960).

[5]Clark, J. B., and Rhines, F. N., Trans. ASM 51, 199 (1958).

TABLE VII. Variation of Tensile Properties with Temperature in Homogenized and Quenched U-Pu-Zr and U-Pu-Ti Alloys[a]

Alloy, nominal w/o			Temp, °C	U.T.S., kg/mm^2	Y.S.,[b] kg/mm^2	E, kg/mm^2 x 10^{-3}	Type of Failure
U	Pu	Zr					
82.6	11.1	6.3	25	18.1	-	17.4	Brittle
			675	1.2	1.1	1.4	Ductile
77.1	16.6	6.3	25	4.0	-	10.6	Brittle
			675	1.2	1.1	1.6	Ductile
67.4	18.5	14.1	25	7.7	-	13.0	Brittle
			675	2.9	2.8	1.9	Ductile
U	Pu	Ti					
90.9	0	9.1	25	14.7	-	22.7	Brittle
			675	26.3	-	3.0	Brittle
85.2	11.4	3.4	25	30.8	-	17.9	Brittle
			675	5.5	5.2	2.4	Ductile
75	15	10	675	7.0	6.5	3.0	Ductile

(a) All specimens were tested in creep prior to the tensile tests, and therefore contain some (<5%) hot work.
(b) Yield strength at 0.2% offset. Brittle specimens did not attain this before fracturing.

Plutonium additions have an embrittling effect on the U-Pu-Zr alloys at low temperatures, and very little effect on ductility and strength at 675°C. Zirconium additions strengthen the alloys somewhat at 675°C.

The U-Pu-Ti alloys are stronger at 675°C than the U-Pu-Zr alloys, and titanium additions strengthen the alloys more effectively than zirconium additions in the U-Pu-Zr alloys. The effect of plutonium additions is not clear in the U-Pu-Ti alloys, except that, as a consequence of lowering the temperature of transformation from the gamma to U_2Ti phases to below 675°C, tests of the alloys containing plutonium were above the transformation and below it in the U_2Ti alloy.

The tensile behavior at slow strain rates between 600 and 700°C was also investigated for these alloys. The times to reach 2% strain for several stresses below the short-time ultimate tensile stresses (UTS) are given in Table VIII. It requires only minutes at about 1 kg/mm^2 to reach 2% strain at 675°C. In general, the strain-time relationship is nearly a straight line when plotted on log-log coordinates.

TABLE VIII. Time (in minutes) to Attain 2% Strain in U-Pu-Zr and U-Pu-Ti Alloys

Alloy Composition, w/o			Load, kg/mm²	Temp, °C				
				600	625	650	675	700
U	Pu	Zr						
82.6	11.1	6.3	0.5	-	-	-	15	-
			1.0	-	-	-	5	-
			2.0	-	-	-	3	-
			4.0	-	5	-	1	-
77.1	16.6	6.3	0.5	-	-	-	10	-
			1.0	-	5,000	-	1	-
			2.0	-	210	-	-	-
			4.0	-	10	-	-	-
75	15	10	0.5	-	-	5,000	-	-
			1.0	-	5,000	80	-	-
			2.0	-	210	1	-	-
			4.0	-	10	-	-	-
67.4	18.5	14.1	0.5	100,000	-	5,000	45	40
			1.0	10,000	-	80	5	5
			2.0	800	-	1	1	1
			4.0	70	-	-	-	-
U	Pu	Ti						
85.2	11.4	3.4	0.5	-	-	-	-	-
			1.0	-	20,000	-	2,000	-
			2.0	-	350	-	60	-
			4.0	-	5	-	1	-
75	15	10	0.5	400	-	110	-	45
			1.0	20	-	5	-	5
			2.0	-	-	-	-	-
			4.0	-	-	-	-	-

The creep strength is not appreciable in any of the alloys at 650°C, the lowest temperature expected in the FARET Core I fuel.

Thermal conductivity tests to 900°C and thermal cycling tests to 700°C for several U-Pu-Zr and -Ti alloys have been completed and the data are being analyzed. Corrosion tests of these alloys in air have shown them to be very corrosion resistant. Specimens exposed to flowing room-temperature air with a variation in relative humidity from 25 to 55% for periods up to nine months have remained bright and have gained no weight.

2. Jacket Materials

a. Vanadium Alloys. A "scale up" in the fabrication development of the V-Ti-Cr alloys, in particular of the V-15 w/o Ti-7.5 w/o Cr alloy, is now underway.

As expected, a significant loss of chromium occurs on melting under vacuum (either electron beam or arc melting) because of the high vapor pressure of chromium. Double arc-melting under a partial pressure

is expected to reduce losses of chromium and to improve both the alloy homogeneity and process reliability.

Annealing studies of rolled sheet have shown that the V-Ti-Cr alloys are quite susceptible to variations in precipitate morphology and in macrohardness as a function of annealing temperature. Mechanical properties, corrosion resistance, and fabricability may be significantly influenced by such changes.

3. Carbide Fuel Elements

a. Compatibility of (U, Pu)C with Jacketing Materials. The initial phase of the study of jacketing materials for uranium-plutonium mixed-carbide fast reactor fuels has consisted of heat treating and evaluating diffusion couples of single-phase $(U_{0.8}Pu_{0.2})C$ with various metals and alloys.

Chemical analysis of the (U, Pu)C pellets showed a carbon content of 4.74 w/o, and oxygen and nitrogen impurities of about 0.09 and 0.03 w/o, respectively. After firing, approximately 0.79 mm was ground off each end of the pellets to reduce the chance of surface impurity phases. Examination of the pellets prepared for compatibility tests showed single-phase monocarbide of approximately 86% of full density. The compatibility tests were run in sealed quartz capsules containing helium.

Results to date are listed in Table IX. In some cases the reaction zone was not a uniform band, but quite irregular owing to reactions

TABLE IX. Reaction of $(U_{0.8}Pu_{0.2})C$ with Potential Jacketing Materials

Material	Temp, °C	Reaction Zone Width, μ			Direction of Reaction Zone	Remarks
		7 days	17 days	42 days		
304 SS	800	Nil	Nil	Nil	-	-
	950	3	-	-	cladding	-
	1100	130	380	melted	cladding	Heavy grain boundary penetration
Hastelloy-X	800	-	5	8	fuel	Continuous band
	950	45	60	75	fuel	Continuous band
	1100	melted	melted	melted	-	-
V-20 w/o Ti	800	-	100 (270)*	-	cladding	Nonuniform continuous band, poorly defined due to reaction along stringers
	950	160 (320)*	-	350 (700)*	cladding	
	1100	750 (>1300)*	-	>1300		
Vanadium	950	Nil	Nil	45	cladding	Irregular second-phase growth along grain boundaries
	1100	165	270	450	cladding	
Niobium	950	2	-	-	cladding	Uniform continuous band
	1100	8	-	-	cladding	Uniform continuous band
Molybdenum	1100	6	-	-	cladding	Uniform continuous band
Tantalum	1100	4	-	-	cladding	Uniform continuous band
Chromium	1100	Nil	-	-	-	-
Tungsten	1100	Nil	-	-	-	-

*Values in parentheses indicate extent of reaction along stringers.

along grain boundaries as in vanadium, or stringers (particles aligned in the extrusion direction) as in V-20 w/o Ti alloy. The values listed in these cases are maximum values. Further tests at 800°C are planned for this material with high-strength iron- and nickel-base alloys.

In most of the specimens to date, the fuel-jacket interface has been found to be broken when examined metallographically. Although we believe that the specimens were in contact at the heat-treatment temperature, subsequent stresses caused by thermal-expansion differences in the specimens and holder on cooling results in broken interfaces. Because of this resulting gap, evaluation of reaction zones is made more difficult. In an attempt to eliminate this problem, we are presently looking at techniques to insure the integrity of the final specimen.

Because of uncertainties encountered in present commercial production of stoichiometric uranium-plutonium monocarbide, we are also studying laboratory procedures pertaining to, and material characteristics of, uranium-plutonium carbides with a variety of carbon contents.

4. Corrosion

a. Corrosion of Fuel-jacketing Materials for Sodium-cooled Reactors. Consistently reliable analyses of oxygen in sodium in the low (0 to 10 ppm) concentration range have not been achieved through use of the mercury amalgamation technique. Since reliable analyses in this oxygen range are necessary in order to achieve meaningful results, studies of corrosion by sodium have been temporarily suspended pending development of a consistently reliable sampling-analytical technique.

A vacuum distillation technique is being explored. Hot gettered (with zirconium) sodium has been sampled at 600°C and at 450°C with either a nickel dip tube or a nickel flushing sampler. Five analyses all yielded results under 10 ppm oxygen. The relatively narrow scatter in the data obtained in this initial effort is encouraging.

Oxygen analyses were also performed with samples taken from a sodium system nominally maintained at 40 to 50 ppm oxygen. The mercury amalgamation method (reasonably satisfactory at this concentration level) yielded a result of 36 ppm; the vacuum distillation method yielded a result of 42 ppm.

With some refinement in technique, it is believed the vacuum distillation method will be a consistently reliable technique for the analysis of sodium containing low concentrations of oxygen.

5. Irradiation Testing

a. High-burnup Irradiation of Uranium-Plutonium Alloys. Post-irradiation examination has begun of a group of five uranium-plutonium-fissium specimens that successfully achieved burnups as high as 8.7 a/o (calculated). A sixth specimen, which was found to have developed a localized jacket rupture after 8.7 a/o burnup, is also being examined. The irradiated specimens are shown in Fig. 11.

The maximum irradiation conditions are shown in Table X. During the later stages of the experiment, plutonium depletion resulted in temperature drops of approximately 150°C. The specimens were irradiated in an instrumented capsule in the CP-5 reactor for 29 months. During this period they were also subjected to several hundred severe thermal cycles because of reactor shutdown.

The purpose of the experiment was to evaluate the effect on achievable burnup of jacket thicknesses heavier than the thin (0.229 mm) jacket used for the EBR-II Mark-I fuel. The predicted achievable burnups based on pressure-volume calculations are shown in the second column from the right in Table X. By comparing this column with the adjoining column to the right, it can be noted that the burnups achieved without clad rupture were, in all but one instance,[6] markedly higher than predicted. The differences may be due to strengthening of the jacketing during irradiation. Consideration is being given to reencapsulating some of the specimens for continued irradiation in order to obtain additional comparisons between predicted achievable burnups at the point of jacket rupture and the burnups that actually can be obtained.

The burnups achieved in this experiment are among the highest ever reported for metal fuels. Successful attainment of these high burnups is regarded as particularly noteworthy in view of the fact that bare uranium-plutonium-fissium alloys were found to swell catastrophically at relatively low temperatures and burnups.[7] The experiment therefore provides a convincing demonstration of the effectiveness of jacket restraint in preventing fuel swelling.

For purposes of comparison, 8.7 a/o burnup in the uranium-plutonium-fissium alloys used in this experiment produced a fission density of 3.3×10^{21} fissions/cm^3. This fission density is equivalent to over 100,000 MWd/T burnup in oxide fuel, and to 80,000 MWd/T burnup in carbide fuel.

---

[6] In this one instance the experiment was terminated before the predicted burnup was attained. There was no jacket rupture.

[7] Horak, J. A., Kettel, J. H., and Dunworth, R. J., ANL-6429 (July 1962).

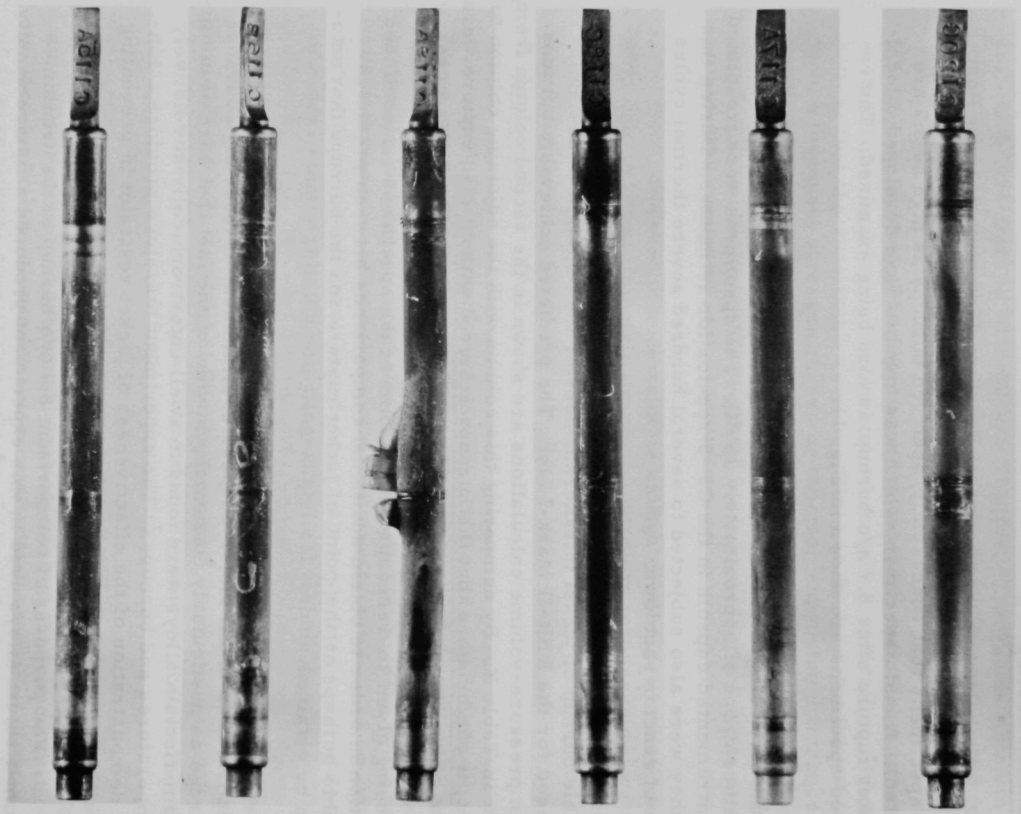

Specimen No.	EI-3908 C-115A	EI-3900 C-116B	EI-3902 C-119A	EI-3906 C-118A	EI-3907 C-117A	EI-3908 C-120A
Calculated Burnup, a/o	7.1	7.1	8.7	8.7	8.7	7.1

Fig. 11. Photographs of Specimens from Irradiation Capsule CP-33 (Mag 1.5X)

TABLE X. Irradiation Conditions for High-burnup U-Pu-Fz Specimens

Specimen No.	Fuel Composition, w/o	Jacket Thickness, in.	Maximum Fuel Temp, °C	Maximum Jacket Temp, °C	Predicted Maximum Burnup to Failure, a/o	Actual Calculated Burnup, a/o
C-115A	U-10 Pu-10 Fz	0.015	590	510	5.0	7.1
C-116B	U-10 Pu-10 Fz	0.020	610	530	5.9	7.1
C-119A*	U-15 Pu-10 Fz	0.015	625	545	5.3	8.7
C-118C	U-15 Pu-10 Fz	0.025	625	545	9.4	8.7
C-117A	U-15 Pu-10 Fz	0.015	625	545	7.2	8.7
C-120C	U-10 Pu-10 Fz	0.025	610	530	6.7	7.1

*Observed to have developed a localized jacket split.

6. Zero-power Reactors

a. Properties of Zero-power U-Pu-based Fuel Alloys. U-Pu-based ternary alloys are being studied as alternates to the U-20 a/o Pu-6 a/o Mo alloy that was developed for zero-power applications. Titanium and zirconium show the most promise as alloying additives. The air-corrosion tests (see Progress Report for July 1965, ANL-7082, p. 23) showed that the U-25 a/o Pu-10 a/o Ti alloy, after an initial weight gain of 0.3% at 13 weeks, showed no further changes after nine additional weeks of exposure. It then began to gain weight slowly and has now gained 0.5% in weight after 30 weeks. The specimen has also powdered and is about 10% disintegrated. The U-25 a/o Pu-12 a/o Ti alloy is still sound and shows no powdering or weight gain after 17 weeks. Although the tests on this alloy have not been in progress as long as the tests for the U-Pu-Mo alloys, the results to date indicate that at least 12 a/o Ti will be needed to give air-corrosion resistance comparable to that of the 6 a/o Mo alloy.

Air-corrosion tests have been started with a series of U-25 a/o Pu alloys with 6, 9, and 12 a/o Zr added. These have all remained sound and have shown no weight gain after five weeks.

Because of the fact that some of the U-20 a/o Pu-6 a/o Mo alloy fuel plates manufactured by NUMEC for the SEFOR fast critical experiments have had carbon contents above the maximum of 1000 ppm called for in the specifications, we have begun air-corrosion tests on NUMEC material reported as containing 1200 and 1800 ppm carbon. (Subsequent analysis has indicated that the actual carbon content is much lower.) The microstructures showed a difference in carbide particle size, but no obvious difference in amount. The higher-carbon specimen has remained sound and shows no significant weight gain after 6 weeks in air. The lower-carbon specimen has become tarnished and cracked after 5 weeks.

Other specimens of U-20 a/o Pu-6 a/o Mo alloy that have been under test for over a year have become very slightly cracked and powdered, whereas our original alloy of U-27 a/o Pu-6 a/o Mo remained sound for 21 months. To see if this cracking might be related to the carbon content, we analyzed the fine powder for carbon and found the carbon content to range from 1200 to 2600 ppm carbon rather than 500 to 700 ppm carbon obtained for the original specimens.

We do not at present understand the mechanism for this buildup of carbon in the corrosion product. The buildup may be due to selective corrosion of the fine UC particles, which we have observed metallographically and have analyzed with an electron-beam microprobe.

These results suggest that the cracking of the U-Pu-Mo alloys after long-time exposure to air is related to the carbon content. We have, therefore, begun a systematic study of the effects of carbon by making a series of U-Pu-Mo alloys with known amounts of carbon added in the range 250 to 3500 ppm.

E. General Fast Reactor Fuel Reprocessing Development

1. Skull Reclamation Process

The skull reclamation process, being developed specifically for recovering and purifying residual uranium left in crucibles after melt-refining discharged fuel pins from the EBR-II reactor, is currently being demonstrated in EBR-II plant-scale (~4.25 kg uranium), remotely operated equipment. This equipment or versions of it will be installed in the Fuel Cycle Facility in Idaho.

Four additional plant-size runs following the modified flowsheet (see Progress Report for June 1965, ANL-7071, pp. 24-25) have been completed in the skull reclamation furnace, which is operated at temperatures between 700 and 810°C. No difficulties were encountered in carrying out any of the mechanical operations, including charging of materials, heating, mixing, sampling, and transferring molten metal and fluxes from the furnace to exterior receivers. Transfers of molten metals and fluxes from the skull reclamation furnace to the transfer receiver equipment are accomplished by means of a heated (~750°C), 1/2-in.-ID transfer line made of molybdenum-30 w/o tungsten.[8] In these runs, the transfer line, which had been rebuilt (see Progress Report for August 1965, ANL-7090, p. 27), continued to operate very satisfactorily. Some 20 troublefree transfers of waste metal supernatants, waste fluxes, and product solutions were easily carried out.

[8]ANL-7020, Chemical Engineering Division Research Highlights, May 1964-April 1965.

The rebuilt transfer line incorporates design changes to improve performance reliability, one of which involves the use of silica-insulated Chromel P wire as a heater cable. In a separate test (ANL-7090, p. 27), the suitability of this heater cable for extended use was examined. No evidence of deterioration of the cable was noted. To date, the accumulated testing time at elevated temperatures has amounted to 158 hr at 900 to 925°C and to 740 hr at 950 to 975°C. Since the performance of this cable for its intended use as a heater cable on the transfer line was very good, no further testing is planned.

Although mechanical operation of the equipment was good, fuming of metal and salt vapors was observed in these runs when the skull reclamation furnace was opened while at operating temperatures for charging. Fuming also occurred, but to a lesser extent, during and following the transfers of metal and salt solutions from the furnace. To overcome this problem, an exhaust manifold for the collection of fumes is being built and tested. The manifold, which is attached to the furnace, is in an early stage of development. However, initial test results indicate that the fuming can be controlled by such equipment.

Retorting is utilized to recover the uranium from the uranium product solution produced in the dissolution step of the skull-reclamation process. In the retorting step, the magnesium-zinc-uranium ingot from the skull reclamation furnace is transferred to a large BeO crucible ($8\frac{1}{2}$ in. in OD by 17 in. of overall height by 1/2-in.-thick wall). The magnesium-zinc is then distilled at 800 to 900°C from the uranium product solution, after which the uranium is melted (~1200°C) to form an ingot. Two preliminary runs using the same BeO crucible (a thixotropically cast crucible) were completed in plant-scale retorting apparatus located in an inert atmosphere enclosure. The charge in each run consisted of a Zn-13.5 w/o Mg (no uranium) ingot weighing about 38 kg, a quantity normally associated with about 4.5 kg of uranium product. Overall performance and apparent distillation rate of the equipment were satisfactory. After these two runs, the BeO crucible was found to be in excellent condition. In future runs, feed charges to the BeO crucible will contain uranium.

Pilot-plant demonstration runs (with 1.5 kg U) of the skull-reclamation process were discontinued in June 1965 (see Progress Report for June 1965, ANL-7071, p. 23). However, molybdenum-removal data from one of the last four runs that used the previous flowsheet have become available. (In previous pilot-plant runs, molybdenum removals in the noble metal extraction step have been barely adequate.) Molybdenum analyses of the zinc and flux phases from this step showed that, of the originally charged molybdenum, 56% was extracted into the zinc phase and 37% remained in the flux phase. This suggests that incomplete reduction of the molybdenum is the probable cause of poor molybdenum extraction. The reason for the incomplete reduction is uncertain. Because further molybdenum removal is possible during the product dissolution step, it is believed that overall removals of molybdenum will be satisfactory.

2. Pyrochemical Processes

A general type of flowsheet being investigated for processing uranium and plutonium metal, oxide, or carbide core and blanket material discharged from fast breeder reactors is shown in Fig. 12. The process is based on the selective transport of uranium and plutonium from a Cu-Mg solvent alloy to appropriate Zn-Mg alloys through a salt phase consisting of a mixture of $MgCl_2$, NaCl, and KCl. Because small volumes of metal and salt solutions are required and because separation factors are very high, the process is easily adapted to single-stage batch separations.

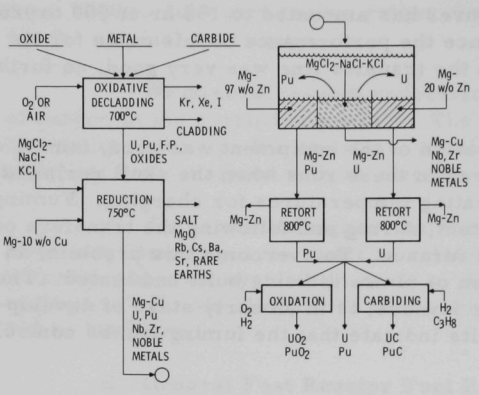

Fig. 12. Conceptual Pyrochemical Batch-extraction Process for Fast Breeder Reactor Core and Blanket Materials

The flowsheet involves, first, an oxidative decladding operation in which oxide fuels would be released from cladding. Carbide and metal fuels would be converted to oxides in such a step. These are then reduced in a Mg-10 w/o Cu alloy. The highly electropositive fission elements, alkali, rare earth, and alkaline earth elements, distribute strongly to the salt phase and are removed in it. Then, by taking advantage of the widely different distribution coefficients and solubilities for uranium and plutonium in metal phases of different compositions, the uranium and plutonium can be separated by selective transfer to separate metal phases. The application to fuel processing of solute transfer between liquid alloys in mutual contact with a molten salt has been discussed by Chiotti.[9] Transfer of uranium and plutonium could be done successively or simultaneously; the latter is shown schematically in Fig. 12.

Results of preliminary experiments related to this flowsheet are very encouraging. The indications are that it should be possible to recover plutonium (well separated from uranium) and uranium with excellent decontamination from fission products.

The study of corrosion is an important adjunct to the development of this process. Corrosion tests of various conventional materials of construction to determine their suitability for this application are in progress (see Progress Report for August 1965, ANL-7090, p. 28). Previous corrosion

[9]Chiotti, P., and Klepfer, J. S., Transfer of Solutes between Liquid Alloys in Mutual Contact with Fused Salt. Application of Fuel Reprocessing, Ind. Eng. Chem., Process Design Develop. 4(2), 232-239 (April 1965).

tests have shown that certain ferrous alloys (304 SS, 405 SS, AISI 4130, and AISI 1020) appear suitable for the containment of liquid Cu-Mg alloys. Since the small amount of corrosion that was observed apparently resulted from the simple dissolution of iron, the solubility of iron in liquid Cu-Mg alloys was determined. The solubility values were low, ranging from 0.14 w/o iron in Cu-9.0 w/o Mg at 850°C down to 0.0115 w/o iron in Cu-33.5 w/o Mg at 600°C. These low solubility values are consistent with the low corrosion rates that have been observed Further, iron at these low concentrations should have no adverse effect on the process.

II. GENERAL REACTOR TECHNOLOGY

A. Experimental Reactor and Nuclear Physics

1. Electron Excitation of ZnS(Ag)

In recent publications,[10-12] there has been recorded a pronounced difference in scintillation decay time of ZnS(Ag) in Hornyak buttons when excited by alpha particles rather than by electrons. Results[13,14] at this Laboratory indicate that, although there may be small differences in scintillation decay shape caused by particles of differing ionization density, the very short (few nanosecond) pulses are due to Cherenkov radiation and luminescence of the transparent media associated with the phototube and coupling media.

Figure 13 shows the fluorescence of ZnS(Ag) powder evaporated on a quartz disc which was bombarded by nanosecond bursts of electrons, with energy less than 75 keV, from a pulsed accelerator.

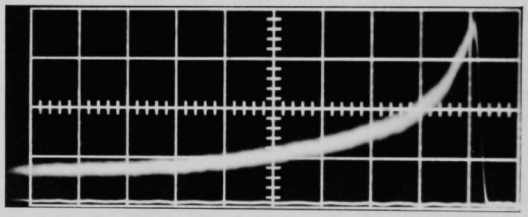

Fig. 13. Fluorescent Emission from ZnS(Ag) Excited by 1.5-nsec Bursts of 70-keV Electrons; Horizontal Scale: 40 nsec/ Major Division (and arbitrary amplitude). The photograph of a sampling oscilloscope shows many superimposed pulses which were triggered by the accelerator. The ZnS(Ag) decay is consistent with a 70-nsec initial decay component; risetime is about 3.0 nsec after subtracting a 2-nsec instrumental integrating time constant.

Under identical conditions, however, narrow pulses have been observed due to fluorescence by electrons in various transparent media and is illustrated in Fig. 14. Decay times of less than 3 nsec have been found

[10] Wraight, L. A., Harris, D. H. C., and Egelstaff, P. A., Improvements in Thermal Neutron Scintillation Detectors for Time-of-flight Studies, Nucl. Instr. Methods 33, 181 (1965).

[11] Bailey, G. M., and Prescott, J. R., Decay Time of the Luminescence of a Zinc Sulphide Neutron Detector for Neutron and γ-ray Excitation, Australian J. Phys. 11, 135 (1958).

[12] Asada, T., et al., Decay Properties of ZnS(Ag) Phosphors, J. Phys. Soc. Japan 14, 1766 (1959).

[13] DeVolpi, A., and Porges, K. G., Rejection of Gamma-background Radiation Pulses in Hornyak Buttons, IRE Trans. Nucl. Sci. NS-9(3), 320 (June 1962).

[14] Porges, K. G., DeVolpi, A., and Polinski, P., Fast Cancellation of Gamma-radiation Background Pulses in Hornyak Buttons with an Active Circuit, Rev. Sci. Instr. 35, 1602 (1964).

for quartz, glass, and Lucite, as well as the sample of clear epoxy in Fig. 14. Longer decay components were measured for polyethylene (17 nsec) and paraffin (24 nsec). All measurements have an estimated relative error of 20%.

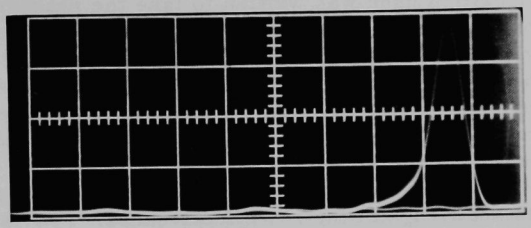

Fig. 14. Electron-generated Fluorescence from a Clear Epoxy Sample at 10 nsec/Major Division (and arbitrary amplitude). This is typical of the type of pulse frequently attributed to ZnS(Ag), but actually produced in many transparent materials.

2. On-line Computer Application

An oscilloscope display has been constructed for the DDP-24 computer. It uses a commercial X-Y oscilloscope driven by resistor-network digital-analog converters connected to two registers. Each register contains ten flip-flop circuits, providing for the equivalent of a 1024-line image. The flip-flops receive signals from the unbuffered parallel output channel. Each output operation causes the plotting of one point. The oscilloscope sweep circuit is used to unblank the beam.

It has been found that letters, numbers, and other symbols and patterns can be generated on the oscilloscope using subroutines that were previously developed for use on the graph plotter.

The oscilloscope is especially intended to give the experimenter a quick look at the data generated during the course of on-line operation. Some use has been made to indicate the proper time to start an asymptotic period measurement.

A motor-control circuit has been developed to control by computer the dual-purpose rod drives on the fast criticals. This circuit uses two flip-flops driving a complementary-symmetry transistor bridge circuit that can run the d.c. motor in either direction.

This motor-control circuit was wired into the ZPR-9 console in such a way that a dual-purpose rod selected by the operator could be moved by computer control instead of manually. This arrangement was used to insert the last rod and make the reactor critical. A number of successful test runs have been with this arrangement.

This work was undertaken as part of a program to develop automatic control for the criticals, and it was done for two reasons: (a) it is most difficult from the standpoint of constructing a suitable algorithm, and (b) at the same time requires the least alteration of the reactor control circuits. The algorithm used was written to take the reactor up to a prescribed power on a prescribed period and level off at the prescribed power. To do this, the algorithm examines the flux behavior and determines if a change in the log of the slope is required to approach the demand trajectory more closely. Having information about the effectiveness of the rod, it decides whether the demand would be most closely approached by moving the rod or leaving it stationary during the next time interval (normally 0.1 sec). By observing the actual response to a given rod motion, the algorithm updates its knowledge of the rod effectiveness. Provision is made to take account of the changes in the log of the slope caused by the approach of delayed-neutron precursors to equilibrium.

The performance of the system was satisfactory, but there were two shortcomings. First, the rod motion was indecisive at low power levels due to noise. Second, the flux had a tendency to overshoot upon reaching the demand level because of limited rod speed. Modifications of the algorithm to overcome these problems are under investigation.

3. Nuclear Constants

a. Radiative Capture. Cross sections of substances important to the fast reactor program are being studied as a function of neutron energy between 4 keV and 3 MeV, covering a large part of the neutron energy spectrum of fast reactors. Capture cross sections are needed to make proper use of materials proposed for structural and control use in reactors. The data are also useful in testing nuclear-reaction theories. The information gained by comparison of experimental data with theoretical values could allow the prediction of other neutron cross sections in the absence of experimental data.

An activation method was employed in which the nucleus being studied was irradiated with a monoenergetic neutron beam and the radioactive species produced counted with a beta counter or a gamma-ray analyzer. The counting data were then converted to capture cross sections by suitable calibrations.

Cross sections have been determined for Lu^{175} and Mo^{98}. In Fig. 15 are shown the capture cross sections of Lu^{175} between 140 keV and 3 MeV. Also shown are data for the low-energy region presented by Gibbons et al.[15] who utilized the detection of capture gamma rays. The agreement between the two sets of data is good. It should be noted that the cross section for Lu^{175} is one of the largest in the fast-neutron region, being nearly as large as that of rhenium.

[15]Gibbons, J. H., Macklin, R. L., Miller, P. D., and Neiler, J. H., Neutron Cross Sections, BNL-325 (1960).

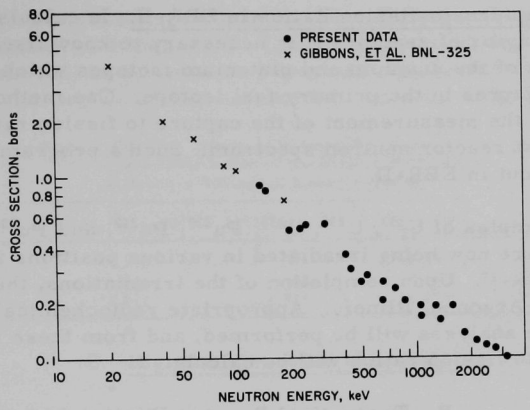

Fig. 15. Radiative Capture Cross Section of Lutetium-175

The experimental data for the capture cross sections of Mo^{98} as a function of neutron energy have been compared with the theoretical formulations of Lane and Lynn[16] by means of the level density formula of Gilbert and Cameron[17] and the neutron strength functions recommended by Moldauer.[18] The results are shown in Fig. 16. The agreement between the experimental and theoretical values is reasonably good.

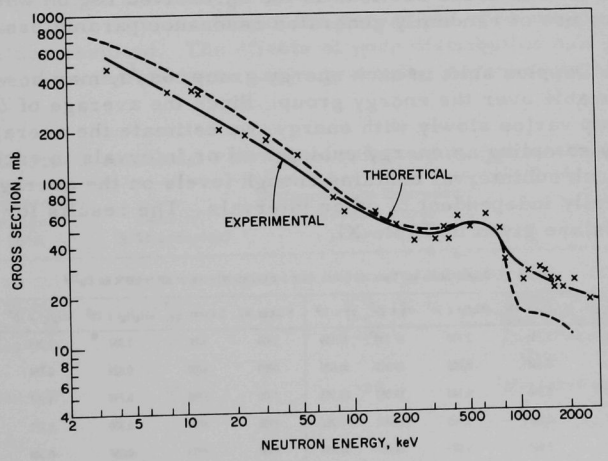

Fig. 16. Radiative Capture Cross Section of Molybdenum-98

[16] Lane, A. M., and Lynn, J. E., Proc. Phys. Soc. A70, 557 (1957).

[17] Gilbert, A., and Cameron, A. G. W., A Composite Nuclear Level Density Formula with Shell Corrections, Goddard Space Flight Center (NASA) (Preprint).

[18] Moldauer, P., Phys. Rev. 123, 968 (1961).

b. Capture-to-fission Ratios in EBR-II. In calculations of the long-term behavior of reactors it is necessary to know fission and capture cross sections of the uranium and plutonium isotopes which build up through successive captures in the primary fuel isotope. One method of obtaining this data is by the measurement of the capture to fission ratio of an isotope in a typical fast reactor neutron spectrum. Such a program is currently being carried out in EBR-II.

Samples of U^{233}, U^{235}, U^{238}, Pu^{239}, Pu^{240}, and Pu^{242} have been prepared and are now being irradiated in various positions in the core and blankets of EBR-II. Upon completion of the irradiations, the samples will be returned to Argonne, Illinois. Appropriate radiochemical and mass spectrographic analyses will be performed, and from these results the desired capture to fission ratios will be calculated.

B. Theoretical Reactor Physics

1. Effects of Randomness on Group Cross Sections

Work on the effective Pu^{239} cross sections (see Progress Report for August 1965, ANL-7090, p. 32) has been extended to cover the unresolved energy range from 10 keV to 200 eV. Below this range resolved resonance levels for Pu^{239} have been used to calculate the Doppler shift in group cross sections by a homogeneous version of RIFF RAFF[19] and are thus numerically precise. The cross sections in the unresolved region were similarly computed by use of randomly generated resonance parameters.

The Doppler shift in each energy group, $\delta\sigma/\sigma$, may be viewed as a random variable over the energy group. Since the average of $\delta\sigma/\sigma$ over an energy group varies slowly with energy, we estimate the average and the variance by sampling an energy subinterval or intervals in each wide group such that each subinterval contains enough levels on the average to be viewed as statistically independent of other intervals. The results for a variety of subintervals are given in Table XI.

TABLE XI. Doppler Shifts and Their Variances, Codd and Collins Mixture, at 300 to 600°K for Pu^{239}

E Upper, eV	E Lower, eV	$(\Delta I_a/I_a) \times 10^3$	$(\Delta I_f/I_f) \times 10^3$	$\sigma_a^2 \times 10^6$	$\sigma_f^2 \times 10^6$	E Upper, eV	E Lower, eV	$(\Delta I_a/I_a) \times 10^3$	$(\Delta I_f/I_f) \times 10^3$	$\sigma_a^2 \times 10^6$	$\sigma_f^2 \times 10^6$
500	300	5.186	2.755	27.249	35.159	5900	5700	1.357	1.069	34.209	42.490
900	700	6.644	6.002	35.418	36.026	6900	6700	0.829	0.784	31.72	39.112
1900	1700	6.346	6.148	19.062	23.963	7900	7700	0.798	1.037	29.727	37.032
2900	2700	0.857	1.563	505.801	470.262	8900	8700	0.300	0.271	17.328	22.772
3900	3700	3.910	3.949	28.042	31.858	9900	9700	-0.057	-0.148	17.305	23.058
4900	4700	1.725	1.756	35.317	43.130						

Notes: E Upper to E Lower is the energy subinterval.

$\Delta I_a/I_a$ is the Doppler shift in the absorption resonance integral and $\Delta I_f/I_f$ the Doppler shift in the fission resonance integral of Pu^{239} over the energy subinterval for a temperature change of 300 to 600°K.

σ_a^2 and σ_f^2 are the variances of $\Delta I_a/I_a$ and $\Delta I_f/I_f$, respectively.

[19] Kier, P. H., RIFF RAFF, A Program for Computation of Resonance Integrals in a Two-region Cell, ANL-7033 (August 1965).

The fission widths were assumed to be distributed according to a chi-square distribution of degree 2. The effect of using degree 1 or 4 is shown (see Table XII) to be about as expected: the fission Doppler shift increases with the degree of the distribution, but only slightly.

TABLE XII. The Effects of Varying the Degree of the Chi-square Distribution of the Fission Width with E Upper = 900 and E Lower = 700 eV

Degree	$(\Delta I_a/I_a) \times 10^3$	$(\Delta I_f/I_f) \times 10^3$	$\sigma_a^2 \times 10^6$	$\sigma_f^2 \times 10^6$
1	7.105	5.821	31.291	48.407
2	6.644	6.002	35.418	36.026
4	7.112	6.561	36.872	38.762

C. High-temperature Materials

1. Ceramic Fuel Materials

a. Microhardness of PuS, Pu_2S_3, and PuP. The DPN hardness values for PuS, Pu_2S_3, and PuP shown in Table XIII were measured with a Kentron microhardness apparatus and a load of 25 g on the indentor. This load gave an impression approximately 10 μ in width which left a distance of about 5 μ between the impression and the nearest pore in samples with densities of less than 90%. Samples 90 to 91% of full density had widely spaced pores, and the distance between the impression and the nearest pore in these samples was about 50 μ. Heavier loads increased the size of the impressions so that they overlapped the pores, and erroneously low microhardness values resulted. The effects of pore distribution can be seen from Table XIII because the hardness range generally increased with increasing density.

TABLE XIII. Microhardness Values for the Sulfides and Phosphides of Plutonium

Material	Microhardness Range, DPN	Density, % Theoretical	Distance from Impression to Nearest Pore, μm	Comments
PuS				
Sample 1	220-250	80	~5	Single Phase.
Sample 2	280-320	88	~5	Single Phase.
Sample 3	360-410	90	~50	Pu_2S_3 Precipitate in PuS Grain.
Pu_2S_3	520-600	90	~50	Measured on Pu_2S_3 Phase in Sample that Contained Some PuS
PuP				
Sample 1	230-310	87	~5	Single Phase.
Sample 2	220-370	87	~5	Single Phase.
Sample 3	320-370	89	~5	Single Phase.
Sample 4	350-420	91	~50	Impurity-phase Precipitate in PuP grains.

The microhardness of fully dense PuS and PuP is thought to be about 400 DPN. Samples that showed values of this magnitude also contained a second phase within the grains. The small amount of these impurities would not be expected to change this overall hardness significantly. Plutonium sesquisulfide is harder than the monosulfide.

b. Anelasticity of Some Uranium Compounds. The elastic modulus of nonporous uranium dioxide at room temperature was determined by least-squares fitting of data for porous UO_2 into the expressions

$$E = E_0 e^{-bP} \quad (1)$$

and

$$E = E_0(1 - AP), \quad (2)$$

where E is the elastic modulus of the porous polycrystalline material, E_0 is the elastic modulus of the nonporous polycrystalline material, b and P are empirical constants determined by least-squares fittings, and P is the volume fraction porosity.[20] Expression (1), proposed by Spriggs,[21] is based on a relation between strength and porosity postulated by Knudsen.[22] Equation (2) was presented by Hasselman[23] and derived from the equation deduced by Hashin.[24]

Values for E_0, b, and A are presented in Table XIV. The values obtained for E_0 fall within the range mentioned by Wachtman et al.,[25] who asserted that Young's modulus for nonporous polycrystalline UO_2

TABLE XIV. Values of E_0, b, and A Obtained by Least-squares Fitting of Exponential and Linear Equations

Equation	E_0(kbar)	b	A
$E = E_0 e^{-bP}$	2243.56 ± 22.10	2.512	-
$E = E_0(1 - AP)$	2233.85 ± 22.05	-	2.277

[20] Volume Fraction Porosity = Void Volume/Total Specimen Volume.

[21] Spriggs, R. M., Expression for Effect of Porosity on Elastic Modulus of Polycrystalline Refractory Materials, Particularly Al_2O_3, J. Am. Ceram. Soc. 44, 628-629 (1961).

[22] Knudsen, F. P., Dependence of Mechanical Strength of Brittle Polycrystalline Specimens on Porosity and Grain Size, J. Am. Ceram. Soc. 42, 376-387 (1959).

[23] Hasselman, D. P. H., On the Porosity Dependence of the Elastic Moduli of Polycrystalline Refractory Materials, J. Am. Ceram. Soc. 45, 452-453 (1962); Relation between Effects of Porosity on Strength and on Young's Modulus of Elasticity of Polycrustalline Materials, ibid., 46, 564-565 (1963).

[24] Hashin, Z., Elastic Moduli of Heterogeneous Materials, J. Appl. Mechanics 29, 143-150 (1962).

[25] Wachtman, J. B., Jr., Wheat, M. L., Anderson, H. J., and Bates, J. L., Elastic Constants of Single Crystal UO_2 at 25°C, J. Nucl. Materials 16(1), 39-41 (1965).

without preferred orientation should lie between 2170 kbar (Reuss average) and 2440 kbar (Voight average). A mean of both averages gives a value of 2305 kbar, which is slightly higher than the values of the present investigation. The same authors[25] claim that by extrapolating the results published by Lang,[26] a value of 2280 kbar was obtained for nonporous uranium oxide. That also agrees with the present results. It should be pointed out that some of the specimens tested by Lang were not stoichiometric.

Using the least-squares fitting of our data, we calculated the elastic modulus for UO_2 of zero to 0.4 volume-fraction porosity (see Fig. 17). The linear and exponential equations give similar results for values of volume-fraction porosity lower than 0.1. Beyond that the exponential expression gives higher values of the elastic modulus, because this relation does not fulfill the boundary condition for P = 1. The linear equation gives zero elasticity for a volume-fraction porosity of 0.438, consistent with the postulate of Marlowe and Wilder[27] that a material of initial uniform particle size should approach zero elasticity at porosity less than 0.4764 volume-fraction porosity.

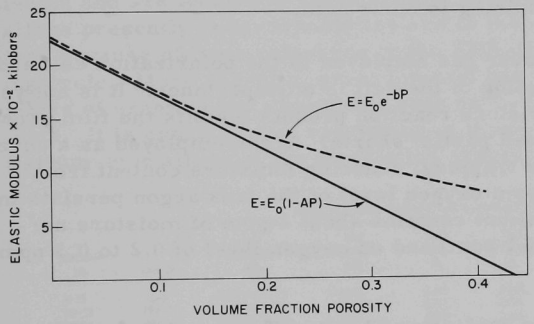

Fig. 17. Calculated Values of Elastic Modulus vs. Porosity

c. Uranium-mixed-anion Systems. It has been reported that US is soluble in UC_2 up to 50% US. The UC_2 used in the compositions for those equilibrations was made from precipitated UC which was reported to have free carbon present to give a carbon to uranium ratio of 2:1. This material was prereacted to form UC_2. Subsequent chemical analyses revealed quite a large excess of carbon in this material. Consequently a better UC_2 was needed. A new batch of UC_2 was formed by reacting at 1775°C high-purity carbon with arc-melted UC that was assumed to be stoichiometric. Carbon was added in an amount to form $UC_{1.96}$, the reported stoichiometry of tetragonal UC_2. Chemical analyses indicated the carbon-to-uranium ratio of the new material to be within 0.02 of the stoichiometric composition. X-ray diffraction produced only one very weak extraneous reflection, the 220 reflection for U_2C_3. This material will be used in further equilibrium studies.

---

[26]Lang, S. M., Properties of High-temperature Ceramic and Cermets. Elasticity and Density at Room Temperature, National Bureau of Standards Monograph 6 (1960).

[27]Marlow, M. O., and Wilder, D. R., Elasticity and Internal Friction of Polycrystalline Yttrium Oxide, J. Am. Ceram. Soc. 48, 227-233 (1965).

2. Liquid-metal Corrosion

a. Polarization Studies. Conditions to yield corrosion films on zirconium suitable for polarization experiments in sodium have been more completely defined. Overnight exposure of a smooth zirconium rod sample (0.38-μ polish, nominal), having a hemispherical tip, to highly oxygenated sodium at 580°C appears to be sufficient. Subsequent anodic polarization of a portion of the corroded surface at 400°C in the same sodium results in cell voltages of the order of 100 mV at a current density of 1 mA/cm^2. After test, capacitances may be successfully measured between sample metal and a liquid-metal environment at room temperature without the necessity of intermediate anodizing in boric acid.

The dryness of cover gas employed in the polarization cell and of glovebox helium during loading of the cell is of importance. It is not yet clear whether the sodium-moisture reaction product inhibits the film growth or is a direct cause of localized partial shorts. Argon employed as a cover gas presently is dried by cold trapping, reducing moisture content from about 20 to 4 ppm. The 2-3-ppm oxygen level of the tank argon persists in the purified gas. Glovebox helium contains about 2 ppm of moisture normally (and has been as low as 1 ppm) and an oxygen level of 0.2 to 0.3 ppm is indicated.

b. Lithium Corrosion Studies at Elevated Temperatures. Two molybdenum alloys, Mo-0.5 w/o Ti and Mo-0.5 w/o Ti-0.08 w/o Zr (TZM) were exposed to pure lithium at 1200°C for 8.7 days. The specimens were contained in pure molybdenum capsules and tested in a horizontal resistance furnace under a positive helium pressure of about 38 Torr.

Results indicated that the Mo-0.5 w/o Ti alloy was partially recrystallized, but TZM exhibited no apparent change in microstructure. No evidence of corrosion was detected on either material.

An attempt was also made to study the effect of a metallic additive to the lithium-tantalum system. The test was conducted in a manner similar to that mentioned above except that a small amount (0.36 g) of thorium was introduced to the system. After 8.7 days at 1200°C, it was shown that the lithium corrosion of tantalum with thorium additive was greatly accelerated. The gross attack was both inter- and transgranular in nature. The thorium was partially disintegrated.

Since the ultrahigh-vacuum furnaces are not yet ready for use, inhibitor studies at the 1200°C level will be continued.

3. Irradiation Testing

a. Introduction. A large and expanding program of irradiation studies on fast reactor materials is in progress at the Laboratory. Materials

under irradiation include both ceramic and metallic fuels in various fuel-jacket alloys. The reactors being used include CP-5, MTR, and EBR-II. It is expected that ETR will also soon be used, so that transfer of experiments from MTR will be minimized when it is made unavailable for capsule experiments.

b. Metallic-fuel Irradiations. The forty-six irradiations presently underway are shown in Table XV. The specimens being irradiated in CP-5 are from 10.16 to 15.24 cm long and are in instrumented capsules. Those in MTR are full-length EBR-II size (45.72 cm long) and are in instrumented, temperature-controlled capsules. The specimens in EBR-II are also full length and are located in three special subassemblies. Most of the fuel alloys presently under irradiation are of the uranium-plutonium-fissium type because of their relevance to the EBR-II pyrometallurgical reprocessing cycle. More recently, great interest has developed in high melting alloys of uranium and plutonium, such as U-Pu-Ti and U-Pu-Zr compositions. It is expected that specimens of these alloys will replace most of the fissium-type alloys in the irradiation program.

TABLE XV. Status of Metallic Fuel Irradiations in Progress

Specimen No.	Reactor	Fuel Composition, w/o	Clad Composition, w/o	Clad ID, in.	Clad Thickness, in.	Maximum Clad Temp, °C	Calculated Burnup to Date	
							a/o	(f/cm^3) x 10^{-21}
N-15	CP-5	U-19 Pu-14 Zr	V-20 Ti	0.175	0.015	600	4.2	1.4
ND-23	EBR-II	U-15 Pu-10 Zr	V-20 Ti	0.177	0.016	540	0.22	0.058
ND 24	EBR-II	U-15 Pu-10 Zr	V-20 Ti	0.177	0.016	540	0.22	0.058
N-14	CP-5	U-15 Pu-10 Ti	V-20 Ti	0.173	0.015	560	4.6	1.7
NC-17	EBR-II	U-15 Pu-10 Ti	V-20 Ti	0.177	0.016	540	0.22	0.058
NC-23	EBR-II	U-15 Pu-10 Ti	V-20 Ti	0.177	0.016	540	0.22	0.058
N-10	CP-5	U-10 Pu-10 Fz	V-20 Ti	0.165	0.016	540	4.0	1.5
N-11	CP-5	U-10 Pu-10 Fz	V-20 Ti	0.161	0.016	540	4.0	1.5
N-12	CP-5	U-10 Pu-10 Fz	V-20 Ti	0.157	0.016	540	4.0	1.5
CK-01	MTR	U-10 Pu-10 Fz	Nb-1 Zr	0.156	0.015	555	2.9	1.1
CG-02	EBR-II	U-10 Pu-10 Fz	Nb-1 Zr	0.156	0.009	440	0.20	0.076
CG-03	EBR-II	U-10 Pu-10 Fz	Nb-1 Zr	0.156	0.009	440	0.18	0.068
CJ-01	EBR-II	U-10 Pu-10 Fz	Nb-1 Zr	0.156	0.009	435	0.16	0.062
PB-02	EBR-II	U-10 Pu-10 Fz	Nb-1 Zr	0.156	0.009	440	0.18	0.068
TC-1	CP-5	U-15 Pu-10 Fz	Nb-1 Zr	0.156	0.009	550	1.3	0.30
C-152 P	CP-5	U-15 Pu-10 Fz	Nb-1 Zr	0.156	0.009	550	1.3	0.30
C-153 P	CP-5	U-15 Pu-10 Fz	Nb-1 Zr	0.156	0.009	550	1.3	0.30
C-155 P	CP-5	U-15 Pu-10 Fz	Nb-1 Zr	0.156	0.009	590	1.3	0.30
C-156 P	CP-5	U-15 Pu-10 Fz	Nb-1 Zr	0.156	0.009	590	1.3	0.30
C-159 P	CP-5	U-15 Pu-10 Fz	Nb-1 Zr	0.156	0.009	590	1.3	0.30
N-1	CP-5	U-15 Pu-10 Fz	V-20 Ti	0.157	0.016	575	5.7	2.2
N-2	CP-5	U-15 Pu-10 Fz	V-20 Ti	0.157	0.016	575	5.7	2.2
N-3	CP-5	U-15 Pu-10 Fz	V-20 Ti	0.165	0.016	575	5.7	2.2
N-4	CP-5	U-15 Pu-10 Fz	V-20 Ti	0.161	0.016	575	5.7	2.2
N-5	CP-5	U-15 Pu-10 Fz	V-20 Ti	0.161	0.016	575	5.7	2.2
N-6	CP-5	U-15 Pu-10 Fz	V-20 Ti	0.169	0.016	575	5.7	2.2
N-7	CP-5	U-15 Pu-10 Fz	V-20 Ti	0.165	0.016	540	4.0	1.5
N-8	CP-5	U-15 Pu-10 Fz	V-20 Ti	0.161	0.016	540	4.0	1.5
N-9	CP-5	U-15 Pu-10 Fz	V-20 Ti	0.157	0.016	540	4.0	1.5
CE-03	MTR	U-15 Pu-10 Fz	Nb-1 Zr	0.156	0.015	555	2.9	1.1
EC-01	MTR	U-15 Pu-10 Fz	V	0.156	0.015	555	2.9	1.1
CA-01	EBR-II	U-15 Pu-10 Fz	Nb-1 Zr	0.156	0.009	450	0.20	0.077
CB-02	EBR-II	U-15 Pu-10 Fz	Nb-1 Zr	0.156	0.015	445	0.19	0.073
CB-03	EBR-II	U-15 Pu-10 Fz	Nb-1 Zr	0.156	0.015	445	0.18	0.070
CB-04	EBR-II	U-15 Pu-10 Fz	Nb-1 Zr	0.156	0.015	445	0.18	0.068
CD-01	EBR-II	U-15 Pu-10 Fz	Nb-1 Zr	0.156	0.009	435	0.18	0.068
CD-02	EBR-II	U-15 Pu-10 Fz	Nb-1 Zr	0.156	0.009	435	0.15	0.059
LA-02	EBR-II	U-15 Pu-10 Fz	Hastelloy-X	0.153	0.011	440	0.17	0.063
PA-01	EBR-II	U-15 Pu-10 Fz	Nb-4 V	0.156	0.009	435	0.17	0.063
C-93	EBR-II	U-20 Pu-10 Fz	Nb-1 Zr	0.156	0.009	430	0.17	0.064
C-97	EBR-II	U-20 Pu-10 Fz	Nb-1 Zr	0.156	0.009	430	0.16	0.060
C-98	EBR-II	U-20 Pu-10 Fz	Nb-1 Zr	0.156	0.009	430	0.15	0.056
C-99	EBR-II	U-20 Pu-10 Fz	Nb-1 Zr	0.156	0.009	430	0.15	0.057
C-100	EBR-II	U-20 Pu-10 Fz	Nb-1 Zr	0.156	0.009	430	0.15	0.058
C-101	EBR-II	U-20 Pu-10 Fz	Nb-1 Zr	0.156	0.009	430	0.16	0.061
CM-01	EBR-II	U-20 Pu-10 Fz	Nb-1 Zr	0.156	0.015	435	0.16	0.062

c. Mixed-carbide Irradiations. Two forms of mixed carbide are being irradiated: physical mixtures of powders of UC and PuC, and solid solutions of (U,Pu) C. The physical mixtures are being studied in the form of vibratorily compacted rods. The solid-solution material is being studied as both vibratorily compacted rods and sintered pellets. The irradiations in MTR are on specimens approximately 7.62 cm long in instrumented, temperature-controlled capsules. The specimens in EBR-II have a 33.02-cm fuel length and are located in a special subassembly. The status to date is given in Table XVI.

TABLE XVI. Status of UC-20 w/o PuC Irradiations in Progress

Specimen No.	Reactor	Clad Composition, w/o	Clad ID, in.	Clad Thickness, in.	Maximum Clad Surface Temp, °C	Calculated Burnup to Date	
						a/o	$(f/cm^3) \times 10^{-21}$
MV-1	MTR	Nb-1 Zr	0.257	0.012	630	2.8	0.73
MV-2	MTR	Nb-1 Zr	0.257	0.012	650	3.9	1.0
MV-3	MTR	Nb-1 Zr	0.257	0.012	800	4.3	1.1
MV-4	MTR	Nb-1 Zr	0.257	0.012	660	3.3	0.87
MV-5	MTR	Nb-1 Zr	0.257	0.012	790	4.0	1.0
MV-6	MTR	Nb-1 Zr	0.257	0.012	620	4.1	1.1
SMV-2	EBR-II	304 SS	0.257	0.020	600	0.21	0.055
HMV-5	EBR-II	Hast.-X	0.267	0.015	600	0.21	0.055
NMV-11	EBR-II	Nb-1 Zr	0.257	0.012	600	0.21	0.055

d. Uranium Sulfide Irradiations. Earlier irradiations of uranium sulfide have shown it to be a fuel with highly promising behavior. The material is highly stable under irradiation and releases fission gas at rates significantly lower than from other ceramic fuels. Table XVII summarizes the irradiations now in progress. All specimens, clad in Nb-1 w/o Zr of

TABLE XVII. Status of Uranium Sulfide Irradiations in Progress

Specimen No.	Maximum Clad Surface Temp, °C	Calculated Burnup to Date	
		a/o	$(f/cm^3) \times 10^{-21}$
S-7	560	2.9	0.69
S-8	740	4.5	1.1
S-9	750	4.5	1.1
S-10	730	4.5	1.1
S-11	520	2.3	0.49
S-12	650	3.0	0.71
S-13	670	3.6	0.76
S-14	670	3.5	0.88
S-15	570	1.8	0.33
S-16	660	3.6	0.76
S-17	780	4.1	1.0
S-18	660	2.4	0.50

0.257-in. ID and 0.012-in. thickness, are in instrumented temperature-controlled capsules in the MTR. The specimen lengths are of the order of 7.62 cm.

D. Other Reactor Fuels and Materials Development

1. Nondestructive Testing

a. Ultrasonic Instrument and Transducer Development. The measurement of velocities and attenuation in several samples of porous stainless steel continued in order to determine the feasibility of using them as backing members in ultrasonic transducer probes. A linear relation between sample density and longitudinal wave velocity was shown, low-density samples having a smaller velocity. An increase of approximately 0.062×10^3 m/sec per % of density increase was determined, with an assumed velocity of 5.75×10^3 m/sec at 100% density.

The longitudinal wave velocity and the density of polarized PZT-4 ceramic was also determined. This is the transducer material that is to be matched. The acoustic impedance in this material was determined to be 34×10^6 kg/(m^2-sec). From the graph of velocity (of porous stainless steel) versus density, it has been determined that a sample of 90% dense material should have the same acoustic impedance as the PZT-4. The manufacturer has been notified of our findings and has started the fabrication of a 90% dense sample disc of Type 316 stainless steel.

b. Elastic Moduli of Fuel-jacket Materials. The results of room-temperature measurements are given in Table XVIII.

TABLE XVIII. Room-temperature Elastic Properties

Material, w/o	Longitudinal Wave Velocity, 10^5 cm/sec	Shear Wave Velocity, 10^5 cm/sec	Density, gm/cm^3	Young's Modulus, 10^{12} dyne/cm^2	Shear Modulus, 10^{12} dyne/cm^2	Poisson's Ratio
V-30 Ti-10 Cr as rolled	6.03	2.71	5.63	1.08	0.413	0.374
V-20 Ti-5 Cr annealed	6.12	2.86	5.76	1.28	0.469	0.362
V-20 Ti-2 Mo annealed	6.22	2.72	5.76	1.18	0.426	0.382
V-20 Ti-2 Ta annealed	6.10	2.90	5.78	1.40	0.522	0.376
V-15 Ti-7.5 Cr annealed	6.20	2.79	5.89	1.26	0.459	0.373
V-15 Ti-5 Cr annealed	6.12	2.76	5.87	1.23	0.449	0.372
V-20 Ti-2 Nb annealed	6.07	2.74	5.75	1.19	0.432	0.372
V-5 Ti-15 Cr as rolled	6.12	2.90	6.19	1.41	0.519	0.356
V-30 Ti-5 Cr as rolled	6.00	2.74	5.61	1.16	0.420	0.369

c. Development of a Neutron-image-intensification System. A second neutron-image-intensifier tube has been received and is being tested at Juggernaut reactor. The second tube contains a glass window similar to the one on the original tube except for two differences. The radius of curvature of the window of the new tube is larger than that of the original tube window (see Progress Report for February 1965, ANL-7017, p. 57), thereby contributing to a reduced spacing between the window and the input target. This should lead to improved resolution capability for the new tube. Tests to determine the resolution of the new tube are now in progress.

Secondly, the new tube window is reported to contain less boron than that of the original tube. This should lead to improved output phosphor brightness, a fact apparently confirmed by visual inspection. A more nearly complete comparison of brightness outputs for the two tubes will be made. Preliminary brightness measurements for the new tube indicate an improvement of about 30% over the excellent brightness characteristics of the original tube.

A comparison of the neutron transmission of the materials of the old and new windows is also planned.

d. Infrared Systems. Analysis of the indium antimonide infrared-detection system has been in progress for several months. During the inspection of a flat plate sample, a gradual shift of the baseline of the pen recording was observed, accompanied by a loss in sensitivity and resolution. Investigation revealed a heat buildup in the detector section of the system. To maintain the detector at a constant temperature, a Borg-Warner thermoelectric cooler was installed.

Surfaces not of uniform emissivity introduce erroneous signals, degrading system performance. Tests are being conducted to compare emissivity effects on InSb radiometer and thermistor systems.

e. Thermal Conductivity of Irradiated Fuel versus Burnup and Temperature. Because of the high cost and long period of time required for the preparation of the transverse and longitudinal specimens made from each fuel pin, only the uranium alloy presently used as a reactor fuel, U-5 w/o Fs, is under consideration for investigation. Specimens are being made from five irradiated fuel pins of this alloy. Measurements at room temperature will begin as soon as the samples are received. A final trial run of unirradiated fuel is presently being made in the cave.

E. Engineering Development

1. Two-phase Flow

a. Void Fraction--Pressure-drop Facility. An additional 300 hr of boiling runs have been made in the range from 1300 to 1600°F in an attempt to reproduce earlier data, as it has been found that the boiling is not as stable as that of 6 to 9 months ago. Possible reasons for this new behavior are under study.

The void-fraction data appear consistent with all previous runs. Calculations of the slip ratio yielded results approximately four times higher than those predicted from results of other experiments with lower-temperature water or water-air. This discrepancy may be peculiar to liquid metals or it may be charged to errors in quality measurements and calculations owing to nonequilibrium effects. As soon as these final experiments are complete, a topical report will be issued.

2. Boiling Liquid-metal Technology

a. Niobium-1% Zirconium Loop. All loop-support components are being thoroughly cleaned in the storage and assembly room. Procedures have been selected and personnel assigned for the task of completing the loop-support structure and attaching the main sodium loop assembly. The stainless steel support hangers and straps have been completed. Four of the tantalum rods for the thermal-radiation shield shutters were found to be defective when received from the vendor. To avoid additional delay, the rods will be reworked in Central Shops; this procedure will not affect the integrity of the rod support. Tantalum sheet, round, and bar stock has been received for the assembly of the shield shutters, reflector and balancing assembly, and the reflectors for the preheater.

Instrumentation procurement and assembly are still in progress. Because of insulator difficulties, some of the Chromel-Alumel niobium-sheathed thermocouples are being reworked. Tests and calibration of the pressure transducers have revealed the necessity of a temperature-controlled environment for the electronic readout system. Equipment for the sodium-sampling and -purification system has been received and the system is being fabricated. The data-acquisition system has been integrated into the instrumentation system and channel-identification procedures are complete. The partial-pressure analyzer has been attached to the vacuum chamber and will be calibrated with nitrogen after pump down.

b. Heater Experiments

(i) Electron-bombardment Heater Experiment. The defective alumina insulator has been replaced and testing of the heater has resumed. No results pertinent to the final design of the large Nb-1% Zr boiler are available.

3. General Heat Transfer

a. Countercurrent Liquid-metal Heat Exchanger. Investigation of a double-pipe, countercurrent liquid-metal heat exchanger has started.

A general theory for arbitrary velocity profiles is being developed which will apply to a plug-flow model. An exact solution for the energy conservation equation, neglecting axial heat conduction, is being developed.

Previous work on countercurrent flows is being investigated and rederived.

The existing liquid-metal loop in Building 11 can be modified to attain countercurrent flow for an experimental check of the analysis.

4. Manipulators for Handling Radioactive Materials

The Electric Master-Slave Manipulator Mark E4 will have a number of improvements over the existing Model E3: greater coverage of working volume, ability to approach work from a wider variety of directions, improved mechanical and electrical repairability, greater allowable distance between master and slave working stations and fewer conductors in the electrical cables. In addition, although the Mark E4 will have the same maximum 50-lb load capacity as the Model E3, the improved cooling will allow handling of this load for a longer period of time. A pair of Mark E4 slave arms is illustrated in Fig. 18.

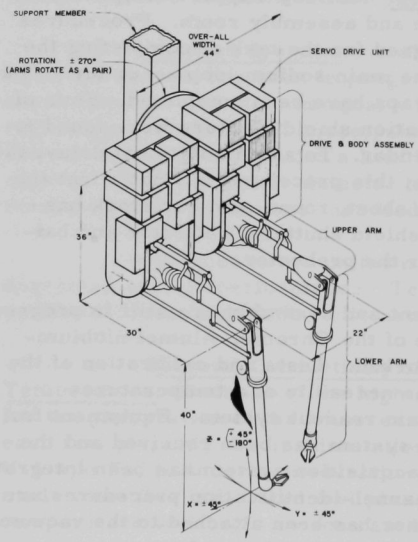

Fig. 18. A Pair of ANL Mark E4 Slave Arms

The servo drive units, tongs, and wrist joints have been fabricated for two slave and two master arms. Fabrication of the parts for one Upper and one Lower Slave Arm is complete except for the "X" motion drive gears, which have a December delivery date. Many parts have been assembled. The Upper and Lower Slave Arms are designed completely.

The layout drawings of the Drive and Body Assembly are finished. The body structure will include integral cooling ducts and integral gear housings for the "Y" and "Z" motions. The output drums and "Y" and "Z" motion output drive gears are in fabrication. Brakes for each motion are yet to be designed.

The layout work on the master arm is about 35 percent complete. The master arm will employ tapes rather than cables to provide lower friction and thus give the operator better "feel."

A second amplifier console is approximately complete (one console is required for each master-slave arm). These consoles are designed to deliver full power in ambient temperatures up to 115°F. Designs have been worked out and tested which will allow operation in ambients up to 135°F when required.

F. Chemical Separations

1. Fluorination and Volatility Separations Processes

a. Recovery of Uranium from Low-enrichment Fuels: Laboratory Support Work

(i) Thermal Decomposition of Plutonium Hexafluoride. In one concept of the fluid-bed fluoride volatility process for low-enrichment oxide fuels, uranium and plutonium oxides are fluorinated with fluorine to produce volatile uranium and plutonium hexafluorides which are separated from one another by thermal decomposition of plutonium hexafluoride to produce solid plutonium tetrafluoride. Data on the kinetics and mechanism of the thermal decomposition of PuF_6 have been reported previously[28] as well as the results of tests confirming the feasibility of separating plutonium from gaseous mixtures of UF_6 and PuF_6 by thermal decomposition of plutonium hexafluoride.[29] Recent laboratory support studies have been devoted to observing the behavior of volatile fission product fluorides during the thermal decomposition process with particular emphasis on determining the effect of these fluorides on the rate of PuF_6 decomposition and on the purity of the PuF_4 product.

The experiments involved the continuous recycle of a gaseous mixture containing UF_6, PuF_6, volatile fission product fluorides (MoF_6 and TeF_6), and nitrogen at 300°C through a vessel packed with nickel balls. The decomposition rate of PuF_6 was estimated from periodic analysis of samples of the gas phase. The results indicated that the presence of MoF_6 and TeF_6 in the gas mixture did not affect the PuF_6 decomposition rate. The data also showed no clear indication of any effect of the quantity of PuF_4 initially present in the decomposition vessel on the decomposition rate. Analyses of the PuF_4 deposit showed a maximum uranium content of 0.04 w/o and a molybdenum concentration of 0.016 w/o. A suitable method for determining tellurium content of the solids is being developed.

---

[28] Fischer, J., Trevorrow, L. E., and Shinn, W., The Kinetics and Mechanism of the Thermal Decomposition of PuF_6, J. Phys. Chem. 65, 1843 (1961).

[29] Trevorrow, L., Fischer, J., and Riha, J., Laboratory Investigations in Support of Fluid-bed Fluoride Volatility Processes. Part III. Separation of Gaseous Mixtures of Uranium Hexafluoride and Plutonium Hexafluoride by Thermal Decomposition, ANL-6762 (August 1963).

(ii) Corrosion of Nickel and Nickel Alloys by Volatile Fluoride Compounds. A laboratory-scale program has been established to evaluate the corrosion of nickel and nickel alloys by certain volatile fission product fluorides. A series of tests were performed to determine the rate of corrosion of nickel and nickel alloys by TeF_6 and to compare the corrosion rates with those obtained with SeF_6 and SF_6. In a test in which nickel-200, Monel, and Inconel coupons were exposed to TeF_6 at 500°C for 19 hr, it was observed that the consumption of TeF_6 was very rapid and it was frequently necessary to add TeF_6 to the system to maintain a TeF_6 pressure of 100 mm. At the conclusion of the test it was observed that the nickel reaction vessel was filled with a light-grey fluffy solid. The corrosion rates for the specimen coupons based on weight loss varied widely: for nickel-200, 0.017 to 0.078 mil/hr; for Monel, 0.000 to 0.016 mil/hr; and for Inconel, 0.001 to 0.028 mil/hr. Intergranular attack to a depth of 0.2 mil was observed on nickel-200 specimens. No intergranular attack was found on the Monel or Inconel specimens. X-ray diffraction analyses of the corrosion deposits indicated the presence of $NiTe_2$, NiTe, NiF_2, and (for Monel) $Cu_{2-x}Te$.

Comparison of intergranular-penetration data obtained in tests with SF_6, SeF_6, and TeF_6 indicate that the intergranular attack on nickel and nickel alloys produced by TeF_6 is significantly less than that produced by either SF_6 or SeF_6. It should be noted, however, that TeF_6, unlike SF_6 and SeF_6, does cause corrosion of nickel, Monel, and Inconel, probably by a surface reaction to form tellurides of nickel and copper and, to a lesser extent, to form NiF_2. Previous tests in which mixtures of TeF_6 and fluorine were used resulted in comparatively low corrosion rates.

Further work in this program will concern measuring the rates of corrosion of nickel and nickel alloys by MoF_6 and UF_6.

(iii) Neptunium Fluoride Chemistry. Neptunium-237 can be expected to be a significant contaminant in highly irradiated low-enrichment fuels. A knowledge of the pertinent physical and chemical properties of neptunium fluorides (NpF_4 and NpF_6) is necessary in order to devise methods for achieving complete separation of uranium and plutonium from neptunium by the fluoride volatility process. Recent work has been concerned with the measurement of the rate of reaction between NpF_4 and fluorine at various temperatures to form NpF_6 and the determination of whether or not any intermediate fluorides are formed during the fluorination of NpF_4.

The NpF_4 used in this study was prepared by reaction of NpO_2 at 500°C with hydrogen fluoride in the presence of oxygen. Reaction rates were measured for the fluorination of NpF_4 at 250 and 300°C. The reaction-rate data were treated by means of a diminishing-sphere model in which F, the fraction of NpF_4 reacted, is related to a rate constant k' and a reaction time t by the expression

$$(1 - F)^{1/3} = 1 - k't.$$

Values of k' calculated for the reaction of NpF_4 with fluorine at 250 and 300°C were 0.0010 to 0.0065 min^{-1}, respectively. Based on these values, an apparent activation energy for the reaction $NpF_4 + F_2 \rightarrow NpF_6$ was calculated to be approximately 22 kcal/mole. Chemical and X-ray analyses of samples of the residue taken during the fluorination tests will be used to determine if any intermediate fluorides are formed during the fluorination reaction.

b. Recovery of Uranium from Low-enrichment Fuels: Engineering Work

(i) Engineering-scale Alpha Facility. Final shakedown experiments prior to the introduction of plutonium into the engineering-scale alpha facility have been completed. These experiments consisted of a two-zone oxidation-fluorination test with a charge of 8.8 kg of UO_2 pellets and a test simulating the separation of PuF_6 from gaseous mixtures of PuF_6-UF_6 by thermal decomposition of PuF_6 to solid PuF_4. In general the tests were considered satisfactory and provided not only additional operating experience but also a thorough check of operating procedures.

Concurrent with the final shakedown tests, leak testing and sealing of the large alpha box containing the process equipment were accomplished in preparation for experiments with plutonium-containing materials.

(ii) Fluorination of UO_2-PuO_2-fission Product Pellets. Development studies are being performed in a 2-in.-dia fluid-bed reactor to determine optimum conditions for fluorinating UO_2-PuO_2 pellets containing fission products and to establish those conditions that would result in a minimum retention of uranium and plutonium on the fluid bed of alumina particles. A run was completed in which a 2-in.-deep bed of UO_2-PuO_2-fission product pellets was reacted by the following reaction sequence: (1) a two-zone oxidation-fluorination step at 450°C for 3 hr, (2) a single-zone fluorination step at 450°C for 2 hr with 7 v/o fluorine in nitrogen introduced at the bottom of the reactor, and (3) a recycle-fluorination step with 90 v/o fluorine at 450°C for 1 hr, 500°C for 3 hr, and 550°C for 8 hr. During the two-zone and single-zone fluorination steps, the fluidized-packed bed was pulsed every 40 sec with nitrogen (50 psig N_2, pulse duration 0.04 sec) to agitate the pellets and thereby increase the fluorine utilization. Caking of the alumina bed (a difficulty which had been experienced in previous tests, see Progress Report for June 1965, ANL-7071, pp. 44-45) was avoided by slowly increasing the fluorine concentration during the initial stages of the recycle-fluorination step and thereby avoiding localized temperature excursions.

The final alumina bed from this run was entirely free-flowing; no caking of alumina particles was observed. The final uranium and plutonium concentrations in the alumina bed were 0.004 and 0.007 w/o, respectively, representing uranium removals of >99.9% and plutonium removals of 97% for a single use of the alumina bed.

(iii) Cleanup of Cell Exhaust Air Contaminated with Plutonium Hexafluoride. Studies continued of the cleanup of air contaminated with plutonium hexafluoride. Current studies have involved the evaluation of performance of filter media in the filtration of aerosols. In previous experiments[30] in which PuF_6 was released into air containing an excess of moisture, it was observed that the fraction of plutonium penetrating two successive AEC filters in series ranged from 10^{-6} to 10^{-9}. The extent of this variation which could be attributed to the filters has not been determined. Small sections of filter media might be expected to have inherent large variations in performance, much greater, in fact, than larger sections of filter media, since in larger sections the variations are averaged. Equipment was constructed to evaluate the filtration performances of filters after the filters are mounted in holders that are used in experiments. The principal components of the equipment are an aerosol generator and a light-scattering photometer to measure the aerosol concentration.

In the aerosol generator,[31] DOP [di(2-ethylhexyl)-phthalate] is dispersed by an air jet submerged in the liquid. The coarse particles in the aerosol are removed by a jet impaction stage. The aerosol concentration was measured with a light-scattering device with a 90° average scattering angle.

The quantity of aerosol penetrating the test filters was determined from four photometer readings which included two readings of the raw smoke (at the beginning and end of the test), a background reading for clean filtered air, and a reading of the filtered smoke. After correcting each reading for the background, the filter penetration was computed by dividing the filtered smoke reading by the average of the two readings for the raw smoke. In general the raw smoke readings differed by approximately 3%.

The effect of air-flow rate on filter penetration and the effect of a small hole on filter behavior were examined with 10-cm-dia discs cut from a sheet of AEC filter media. When the air-flow rate was reduced from 115 to 30% of rated flow (2.5 cm/sec) for this type of filter media, the penetration of the media rapidly decreased from 0.03 to 0.002%.

---

[30] Chemical Engineering Division Summary Report July, August, September 1962, ANL-6596, pp. 123-125, 1963.

[31] Echols, W.H., and Young, J. A., Studies of Portable Air-operated Aerosol Generators, NRL-5929 (July 1963).

However, for the same disc with a pin hole in it (area of hole 6 ppm of entire filter area), the penetrations were higher by an order of magnitude and increased with a decrease in flow rate since at the lower flow rate a greater fraction of the air passed through the hole. The high penetration of a primary AEC glovebox filter in an accidental PuF_6 release (see Progress Report for June 1965, ANL-7071, pp. 45-47) was attributed to the presence of a small hole in the filter. In this case the penetration of plutonium through the torn filter media was higher by an order of magnitude than through a perfect filter. In the case of the accident the plutonium was stopped by additional filters in series.

The penetration values obtained from several discs cut from the sheet of filter media indicated that there was a slight variation in penetration among the discs. The penetration at 30% rated flow averaged 0.0012% with a standard deviation of 19% for the individual values. At 100% rated flow, the average penetration was 0.023% and the standard deviation for the individual values was 8%. Although these variations are not considered to be significant in terms of the results of previous studies on the gas-phase hydrolysis of PuF_6, the variations may, however, be highly significant in a refined experimental program on the evaluation of filter performance.

(iv) Studies with Irradiated UO_2-PuO_2 Fuels. Studies with irradiated oxide fuel materials are being conducted in a bench-scale fluid-bed unit installed in the Chemical Engineering Division senior cave. The facility consists of a $1\frac{1}{2}$-in.-dia fluid-bed reactor and a packed bed filter with associated equipment for the containment of volatile chlorides and fluorides produced in the process (see Progress Report for May 1964, ANL-6904, pp. 89-90).

Two experiments were performed with UO_2 fuel, which had been irradiated to 20,000 MWd/ton and cooled 18 months, by means of a two-step reaction sequence: (1) the pellet fuel was reacted with 48 v/o HF in oxygen at 400°C for 4 hr, and (2) the powdered material from step 1 was reacted with 2 to 20 v/o F_2 in nitrogen for 3 hr at 400 to 450°C. Less than 0.4% of the gross beta-gamma activity volatilized from the reactor during the HF oxygen treatment. During this treatment, the activities which were partly volatile were Sb, Mo, Tc, and apparently Ru. The nonvolatile activities during the fluorination step were the rare earths, Sr, Zr, and Cs. During fluorination, Sb, Ru, and Nb were only partly volatilized. The decontamination factors for uranium collected on a sodium fluoride trap ranged from 1.5×10^2 to 10^5 from various fission products. Decontamination from Mo and Tc was low since these elements are collected with the uranium product on the sodium fluoride trap. Uranium losses to the reactor and packed-bed filter beds were about 0.25 w/o of the uranium charged.

In an experiment with Zircaloy-clad UO_2 fuel material, the processing sequence involved (1) decladding of the fuel with HCl at 400°C for 1.5 hr, (2) oxidation of the fuel with 20 v/o oxygen in nitrogen at 450°C for 4 hr, and (3) fluorination with 10 to 83 v/o fluorine in nitrogen at 450 to 550°C for 15.5 hr. The UF_6 product was collected in a series of refrigerated condensers; no sodium fluoride purification traps were used in this experiment. The results indicated the following:

(1) About 1.2% of the beta and 4.5% of the gamma activities volatilized from the reactor during the decladding step.

(2) About 0.2% of the beta and 0.7% of the gamma activities volatilized from the reactor during the oxidation step.

(3) Uranium decontamination factors from beta and gamma activities for the primary separation from the reactor to the UF_6 product condensers were approximately 30.

(4) The uranium loss to the reactor and filter beds after fluorination was about 0.4% of the uranium charged.

G. Sodium Coolant Chemistry

1. Chemistry of Carbon in Liquid Sodium

a. Reactions of Carbon Compounds with Sodium. A study on the reactions of carbon compounds with sodium at elevated temperatures has been initiated. This study will employ gas chromatography and other chemical techniques for the analysis of the solid, liquid, and gaseous reaction products. In order to gain experience with these techniques, several preliminary experiments were performed with sodium-Na_2CO_3, a previously investigated reaction, and with sodium-lampblack and sodium-graphite systems.

The experiments consisted of heating 2 g of reactor-grade sodium[32] with 0.1 g of the carbon compound for 2 to 16 hr at 700°C in stainless steel or nickel capsules in a helium atmosphere. After cooling, the (unfiltered) reaction products were hydrolyzed in dilute sulfuric acid; the gases evolved were analyzed by gas chromatography. The experimental results may be summarized as follows:

1) U.S.I. reactor-grade sodium contains about 6 ppm carbon as carbonate.

2) Sodium carbonate is unstable in liquid sodium at 700°C, yielding decomposition products whose relative amounts vary with heating time. Sodium carbonate decomposes to

[32]United States Industrial Chemical Co. sodium containing 29 ± 5 ppm total carbon.

a carbide or carbide-like compound as shown by the evolution of C_2H_2 on hydrolysis of the sodium reaction product. The final product of Na_2CO_3 decomposition appears to be carbon (observed in the form of insoluble, black particles after the hydrolysis).

3) Lampblack and graphite do not react with sodium at 700°C to give carbides, as indicated by the absence of any significant amounts of carbon-containing gaseous hydrolysis products.

These results are in accord with the findings of Hobart, at Pratt and Whitney Aircraft-CANEL, who has made a more extensive study of the reactions of sodium and Na_2CO_3 at elevated temperatures.

Several experiments similar to those above were made in which sodium was heated in nickel capsules in the presence of nitrogen, nitrogen and Na_2CO_3, or $(NH_4)_2C_2O_4$. In all cases cyanide was found in the aqueous hydrolysis products, as previously reported.[33]

b. Total Carbon Analysis. A series of experiments with respect to determination of graphitic carbon in sodium has been completed. Graphite thread (Union Carbide, Grade WCB, 99.96% graphitic carbon) was added to samples of U.S.I. sodium which were then carried through the analytical procedure.[34] The results, shown in Table XIX, indicate that elemental carbon in sodium can be determined by our usual analytical procedure. However, the variability in recovery found at the higher carbon concentrations is somewhat surprising.

TABLE XIX. Recovery of Graphitic Carbon Added to Sodium

Weight of Sodium, g	Carbon, μg				
	In Sodium	In Graphite Thread	Total	Found	% Recovery
0.71	20	44	64	67	105
0.94	27	38	65	52	80
0.97	28	189	217	187	86
0.57	16	224	240	245	102
1.09	31	337	368	324	88
1.01	29	275	304	289	95

[33]Hobart, E. W., and Bjork, R. J., TIM-90 (May 10, 1965).

[34]Combustion in an alumina boat with pure oxygen, followed by dissolution in dilute sulfuric acid and manometric measurement of liberated CO_2.

2. Control of Sodium Oxide Impurity

Evaluation of the two new electrochemical oxygen-analysis cells developed by United Nuclear Corporation (see Progress Report for August 1965, ANL-7090, p. 53) continued.

H. Plutonium Recycle Reactors

1. EBWR Plutonium Recycle

During the early part of September, preparations were completed for the initial loading of the plutonium elements to be used in the Plutonium Recycle Program. Thirty-six of the plutonium elements were brought into the containment shell and placed in wet storage. Multiplication measurements were made of the storage rack to insure against inadvertent criticality.

All work on systems needed for use in the critical program was completed, including the nondestructive testing and repairing of welds.

Several areas of the cladding inside the primary pressure vessel were prepared for observation during the course of the program by removing the stainless steel cladding. The areas were measured and identified so that the effect of operation may be determined using a measuring microscope and other nondestructive techniques. Two windows, each 15 in. square, were cut in the shock shield to permit access to the test areas during shutdown between periods of operation.

The reactor vessel internals, steam duct, shock shields, and sample-irradiation tubes which had been removed for vessel inspection were replaced. Special instrumentation was procured, and certain of the regular instrument detectors were relocated to provide six startup channels.

Loading began on September 13; criticality was achieved on September 22, 1965, with 22 plutonium elements in a 4 x 5 slab array, plus an additional element on each end.

Calibrations using a four-group, one-dimensional (cylindrical) diffusion theory predicted a critical mass with 17.7 elements.

The observed configuration will be compared with two-dimensional calculations to aid in resolving the loading discrepancy. These calculations will make use of the recently revised THERMOS code[35] to generate thermal-group cross sections. Previous calculations used the space-independent SOFOCATE code in conjunction with the DTK code to account for spatial flux-weighting effects.

---

[35]Toppel, B. J., and Baksys, I., The Argonne-Revised THERMOS Code, ANL-7023 (March 1965).

III. ADVANCED SYSTEMS RESEARCH AND DEVELOPMENT

A. Argonne Advanced Research Reactor (AARR)

1. General

The architect-engineer for the AARR Project, Burns and Roe, Inc., has completed the initial planning phase of the Title I effort. All available preliminary design studies, evaluations, and contributing data have been reviewed by A-E key personnel, and the Title I design effort has been planned in detail. PERT/TIME networks have been prepared and incorporated into the overall project PERT system. Resource estimates for inclusion in the PERT/COST system have also been supplied. The A-E has now been given approval to start the Title I design phase.

2. Critical Experiments

Experimentation has started to supply information needed to locate neutron detectors in AARR. Important advantages would exist if most of the neutron detectors could be placed in the lateral shield, just outside the pressure vessel. For these detectors to be operationally useful at this location, the neutron-flux levels at the detectors must be raised substantially. There would be corresponding increases in the rate of radiation damaging of the vessel, by fast neutrons, and in the thermal stresses in the vessel, because of capture of gamma rays. In evaluating the merits of a device which would raise neutron-flux levels, these associated effects must be considered.

For the case of a full water thickness (no windows), radial traverses of neutron activation rates have been made with indium foils. The data were accurate up to a radial distance of 80 cm. Beyond 80 cm, the activation levels were too low for reliable measurements with the indium. Overlapping measurements were made with a movable BF_3 counter, which provided data at greater distances in water, up to and beyond the tank wall (inside surface at 152.4 cm). The radial traverses indicated that the activation levels is reduced by more than 5 decades from the outer edge of the beryllium reflector to the reference location of the inside surface of the AARR pressure vessel.

To measure the effectiveness of a graphite "window," a graphite block (52 cm wide, 42 cm high, and 52 cm thick) was positioned at the inside surface of the tank wall. This block raised the activation level of the BF_3 counter, positioned just beyond the tank wall, by two orders of magnitude. This level should be adequate for the needs of the operational nuclear instrumentation of AARR.

Similar measurements were made with a somewhat smaller stack of aluminum, composed of 24 pieces of solid aluminum, each of dimensions 46 cm x 46 cm x 2.54 cm thick. For direct comparison, a graphite block

of increased thickness (~60 cm) was used. On the basis of data obtained with a BF_3 counter at the outside surface of the thin steel tank, when these blocks were pushed back against the tank wall, the aluminum and the graphite were of comparable effectiveness as neutron windows.

Radial traverses have been made, with indium foils, through the aluminum stack and through a thinner graphite block. The displacement of water by the stack raised the activation levels so that indium-foil data were accurate at much greater radial distances.

This program of experiments is continuing. Also, an effort is being made to measure relative magnitudes of gamma flux, at the radial distance corresponding to the reference radius of the pressure vessel for AARR, for various neutron windows.

The present schedule of the fuel-foil supplier calls for final shipments of fuel foils during the week of October 18, 1965. Therefore, it is unlikely that experiments with the next loading of fuel foils could begin before the middle of November 1965.

3. Theoretical Analyses of the Critical-facility Reactors

New 16-group cross-section sets have been constructed for diffusion-theory calculations for each of 4 loadings of fuel foils and boron-stainless steel (B-SS) poison strips: (1) 315 fuel foils; no boron; (2) 615 foils; 420 B-SS strips; (3) 810 foils; 810 B-SS strips; and (4) 1215 foils; 2000 B-SS strips. The first three systems represent actual critical-facility loadings that have been studied experimentally.

For the above-thermal groups, these sets are identical to cross-section sets selected earlier and used in various reactivity computations (see Progress Report for March 1965, ANL-7028, pp. 73-74). The cross sections for the two thermal groups have been revised, principally the transport cross sections and the cross sections for net downscattering from group 15 (0.1 to 0.4 eV) to group 16 (0 to 0.1 eV). In getting these cross sections for the thermal groups, the THERMOS program[36] was applied to infinite-medium calculations, using the Nelkin kernel for the scattering matrix of water.

By means of these new cross-section libraries, 16-group diffusion-theory calculations have been made of the reactivity and of various coefficients of reactivity of systems (1) to (4). Results of some of these calculations are summarized below.

[36]Honeck, Henry C., THERMOS, A Thermalization Transport Theory Code for Reactor Lattice Calculations, BNL-5826 (Sept 1961).

For the 315-fuel-foil loading, with 10% Lucite in the beryllium reflector, the calculated k_{eff} is 1.052. From this must be subtracted the reactivity effect of the gross heterogeneities in the spatial distribution of fuel foils, estimated to be 3.0% (see Progress Report for March 1965, ANL-7028, p. 74). The net mismatch between theory and experiment then is approximately 1.6%, with calculation overestimating reactivity. For this loading, reactivity coefficients were computed for small percentages of voids in water in the reactor. A 10% uniform void in the Internal Thermal Column (ITC) corresponded to a reactivity gain of 0.37%. A uniform 10% void of water in the active core zone was calculated to reduce reactivity by 2.7%; the corresponding measurement was -0.16%/% void in the core water (see Progress Report for May 1965, ANL-7046, p. 69).

For the 615-fuel-foil loading with 420 B-SS strips, the calculated reactivity was 5.0%. From this must be subtracted the reactivity effect of the still heterogeneous loading of fuel foils (this has not been calculated yet). The net available reactivity of this system was measured to be 3.7% (see Progress Report for December 1964, ANL-6997, p. 55). The net mismatch is estimated to be approximately 1/2% to 1%, with theory overestimating the reactivity. With the Lucite removed from the beryllium reflector, the calculated reactivity was 6.0%; the measured reactivity was 4.9% (see Progress Report for March 1965, ANL-7028, p. 75), but part of the mismatch is due to the aforementioned fuel heterogeneity. For a 10% void in the core water, calculation yielded a reactivity loss of 2.5%; the measured coefficient was -0.23%/% void in core water (see Progress Report for February 1965, ANL-7017, p. 75). For small percentages of voids in the ITC, calculation indicated +0.032%/% void; measurement yielded +0.05%/% void. Removal of the boron from the core corresponded to a calculated reactivity gain of 10.5%; removal of only half of the full boron loading was calculated to be worth 5.2%. Thus, for this fuel loading, 220 g natural boron control 10.5% in reactivity. For the conversion from a reflector with 10% Lucite and 90% beryllium, to a 100% beryllium reflector, calculation indicated a reactivity gain of 1.0%; the measured value was +1.2%.

For the current loading of 810 fuel foils and 810 B-SS strips, the calculated reactivity was 4.4%; the measured value was 2.9% (see Progress Report for May 1965, ANL-7046, p. 68). For small ITC voids, calculation indicated a reactivity effect of +0.034%/% void; the measured value was 0.05%/% void. For small, uniform voids in core water, calculation predicts -0.22%/% void in core water; the measured value was -0.19%/% void. Removal of half of the boron provided a computed reactivity gain of 6.6%; an additional 7.9% was gained by removing the remaining 50% of the boron. Thus, 425 g natural boron control 14.5% in reactivity, for this loading.

It was calculated that a loading of 1215 standard (0.0044-in.-thick) fuel foils and 2000 B-SS strips would be supercritical by 0.9%, and that,

for small changes in this number of B-SS strips, the reactivity effect of removing boron is +1.0% per 100 B-SS strips (containing 52.5 g natural boron). Thus, assuming that the reactivity mismatch is, say, $1\frac{1}{2}$%, a loading of 1215 fuel foils and 1750 B-SS strips would be supercritical by approximately 2%.

4. Heat Transfer

a. Analytical Studies. A summary of previous (see Progress Report for August 1965, ANL-7090, pp. 60-62) and supplementary hot-channel calculations for AARR transients is given in Table XX, in which Φ_{DNB} is the maximum surface heat flux which can be maintained with nucleate boiling, f_r the fraction of heat going into voids, and τ is the bubble collapse (or removal) time.

TABLE XX. Summary of Conditions for AARR Hot-Channel, Transient Calculations at 100 MW

Run No.	$\Phi_{DNB} \times 10^{-6}$, Btu/hr-ft^2	f_r	τ, msec	Reactivity Insertion	Axial Heat Generation Distribution
8A*	6.25	0.1	10	$1.00 step	Skewed
201	5.0	0.075	10	$1.00 step	Skewed
202	5.0	0.05	10	$1.00 ramp**	Skewed
203	6.19	0.05	10	$1.00 ramp	Skewed
204	6.19	0.05	10	$1.00 ramp	Cosine
205	6.25	0.1	10	$1.00 step	Cosine
206	5.0	0.05	10	$1.00 ramp† with rod action	Skewed
207	5.0	0.05	10	$1.50 ramp† with rod action	Skewed

*In Run 8A, the initial fluid velocity through the channel was 45 ft/sec. In all other runs, the initial velocity was reduced by a factor of 1.08.
**All ramp reactivity additions were accomplished in 33 msec.
†Control rods assumed inserted with four "g" acceleration following a 10-ms delay. Signal given at 130% of initial power.

The magnitude of large pressure surges predicted during certain transients is affected strongly by the number of equal sections into which the axial length is divided for the computation. In view of this tendency as well as the errors inherent in neglecting sonic effects and variations of saturation temperature with local pressure, it is believed that the hydrodynamic (pressure) output from CHIC-KIN[37] should be interpreted as providing a qualitative indication of possible trouble rather than as a reliable quantitative indication.

[37]Redfield, J. A., CHIC-KIN - A Fortran Program for Intermediate and Fast Transients in a Water-Moderated Reactor, WAPD-TM-479 (Jan 1965).

A second conclusion is that the CHIC-KIN code predicts no melting of fuel for a one-dollar ramp[38] reactivity addition in 33 msec with subsequent control rod action. This contrasts with results of previous analog studies (see Progress Report for December 1964, ANL-6997, pp. 53 and 54) in which melting was predicted because of the assumption of complete insulation past departure from nucleate boiling (DNB). The CHIC-KIN code makes no such assumption. In this particular transient, transition boiling is predicted past DNB, but the drop in power level results in an insulation decrease and a return to more stable nucleate boiling and convective heat transfer regimes. More information about heat transfer rates beyond the critical heat flux is required to determine if the CHIC-KIN results are accurate.

Finally, it can be concluded that for the same average heat generation in the fuel, an axial cosine distribution of heat generation appears to be a less severe case than the skewed distribution adopted for damage studies, primarily because of the higher local heat fluxes present in the skewed representation.

b. Experimental Program

(i) Steady-state Tests. Heat transfer tests are being conducted to determine the maximum steady-state power level feasible with the AARR Mark-I reference core design. High power levels and associated severe thermal conditions in these steady-state tests have destroyed three test sections by burnout. The problem lays in the inability of the switching equipment of the power supply to reduce power rapidly enough after reaching burnout conditions (see Progress Reports for January 1965, ANL-7003, p. 70; March 1965, ANL-7028, p. 73; April 1965, ANL-7045, p. 54; May 1965, ANL-7046, p. 73; June 1965, ANL-7071, p. 57 and July 1965, ANL-7082, p. 58). It was demonstrated during efforts at circumventing this problem that operation to within a few percent of calculated burnout conditions is possible. Experience and use of the Zenkevich-Subbotin correlation served as guides in the testing of Test Section III.

This third test section was fabricated with rounded corners to reduce local heat fluxes. Single-element pressure drop versus flow curves were directly measured at three powers. The positive-displacement pump-single-channel system was employed; at the operating pressure of the system the demand curve of the pump was considerably steeper than any estimated pressure drop versus flow curve; thus no danger point was expected. At each power the flow was progressively reduced until the system was as close to an expected burnout point as experience has shown to be permissible. During the run at highest power the minimum flow rate was approached too closely and an actual burnout occurred, destroying the section.

[38]The term "melting" is used here to indicate that the melting temperature has been reached and does not consider the time required to melt the fuel.

The results are shown in Fig. 19. Over the ranges tested, there was no minimum pressure drop for any of the three input powers. Also shown is a pump accumulator demand curve.

Test results show that for the three conditions, average power densities of 9.7, 11.8, and 13.2 MW/l were attained. An axial power distribution factor of ~1.42 is estimated for the hottest regions of the test section; therefore, peak power densities of 13.7, 16.75, and 18.7 MW/l were reached. A comparison of the data of condition 3, for which burnout actually occurred, with the Zenkevich-Subbotin correlation indicates that the burnout heat flux was about 5.12×10^6 Btu/ft^2-hr, whereas the maximum heat flux at burnout for the test section was 5.84×10^6 Btu/ft^2-hr.

(ii) Transient Heat Transfer Tests. The effect of rapid power transients upon the heat transfer, fluid flow, and critical heat flux in an AARR coolant channel will be experimentally measured in the transient heat transfer tests intended to check the accuracy of analytical methods for predicting burnout during transients.

In analog studies a 33-msec transport time of the coolant water through the core was used for the time interval during which reactivity is linearly inserted. Reactor power was highest between 35 and 40 msec after start of ramp insertions. Approximately a one-dollar ramp insertion in this time ($30.00/sec) represented the threshold for fuel melting to occur. During this transient, the ratio of peak to initial power was 6:1.

The feasibility of using a 1500-kW d.c. power supply, which consists of four rectifier units controlled by saturable magnetic amplifiers, has been demonstrated. The amplifiers are controlled by bias (excitation) currents which vary the amplifier impedance. The bias-control circuitry has been rewired to allow larger step changes in bias current for a shorter duration. By varing the duration of the bias current, the time of maximum pulsed power can be varied from 30 to 100 msec; by varying the magnitude of the bias current, the ratio of maximum to initial power for each time period can be selected. By use of a single rectifier unit and pulsing it from the lowest possible initial power, it is possible to obtain maximum-to-initial power ratios between 4 and 5 for a pulse duration (and time to maximum power) of 38 msec. This power ratio becomes smaller as the initial power is increased; thus it may be necessary to design different test sections to obtain data at each reactor power level of interest.

A circuit which automatically operates the power supply and instrumentation during power transients has been designed, built, and tested. With this circuit the initial, maximum, and final powers as well as the time to maximum power, can be preselected. The circuit switches the fast-response recorder on, allows time for the recorder to attain correct speed, pulses the power to the test section, and switches the recorder off again.

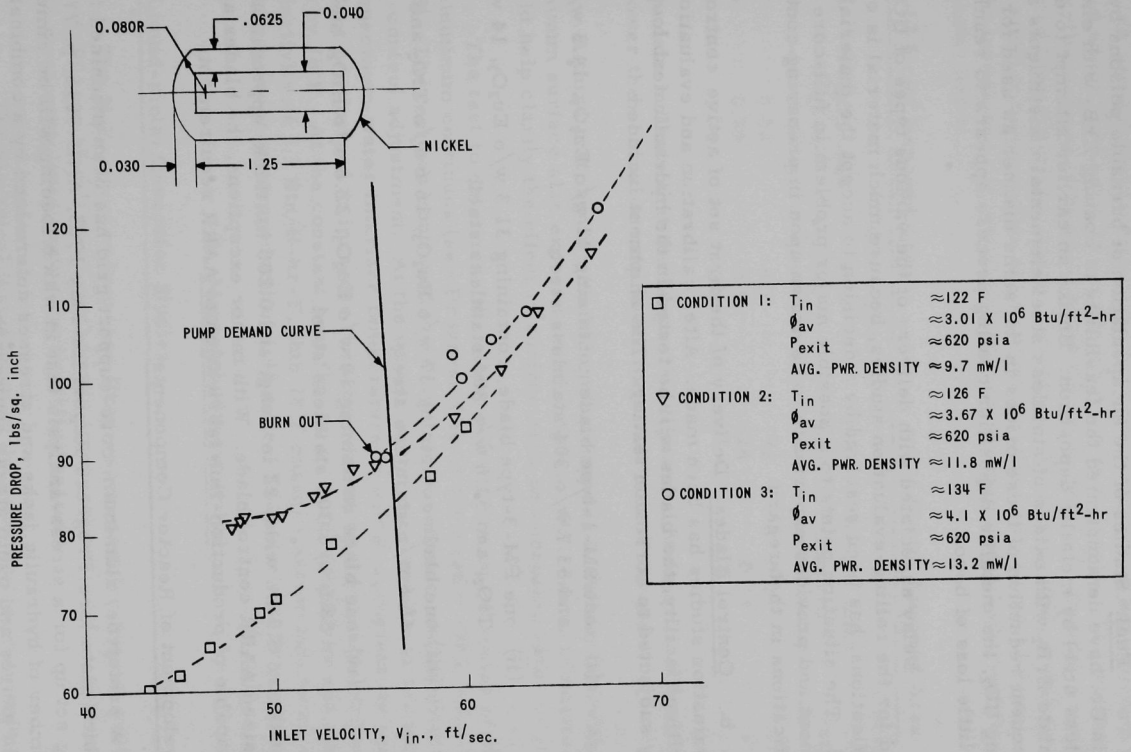

Fig. 19. Results from Test Section III (Rounded Corners); Heated Length was 18 in. (Dimensions in in.)

5. Fuel and Materials Development

a. Fuel. Studies of the encapsulation of burnable poisons by the Martin Co. have demonstrated the feasibility of coating ZrB_2 with elemental stainless steel by metallic deposition. Unlike an earlier attempt to encapsulate ZrB_2 with oxides of stainless steel elemental constituents and subsequent reduction of these oxides in the same manner as used for coating UO_2, the metallic deposition coating process appears to result in very little loss of boron.

Delay associated with delivery of the various types of UO_2 required for the rolling-evaluation studies, because much material is outside specifications, has been resolved by a decision to accept the material produced. The situation points to a possible major problem in full-core procurement and provides experience to be drawn upon in preparing contract specifications in that regard.

b. Control Blades. Delivery of the first set of active control blades for evaluation studies has been made. After calibration and evaluation in the critical facility, the blades will be tested in the hydraulic test loop and finally subjected to corrosion testing. The shipment included:

(i) one SM-1-type blade containing 32 w/o Eu_2O_3, 14.3 w/o TiO_2, and 53.7 w/o 304 stainless steel;

(ii) one PM-3-type blade, containing 31.3 w/o Eu_2O_3, 14 w/o TiO_2, and 54.6 w/o 304 stainless steel;

(iii) one blade containing 37 w/o Eu_2O_3, 16.6 w/o TiO_2 and 46.6 w/o stainless steel;

(iv) one blade containing 19 w/o Eu_2O_3, 22.6 w/o HfO_2, and 58.6 w/o 304 stainless steel.

All blades are 5.5 in. wide, 22 in. long, and 0.200 in. thick, approximating a full-sized AARR control blade. With minor exceptions, the blades appear to be capable of production-line fabrication to AARR requirements.

6. Development of Reactor Components

A prototype, aluminum, core-support grid has been machined from 6-in.-thick plate (see Progress Report for May 1965, ANL-7046, p. 77). It is being set up for a stress-analysis test in which loading will be simulated by a number of hydraulic jacks and stresses determined by a combination of strain gauges and photo stress equipment.

7. Primary System and Components

A second test to determine the corrosion rate of beryllium in deionized water flowing at 44 fps (at 200°F) is in progress. The surface area of beryllium exposed to water (27.6 liters) is 125 cm^2. Results previously reported (see Progress Report for August 1965, ANL-7090, p. 63) were for a similar test in which the exposed beryllium area was 12.5 cm^2. Weight losses and corresponding corrosion rates under both conditions are shown below.

12.5 cm^2 Exposed Area			125 cm^2 Exposed Area		
Time (hr)	Weight Loss (mg/cm^2)	Corrosion Rate (mpy)	Time (hr)	Weight Loss (mg/cm^2)	Corrosion Rate (mpy)
97	0.22	4.1	92	0.16	3.3
478	0.75	2.9	518	0.33	1.2
1150	1.75	2.8			

These data indicate that the larger the exposed surface area of beryllium, the lower the corrosion rate under the conditions of the test.

A third test, again with 125 cm^2 of exposed beryllium but with an aluminum surface also exposed, is in progress; the results of this test should help clarify the effect of surface area on corrosion rate.

The test to determine the effect of heat flux on corrosion of 6061-T6 aluminum continues (see Progress Report for August 1965, ANL-7090, p. 63). The test has continued for 793 hr, with only one interruption for flow-control adjustment. At the middle of the specimen being tested, where the specimen-water interface temperature is 258°F, sufficient corrosion product has formed to increase the temperature on the outside of the specimen by 78°F. At the constant heat flux of 8.2×10^5 Btu/ft^2-hr and a thermal conductivity of 1.3 Btu/ft-hr-F, this 78°F change corresponds to an oxide thickness (corrosion product) of 1.48 mils. This test will be continued.

B. Magnetohydrodynamics

1. Liquid-metal Generator Studies

The NaK-nitrogen loop (see Progress Report for August 1965, ANL-7090, pp. 65-67) has been brought to operational status. The following tasks were completed during the reporting period.

a. The electrical installation of the generator was completed. The generator was coupled to the external variable impedance load and the

entire apparatus was checked out. Calibrations of the thirteen transistor banks were obtained.

b. A closed-circuit television system was installed to view the fluid behavior inside the generator. Observations will be made of the film stability under various operating conditions.

c. The nitrogen-supply system was installed; it includes a series of three orifices and two transducers to cover a mixture quality range of 0-60%.

d. All remaining instrumentation such as pressure transducers, thermocouples, etc., was installed.

e. The entire loop was encased with Lucite and aluminum shielding.

A preliminary design study of a large-scale induction MHD generator suitable for commercial application was started. This study will investigate the effect of such factors as generator wall thickness, wall conductivity, copper electrical loss, iron core temperature, winding geometry, and current on the performance of an induction generator. These parameters, which are of great importance in a practical generator design, have not been considered in the highly idealized models in the literature.

2. MHD Condensing Injector

Studies of liquid-metal MHD power cycles have indicated the potential of the one-fluid condensing-injector cycle. Since the overall efficiency of such a cycle depends on the performance of the condensing injector, preparations are being made for the design, construction, and testing of a Freon-11 condensing injector. For this purpose the Freon Loop heat-exchanger capacity and power input have been balanced and final designs have been established. Two heat exchangers have been fabricated in the shop and a third exchanger has been modified. The dimensions of the resistance-heater sections have been established, with resistances matched to available power.

C. Energy-conversion Systems

1. Regenerative EMF Cells

a. Lithium Hydride Cell Studies. Thermal-analysis studies have continued of various salt systems which have potential application as electrolytes for the lithium hydride emf cell. The electrolyte presently being considered is a ternary mixture of LiH, LiCl, and LiI having a melting point of about 325°C. The solid-liquid equilibrium data defining the three

sides of the ternary diagram, the LiH-LiCl, LiH-LiI, and LiI-LiCl systems, have now been determined. All are simple eutectic systems: the LiH-LiCl eutectic (34.0 m/o LiH) melts at 495.6°C, the LiH-LiI eutectic (23.5 m/o LiH) at 390.8°C, and the LiI-LiCl eutectic (34.0 m/o LiCl) at 368.4°C.

These results indicate that lithium hydride cell operation is possible in an all-lithium electrolyte down to about 350°C. At this temperature, the open-circuit potential of the lithium hydride-saturated cell is about 0.5 V with all components at their standard states [LiH(s), Li(ℓ), 1 atm H_2(g)].

b. Sodium-Bismuth Cell Studies. The cell Na(ℓ)/NaI-NaCl-NaF(ℓ)/Na-Bi liquid alloy (30 a/o Na) has been operated at a temperature of 544°C for seven days. The maximum temperature gradient of the interior of the cell was ±0.6°C and the variation with time was ±1.1°C over the entire period of operation. The temperature uniformity was instrumental in reducing irreversible transfer (irreversible transfer of sodium from the anode to the cathode occurs by two mechanisms: thermal convection and diffusion) to a rate approaching that of diffusion. The initial cell voltage was 0.6084 V and decreased at a linear rate of 4.0×10^{-4} V/hr. This rate of change indicates that a temperature-emf profile cannot be obtained in a single cell experiment designed to yield thermodynamic data because of the changes in concentration of sodium in the cathode.

A single crystal of NaCl machined into a cylindrical cup has been used as a solid electrolyte and as the anode container in cells represented as follows:

$$\text{Na}(\ell)/\text{NaCl(s)}/\text{Na-Bi liquid alloy } (X_{Na} = \text{a/o Na} = 10, 20, 30).$$

Irreversible transfer due to diffusion is very slight in these cells. The internal resistance ranged from 2×10^7 ohms at 250°C to 10^2 ohms at 700°C. Voltages were measured by means of an amplifier using an electrometer input over this entire temperature range. These and other measurements will be used in deriving the required thermodynamic properties of sodium-bismuth alloys at low temperatures for cell design characteristics and at high temperatures to elucidate the regenerative parameters of the system.

c. Vapor-liquid Equilibrium Studies of the Sodium-Bismuth System. As a part of an experimental program to obtain vapor-liquid equilibria data for the high-temperature portion of a sodium-bismuth regenerative cell system, total vapor pressures have been measured both by a boiling point and by quasi-static methods for the binary sodium-bismuth systems containing 90, 80, 75, 60, 50, and 40 a/o sodium. Vapor compositions were measured at 900°C by the transpiration method for the 40 and 20 a/o sodium systems. The results have been incorporated into a virtually complete pressure-composition diagram showing the 900°C isotherms for

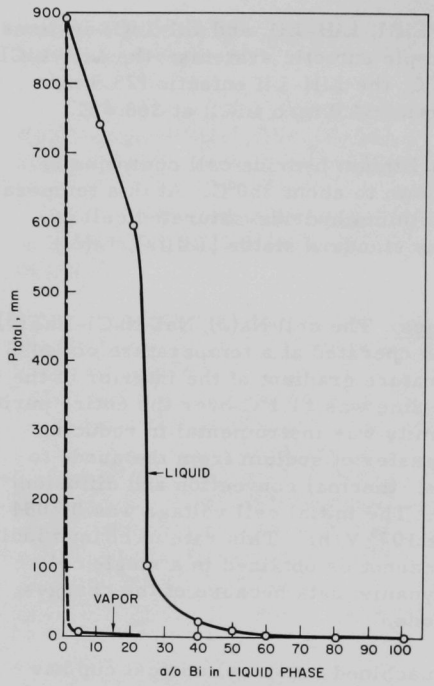

Fig. 20. 900°C Isotherms for Total Pressure in Sodium-Bismuth Alloy System

liquid and vapor equilibrium curves (see Fig. 20). A reasonable, extrapolated part of the vapor equilibrium curve is shown with a dashed line.

We have found the melting point of Na_3Bi to be higher (838°C) than the value reported in the literature[39] (775°C). The entire liquid-solid phase diagram in the literature, therefore, is in doubt.

Previous studies at Argonne of regenerator operation have shown that it is important that the liquid equilibrium curve of the liquid-vapor loop not intersect the liquid-solid regions of the phase diagram. This condition is achieved by selecting a sufficiently high operating pressure. If liquidus isobars, which can be derived from the measured pressure values, are plotted on a temperature-composition diagram together with the liquid-solid regions which may be expected to be in accord with the redetermined melting point of Na_3Bi, one may conclude that a pressure of about 200 to 250 mm will be needed in an operating regenerative sodium-bismuth cell. In turn, this would indicate a probable regeneration temperature of about 1200°C.

A small experimental bimetallic regenerator, similar to the one previously used to regenerate sodium from lead (see Progress Report for April 1965, ANL-7045, p. 58), is being constructed to verify the above conditions for the sodium-bismuth system.

2. Bimetallic Cells

a. Sodium-Lead Bimetallic System. An experimental sodium-lead bimetallic cell apparatus with attached thermal regenerator is being assembled. The cell proper is constructed with a frozen electrolyte-silicone rubber insulator-seal, similar to that of the sodium-bismuth cell now in operation as a battery (see Progress Report for January 1965, ANL-7003, p. 74). The regenerator is constructed of stainless steel and

[39]Hansen, M., and Anderko, K., Constitution of Binary Alloys, McGraw-Hill Book Co., Inc., New York, p. 322 (1958).

is similar to the regenerator previously used to demonstrate the feasibility of regenerating sodium from lead (see Progress Report for April 1965, ANL-7045, p. 58).

b. Multiple Bimetallic Cell. An experimental multiple bimetallic cell system with three cells stacked in series, electrically, is being assembled. The unit is provided with weirs to allow the electrode metals and electrolyte to flow from the top through the three cells to a reservoir at the bottom. The unit can be used with either sodium-lead or sodium-bismuth electrodes.

At present no regenerator is included with the unit; however, in a complete system the spent cathode material from the reservoir at the bottom would be pumped to a regenerator where sodium would be removed by distillation from the lead or bismuth. The separated sodium and lead or bismuth would then be returned to the upper cell anode and cathode, respectively.

A glass and plastic model has been used to check the weir-system design and operation at room temperature. Water (density, 1 gm/cm^5), tetrabromopthane (density, 3 gm/cm^5), and mercury (density, 13.5 gm/cm^5) have been employed to simulate the sodium (density, 0.8 gm/cm^5), electrolyte (density, 2.5 gm/cm^5), and lead alloy (density, ~9 gm/cm^5), respectively. Under these conditions, satisfactory operation was achieved.

IV. NUCLEAR SAFETY

A. Reactor Kinetics

1. Equation of State for Fast Reactor Accidents

Experimental measurements of the shock compression of materials cover an important range of pressure-volume relation between static compression measurements and the range where theories of highly compressed matter are valid. Such measurements usually lead to linear relations between the shock velocity U_s and the particle velocity U_p (in the absence of phase transitions):

$$U_s = C + SU_p. \tag{1}$$

Experiments made with metallic uranium yielded the following values of the constants:

$$C = 2.55 \text{ km/sec}; \quad S = 1.504.$$

In the limit of zero particle velocity, the shock velocity must be the sonic velocity and equal to C, which is available from sonic test data. It can be shown[40] that at zero pressure

$$S = \tfrac{1}{2}(\gamma + 1), \tag{2}$$

where γ is the Grüneisen ratio:

$$\gamma = V\alpha/\kappa C_v, \tag{3}$$

V the specific volume, α the volumetric thermal expansion coefficient, κ the isothermal compressibility, and C_v the heat capacity at constant volume. If the constants C and S are known, then the pressure after a shock, p, is related to the volume by

$$p = \frac{C^2}{V_0}\left(1 - \frac{V}{V_0}\right)\Bigg/\left[1 - S\left(1 - \frac{V}{V_0}\right)\right]^2, \tag{4}$$

and the energy is given by

$$E = E_0{}^\circ K + \frac{C^2}{2}\left(1 - \frac{V}{V_0}\right)^2\Bigg/\left[1 - S\left(1 - \frac{V}{V_0}\right)\right]^2$$

$$= E_0{}^\circ K + \frac{pV_0}{2}\left(1 - \frac{V}{V_0}\right). \tag{5}$$

Here the subscript zero indicates the unshocked state.

[40] Rice, M. H., McQueen, R. G., and Walsh, J. M., "Compression of Solids by Strong Shock Waves," in Solid State Physics, Ed. by F. Seitz and D. Turnbull, Academic Press, N. Y., (1958), Vol. VI.

The sonic velocity can be calculated from the compressibility and S can be estimated from physical properties and Eq. (2). The shock equation of state for various reactor materials is being estimated from measured physical properties and these equations.

An experimental program to measure sonic velocities and derived compressibilities for reactor materials of typical purity and porosity is being initiated. High-temperature measurements are to be made since accidents can be considered to initiate while the reactor is at power.

2. Transients with Thorium-Uranium Fuel

Six EBR-II-type Th-20 w/o U fuel pins have been run in TREAT to a range of conditions extending from no damage to extensive failure. All were exposed, in an inert gas atmosphere, using standard transparent meltdown capsules. Although photographs showed the high-velocity expulsion of bond sodium, resulting from cladding failure, that is characteristic of the sodium-bonded EBR-II fuel type, fuel movement was dominated by gravity rather than by internal pressure (see Progress Report for January 1965, ANL-7003, p. 77).

Metallographic and electron microprobe analyses of samples from the TREAT specimens have been completed. Figure 21 shows a longitudinal section taken from a pin given a power burst of 0.43-sec half-width, and for

Micro BK 271 (Spec. 879) 250X

Fig. 21. Longitudinal Section through the Fuel of Capsule 2. The fiber structure of the original extrusion was not changed by the TREAT experiment.

which maximum cladding surface temperatures of 1330 and 1360°C were measured. The original fiber structure of the uranium phase in a thorium matrix is retained, even though the uranium phase of the alloy must have been above its solidus temperature. Apparently the higher-melting thorium matrix gave support to the alloy as a whole. Thus the metallographic examination, when combined with the postmortem inspection, provides an example of a fuel maintaining its integrity in an excursion during which its solidus temperature is exceeded briefly.

Figure 22 is a transverse section taken from the bottom, in the region of failure, of a pin given an energy input approximately 16.5% greater

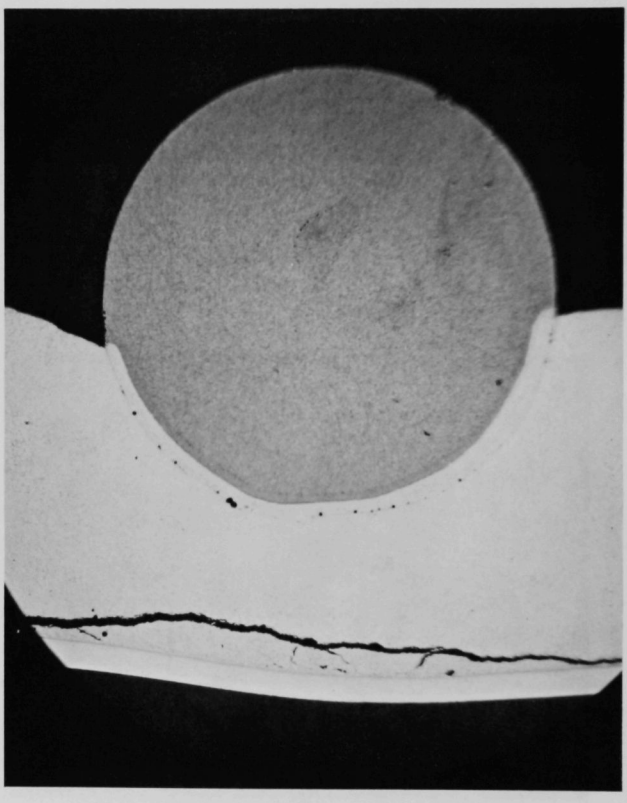

Micro BK 134 (Spec. 882) 22.5X

Fig. 22. Cross Section through Fuel, Molten Material and Stainless Steel Cladding of Capsule 3. The molten metal is bonded with both to the stainless steel cladding and the fuel. The crack through the molten metal was probably formed during or shortly after solidification.

than that received by the sample of Fig. 21. The grey, mottled circle is a cross section of the fuel rod showing the ends of the uranium grains. The semicircular annulus is solidified material from the upper portions of the pin. Although a reaction zone is clearly shown in the fuel, the circular cross section of fuel is retained. The cladding failure in this region was a pressure failure, with the cladding opening up like the pages of a book: the light, nearly horizontal band at the bottom of Fig. 22 is cladding. The gap between fuel and cladding is indicative of the lateral deformation suffered by the fuel, although it maintained its general shape. Figure 22 indicates that cladding failure and escape of sodium occurred appreciably before the light grey alloy ran down the pin, reacted with the fuel, and solidified. Electron microprobe analysis showed this "reaction product" ranging from within the fuel to the cladding to be an alloy of variable composition between the Th-U fuel and the stainless steel cladding. It contained no sodium.

3. Remotely Controlled Camera Stage for Hot Cell Examinations

Post-TREAT examinations of highly irradiated meltdown samples must be conducted remotely in the ANL hot laboratory facilities. A special, remotely controlled, movable horizontal stage has been developed for photographing sample remains in order to provide precision alignment, to speed operations, and to reduce handling by cave manipulators. This stage, or horizontal camera table, has a 56-cm longitudinal by 10-cm transverse travel, and a load capacity of 2.25 kg over the full span of table motion. It is designed to be used with a wall-penetrant hot-cell camera.[41]

A traverse speed of 2.5 cm/sec is obtained by means of standard Bodine motors equipped with all-metal slip-clutches and driving roller chains through sprockets. Self-enclosed V-ways with lightly preloaded roller bearings are used throughout as table supports to reduce drag while retaining maximum load capacity with minimum play and chatter.

Type 6061 aluminum alloy is employed as a structural material throughout. Total weight of the assembled unit, including motors and drives, is 17.7 kg, sufficiently close to the design goal of 16 kg to be accommodated by slight adjustment of the focusing stage counterweights.

Spring-loaded, momentary-contact, double-pole, double-throw switches allow reversing with maximum response and permit the operator to make small incremental movements. Electrical access to the moving platform which houses motors and drives is obtained through a replaceable coiled cable. The unit has been found to operate quite satisfactorily during actual specimen examinations with smooth motion, essentially no coasting or overtravel, and adequate control for closely positioning samples, even with 3X camera magnification.

---

[41]Doe, W. B., Low Power Stereo Camera, Proc. Fifth Hot Lab and Equipment Conference, 1957, Pergamon Press, p. 157 (1957).

4. Fast Neutron Hodoscope

Testing at TREAT was completed with the prototype, 50-channel assembly of the multichannel fast-neutron "camera" (see Progress Report for August 1965, ANL-7090, p. 69). It has been designed to detect and record the extensive coherent motion of fuel inside meltdown loops for conditions which have been hypothesized for meltdown-type accidents. Such motions cannot be followed by conventional means, although the data obtained by other techniques in more idealized experiments is required to analyze the loop results. Results from most of the recent experiments have been analyzed and demonstrated that the system is capable of meeting design objectives as well as providing data of significant value to the Fast Reactor Safety program.

Two single-pin samples were run in standard transparent meltdown capsules, and sample motion was followed by both the neutron hodoscope and by a high-speed optical camera. Preliminary, nonmeltdown check transients were run before each meltdown test. In each case, satisfactory correlations were found between the hodoscope data and the optical-camera Ektachrome-film data, for such phenomena as commencement of sample bending, time of bending, directions of bending, and rupture. For these tests, signal-to-background ratios ~7:1 were achieved by means of a 9% enriched EBR-II pin.

A sodium package loop, loaded with a single 6% enriched EBR-II pin inside a cluster of six dummy pins, also was studied with the hodoscope. In this case, the signal-to-background ratio was only ~2.5:1, adequate for densitometric measurements, as well as visual recognition of gross effects.

Work is now underway on readout techniques, incorporation of improvements based on data from the reactor tests, and on design of the system for extension to a full complement of active channels.

5. Fast Reactor Safety

a. Coolant (Water) Expulsion Studies. The first series of experiments on water expulsion has started. These are investigating effects of energy release rate and inertial loading on coolant expulsion and pressure generation in water contained in an annulus of 19.05-mm ID and 25.4-mm OD. In the 79 experiments that have been conducted, the energy input was varied from 0.44 to 2.96 kW-sec (released in 85 to 148 msec), and the height of water above the 25.4-cm-long heated tube was varied from 0 to 25.4 cm. The water pressure, tube temperature, position of the liquid-vapor interface, voltage drop across the test section, and the current flow were measured.

The magnitude of the pressure transients appears to be independent of the mass of water (in the range investigated) but is proportional to the energy input. Typical pressure pulses measured were 1.97 atm with an energy input of 1.767 kW-sec in 96 msec and 3.33 atm with an energy input of 2.304 kW-sec in 91 msec. In both cases, the initial water temperature was 22°C. High-speed motion pictures taken of the liquid-vapor interface have not yet been interpreted.

After 79 experiments, the thin-wall (0.127 mm) test section was damaged. The equipment was torn down and rebuilt. While the equipment was down, improvements were made on the lighting for photographic purposes; also, an additional thermocouple was placed in the water with suitable circuitry to facilitate fast-response recording.

b. Superheat Experiments. It is planned to measure the degree of liquid superheat required to initiate nucleate boiling in sodium under various conditions simulating a reactor environment. Typical parameters will be varied systematically to determine their independent and combined effects on the liquid superheat necessary to initiate nucleation. The parameters to be covered are: (a) pressure in the range from 50 Torr to approximately 2.5 atm; (b) effects of dissolved gas, such as argon and helium; (c) heat flux in the range of approximately 5×10^4 to 5×10^5 Btu/hr-ft^2; and (d) surface characteristics.

The test apparatus is being constructed of 316 stainless steel. This apparatus consists of a pool boiler pressurized by an inert-gas blanket. Both argon and helium gas blankets will be utilized to aid in the determination of the effect of liquid metal containing soluble cover gas upon the degree of liquid superheat required to initiate nucleate boiling. Testing will be performed at temperatures ranging up to 1700°F.

6. Fast Reactor Control

a. Stability Analysis of Nuclear Power Reactors for Finite Size Disturbances. Two general types of treatments are available for the stability analysis of nuclear reactors. In one, a linear model of the reactor is analyzed to obtain criteria for the local stability of the operating point $\underline{X}_0$. The other deals with the global stability of the reactor; the heat-transfer equations are taken to be linear, and the only nonlinearity considered is that due to the multiplying media in the reactor, thus obtaining criteria for global stability. The criteria for global stability might be unnecessarily restrictive, since disturbances of infinite size are not expected during normal operation; therefore, a criterion which gives the stability conditions for a disturbance of finite size is sought. These criteria hopefully will be less restrictive, since a reactor might be globally unstable but stable in a certain finite region, G, in the vicinity of the operating point $\underline{X}_0$, i.e., if $\underline{X}(t_0) \in G$, then $X(t) \rightarrow \underline{X}_0$ as $t \rightarrow \infty$.

The stability criteria obtained so specify the "size" of the region of attraction G of the point $\underline{X}_0$ and its relation to the reactor power level.

b. Space-Time Reactor Dynamics. In conjunction with the coupled reactor kinetics equations, the space-time effect of the flux distribution of the entire reactor due to the motion of one or more control rods has to be determined first before the stability analysis and control-system design can be made.

In order to have a more accurate description of the control rods effect, the rod motion is considered as the change of the nuclear parameters in the reactor equations, i.e., (D) Σ_a, Σ_f. With this assumption, the multigroup equations have coefficients which are functions of space and time.

As a typical example for a three-dimensional case, the absorption cross section $\Sigma_a(x, y, zt)$ may be written as

$$\Sigma_a = \frac{\Sigma_{a_1} + \Sigma_{a_2}}{2} + \frac{\Sigma_{a_1} - \Sigma_{a_2}}{2} \mathrm{Sgn}[z - f\{x, y, z_1(t), z_2(t), \ldots, z_s(t)\}],$$

where Σ_{a_1} and Σ_{a_2} are the absorption cross sections of the reactor with and without the control rod, respectively. Sgn is a function which is "+1" if $z < f$ and "-1" if $z < f$, and $f\{x, y, z_1(t), \ldots, z_s(t)\}$ is defined as

$$f\{x, y, z_1(t), \ldots, z_s(t)\} = z_k(t) \text{ when} \begin{Bmatrix} x_k \le x \le x_k' \\ y_k \le y \le y_k' \end{Bmatrix}$$

$$= 0 \qquad \text{otherwise}$$

$$k = 1, 2, \ldots, s$$

where

s is the total number of control rods in the reactor

$z_k(t)$ is the time motion of the kth control rod

$\begin{Bmatrix} x_k, x_k' \\ y_k, y_k' \end{Bmatrix}$ are the space coordinates where the kth control rod is located.

The exact solution of the group equation with such parameters are obviously improbable, if not impossible.

An infinite series solution, consisting of the eigenfunctions of the steady-state reactor equation with stationary rods and undetermined coefficients which would be functions of time and rod motion, is possible. The determination of these coefficients may not be simple. If the series is truncated, a simpler class of equations would be obtained. The choice of the set of functions will depend upon the following considerations: (1) the boundary conditions of the reactor equation; (2) whether the set is orthogonal and complete; and (3) the rate of convergence to the true solution. In general, if such a set of functions is chosen, the flux can be written as

$$\phi\{x, y, z_1(t), \ldots, z_s(t)\} = \sum_{ijk} U_{ijk}\phi_{ijk}.$$

If we substitute this expression into the reactor equation and apply the orthogonal property of the set, i.e.,

$$\int_v \phi_{ijk}\phi_{lmn}d_v = \delta_{il}\delta_{jm}\delta_{kn},$$

the reactor equation is reduced to a set of ordinary differential equations:

$$\dot{U}_{lmn} = \sum_{ijk} A_{ijk}^{lmn} U_{ijk},$$

where

$$A_{ijk}^{lmn} = A_{ijk}^{lmn}[z_1(t), z_2(t), \ldots, z_s(t)].$$

At this point, the stability analysis and control-system design is made in the so-called modal approach with respect to this set of equations instead of the original partial differential equations. However, it is also possible to find the solutions of the flux distribution as functions of $z_k(t)$ and evaluate the coupling coefficients, which will also be functions of the control variables $[z_k(t)]$. The choice is arbitrary.

This approach can also be applied to nonlinear cases if we include the heat transfer and hydrodynamics equations. The nuclear parameters will be functions of other dependent variables as well, and the resultant ordinary differential equations will likely be nonlinear, but the application to stability analysis and control-system design will remain the same.

B. TREAT

1. Operations

Metal-water reaction samples CEN 210 through 213 of High Flux Isotope Reactor fuel were irradiated. Three were tested in water initially at 120°C and one in water at room temperature.

An EBR-II type pin in a package sodium loop was subjected to a transient designed to fail the pin in flowing sodium. Data from the fast neutron hodoscope was recorded during this experiment (see Section IV.A.4).

Fuel sample C-3-E, a mixed Pu-U oxide sample irradiated to a burnup of 63,000 MWD/mT prior to the transient irradiation was subjected to a transient irradiation for the General Electric Company.

2. Large TREAT Loop

The large TREAT loop is in its final phase of construction. The assembly of the out-of-pile portion of the loop is proceeding in Idaho. The remaining components still being fabricated are:

1. Lower portion of test section
2. Test section header
3. Test section liner
4. Surge suppressor
5. Crossover bellows for horizontal pipe runs over reactor core
6. TREAT dummy elements
7. Cover-gas system parts
8. Leak-detector drip grids.

The lower portion of the test section is being prepared for the installation of the pressure transducer housings. Although difficulties were encountered in initial attempts, the Conoseal flanges have been welded to the header for the test section, which is now 90% complete.

Fabrication of the Zircaloy liner has started at Dressler Products Company. The liner will isolate the test section and contents from the core so that spilled sodium will not contact the TREAT fuel elements.

As the surge suppressor is approaching the final phase of construction at the Keller Products Company, radiographs of the circumferential

tank weld disclosed incomplete weld penetration. Although rectification of this defect will delay delivery about two weeks, the overall schedule for completing the loop will not be greatly affected.

The Fulton-Sylphon Corporation has mailed radiographs of cross-over bellows welds for examination at the Laboratory.

TREAT dummy elements, which will fill the void region surrounding the core, have been completed and are in storage pending shipment to Idaho.

The gas system has been revised to provide space for pipe support and to accommodate thermal expansion. All the major gas-system components, including valves, gauges, regulators, and pressure switches, are on hand. They are being tested for operation and helium leaktightness before shipment to Idaho.

Circuit components for the sodium leak drip-grids have been constructed. The grids, which will be the last units to go into place, will be located along sensitive loop areas.

Welding of the main 3-in. piping system for the large sodium loop was completed and leak testing of the system is in progress. Recent design changes in the blanket-gas system will cause a delay in completion of the loop because delivery of additional components is not scheduled until the last half of October.

C. Chemical and Associated Energy-transfer Problems in Reactor Safety

1. Metal-Water Reactions

a. Scale-up Metal-Water Experiments in TREAT with UO_2-core Fuel Clusters. Current metal-water reactions in TREAT have utilized 9-pin clusters of UO_2-core fuel clad with either Zircaloy-2 or 304 stainless steel. The pins were 0.42 in. in diameter by $5\frac{5}{8}$ in. long. The total weight of UO_2 core material in each of the experiments was about 750 g. In an experiment, the fuel pin cluster, submerged in water and contained in an autoclave, is subjected to a transient burst of neutrons in TREAT. The fission heat generated in the enriched core of the fuel causes meltdown of the test pins. After the transient, the hydrogen evolved is measured by means of a mass spectrometer, and from this result the extent of reaction of cladding metal with water is computed. Sieve-screen analyses are also made on the residues from the fragmented fuels, and the mean particle size is calculated from the particle size distribution (see Progress Report for January 1965, ANL-7003, p. 76).

Figure 23 is a photograph of a 9-pin, UO_2-core fuel cluster in its original condition. Figure 24 is a photograph of the cluster after a pulsed irradiation in TREAT; the appearance of the residue is typical of both Zircaloy-clad and stainless steel-clad fuels. Burnup analyses performed on each of the ten pellets in a UO_2-core pin which had remained intact during a TREAT transient have shown that the internal heat generation is reasonably uniform over the length of the pin except for the end pellets. This effect is caused by self-shielding. The results of the burnup analyses are summarized in Table XXI.

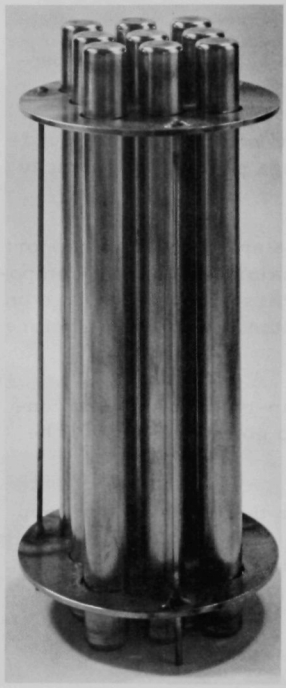

Fig. 23
9-Pin Fuel Cluster before Meltdown in TREAT. (UO_2-core, Type 304 stainless steel-clad fuel elements. Pin dimensions: 0.42 in. dia by 5-5/8 in. long.)

The data from the four UO_2-core scale-up experiments which have been completed to date are shown in Table XXII. Two of the experiments utilized Zircaloy-clad specimens; the other two, stainless steel-clad specimens. No explosive pressure rises were observed for either type of cladding material.

In earlier studies in TREAT, experiments were performed with single UO_2-core pins clad with Zircaloy-2 and with stainless steel (see Progress Reports for June and September 1964, ANL-6912, p. 90, and ANL-6944, p. 82). In the studies with UO_2-core fuel, the scale-up experiments utilized approximately 150 times as much core fuel material as did the single-pin experiments. In Figs. 25 and 26 the extents of metal-water reactions in the present experiments are compared with the results of earlier experiments with single small pins. The extent of reaction with stainless steel is slightly higher for the fuel-pin clusters than for single pins, whereas the extent of reaction with Zircaloy is slightly lower. However, these differences are within the probable limits of reproducibility of the in-pile, transient tests. The comparison indicates that there is no marked change in the extent of metal-water reaction upon fuel meltdown when a nine-pin cluster is used instead of a single pin. This, therefore, lends additional confidence in the application of these results to the behavior of actual reactor cores.

Future scale-up experiments will incorporate two major changes: (1) the reactor transient will be a "flat top" rather than a pulse,[42]

[42] In a "flat top" transient, fission heating remains reasonably constant for a period of about 10 sec. In a pulsed transient, the time scale for heating is about 1 sec, with a Gaussian-shaped power-time heating curve.

and (2) the sample will be located above the water rather than submerged. These conditions will simulate certain aspects of a loss-of-coolant accident, whereas previous experiments have simulated power excursions.

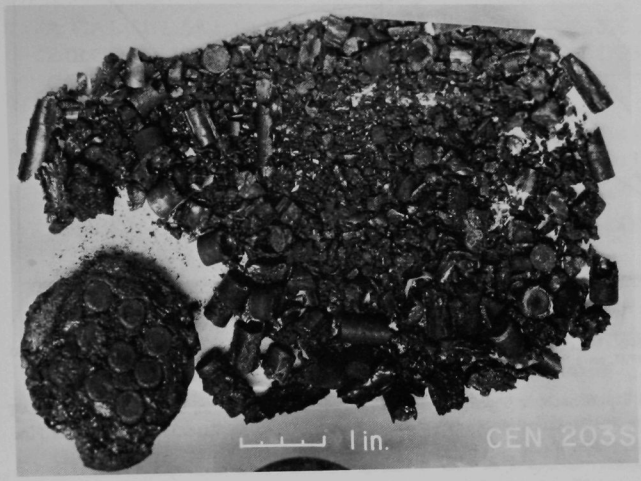

Fig. 24
9-Pin Fuel Cluster after Meltdown in TREAT. (UO_2-core, Type 304 stainless steel-clad fuel elements.)

TABLE XXI. Axial Distribution of Neutron Flux in 10-pellet, UO_2-core Fuel Pin for Scale-up Experiment in TREAT (CEN-202S)

Pellet Number	Vertical Position	Neutron Flux (cal/g UO_2)	Pellet Number	Vertical Position	Neutron Flux (cal/g UO_2)
1	Top	306	5	Center	250
2		238	6		250
3		230	7		244
4		236	8		248
			9		253
			10	Bottom	300

TABLE XXII. Summary of UO_2-core, Metal-clad, 9-pin Scale-up Experiments in TREAT

Conditions:
1. Fuel pins were UO_2, 10% enriched with U^{235}, clad with either Zircaloy-2 or Type 304 stainless steel. Pin dimensions: 0.42-in. dia by 5-5/8-in. long; 10 UO_2 pellets per pin, 25-mil-thick cladding, 3-mil gap between core and cladding.
2. Subassemblies consisted of 9-pin clusters on 9/16-in. centers in 3 by 3 square array.
3. Fuel subassemblies submerged in distilled water initially at ambient reactor temperature (~25°C).
4. 20 psia helium atmosphere above the water.

	CEN-TREAT Transient Number			
	202 S	203 S	208 S	209 S
Period, msec	117	74	87	87
Integrated power, MW-sec	202	373	382	391
Peak power, MW	508	1225	1145	1190
Energy, cal/g UO_2	250	463	475	485
Peak pressure, psig	54	223	110	304
Cladding	Zr-2	SS-304	SS-304	Zr-2
Extent of reaction of metal cladding with water, %	4	24	23	24
Fuel appearance after transient	Cladding started to melt	Complete fragmentation	Complete fragmentation	Complete fragmentation

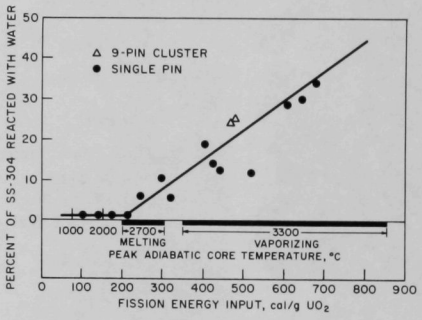

Fig. 25. Results of Meltdown Experiments in TREAT with UO_2-core, Type 304 Stainless Steel-clad Fuel Pins Submerged in Water

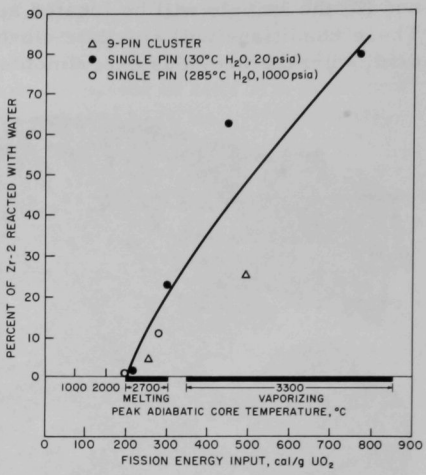

Fig. 26. Results of Meltdown Experiments in TREAT with UO_2-core, Zircaloy-2-clad Fuel Pins Submerged in Water

V. PUBLICATIONS

Papers

A CALCULATION DEMONSTRATING THE EFFECT OF THE ZIRCONIUM-WATER REACTION ON THE ANALYSIS OF A LOSS-OF-COOLANT ACCIDENT

Louis Baker and R. O. Ivins

Proc. Intern. Symp. on Fission Product Release and Transport under Accident Conditions, Oak Ridge, April 5-7, 1965. CONF-650407, Vol. 2, pp. 938-969

FISSION-PRODUCT EFFECTS IN MOLTEN-CHLORIDE FAST-REACTOR FUELS

M. G. Chasanov

Nucl. Sci. Eng. 23, 189-190 (October 1965)

ENGINEERING DEVELOPMENT OF A FLUID-BED FLUORIDE VOLATILITY PROCESS. I. Bench-Scale Studies

Deyabhaktuni Ramaswami, N. M. Levitz, and A. A. Jonke

Nucl. Appl. 1(4), 293-300 (August 1965)

ENGINEERING DEVELOPMENT OF A FLUID-BED FLUORIDE VOLATILITY PROCESS. II. Pilot Scale Studies

J. T. Holmes, Howard Stethers, and J. J. Barghusen

Nucl. Appl. 1(4), 301-309 (August 1965)

PREPARATION OF DENSE URANIUM DIOXIDE PARTICLES FROM URANIUM HEXAFLUORIDE IN A FLUIDIZED BED

Irving E. Knudsen, Norman Levitz, and Albert A. Jonke

Proc. Symp. on Preparation and Processing of Particulate Nuclear Fuels, New York, September 9, 1963

VIBRATORY COMPACTION. Part II. Compaction of Angular Shapes

J. E. Ayer and F. E. Soppet

Bull. Am. Ceram. Soc. 44, 710 (September 1965) Abstract

PROPERTIES OF PLUTONIUM CERAMICS AND THEIR POTENTIAL AS NUCLEAR FUELS

O. L. Kruger and J. B. Moser

Bull. Am. Ceram. Soc. 44, 729 (September 1965) Abstract

PREPARATION OF PuC PELLETS BY VACUUM SINTERING

O. L. Kruger

Nucl. Appl. 1(4), 348-355 (August 1965)

OXIDATION OF URANIUM MONOSULFIDE

D. R. Messier

Bull. Am. Ceram. Soc. 44, 730 (September 1965) Abstract

VIBRATORY GRINDING AND POLISHING OF METALLOGRAPHIC SPECIMENS

S. Matras

Proc. Eighteenth Metallographic Group Meeting, Canoga Park, California, June 22-24, 1964. NMI-5025 (Pt. 1), pp. 185-219 (August 1965)

NEUTRON RADIOGRAPHY

Harold Berger

Elsevier Publishing Company, Amsterdam (1965)

BORAX-V IN-VESSEL INSTRUMENTATION

E. J. Brooks

Proc. Symp. on In-Core Instrumentation, Oslo, June 15-19, 1964. CONF-640607, Vol. 1, Paper B-1

A THREE-DECADE EXPONENTIAL CURRENT GENERATOR FOR TESTING REACTOR PERIOD METERS

J. H. Talboy

Nucl. Appl. 1(4), 356-358 (August 1965)

AARR--A NEW TOOL FOR NUCLEAR RESEARCH

R. C. Skaardal

Teknisk Ukelblad 112(31), 675-679 (September 1965)

CERENKOV COUNTING OF AQUEOUS SOLUTIONS

Alexander DeVolpi and K. G. A. Porges

Intern. J. Appl. Radiation Isotopes 16, 496-498 (1965)

DETERMINATION OF MANGANESE SULPHATE CONTENT FOR NEUTRON SOURCE MEASUREMENTS

Alexander DeVolpi, R. J. Armani, and K. G. A. Porges

J. Nucl. Energy A/B: Reactor Sci. Technol. 19, 597-599 (1965)

EFFECT OF RESONANCE CORRECTION TO GROUP FLUX IN FAST-REACTOR DOPPLER-EFFECT CALCULATION

H. H. Hummel and R. N. Hwang

Nucl. Sci. Eng. 23, 98-99 (1965) Note

DYNAMIC ANALYSIS OF COOLANT CIRCULATION IN BOILING WATER NUCLEAR REACTIONS. I.

C. K. Sanathanan, J. C. Carter, and F. Miraldi

Nucl. Sci. Eng. 23, 119-129 (October 1965)

DYNAMIC ANALYSIS OF COOLANT CIRCULATION IN BOILING WATER NUCLEAR REACTIONS. II.

C. K. Sanathanan, J. C. Carter, and F. Miraldi

Nucl. Sci. Eng. 23, 130-137 (October 1965)

The following appeared in Abstracts of Papers, 150th Am. Chem. Soc. Mtg., Atlantic City, September 12-17, 1965

COMPACT PYROCHEMICAL PROCESSES FOR ADVANCED REACTOR FUELS

Leslie Burris, R. K. Steunenberg, R. D. Pierce, and Milton Levenson

p. 3-R

REPROCESSING SPENT PLUTONIUM AND ENRICHED URANIUM-BEARING FUELS BY FLUIDIZED-BED VOLATILITY METHODS

A. A. Jonke, M. J. Steindler, N. M. Levitz, J. T. Holmes, and Deyabhaktuni Ramaswami

p. 1-R

LIQUID-METAL MELT SALT PROCESSING OF FAST BREEDER REACTOR FUELS

D. A. Wenz, J. B. Knighton, and R. K. Steunenberg

p. 22-R

START-UP EXPERIENCE FOR THE EBR-II MELT REFINING PROCESSING PLANT

C. E. Stevenson, D. C. Hampson, and R. M. Fryer

p. 4-R

ANL Reports

ANL-6776 PHYSICS PERFORMANCE OF THE EBWR IN ITS OPERATION FROM ZERO TO 100 MWt

H. P. Iskenderian

ANL-6883 EXAMINATION OF IRRADIATED Ag-In-Cd ALLOYS

C. F. Reinke

ANL-7013 LABORATORY INVESTIGATIONS IN SUPPORT OF FLUID-BED FLUORIDE VOLATILITY PROCESSES. Part VII. The Decomposition of Gaseous Plutonium Hexafluoride by Alpha Radiation

Raymond P. Wagner, William A. Shinn, Jack Fischer, and Martin J. Steindler